Best Practices for Bridges with Pipe Piles

Research Final Report from Tennessee Technological University | Tim Huff & Dan VandenBerge | July 31, 2024

Sponsored by Tennessee Department of Transportation Long Range Planning Research Office & Federal Highway Administration

DISCLAIMER

This research was funded through the State Planning and Research (SPR) Program by the Tennessee Department of Transportation and the Federal Highway Administration under ***RES2023-04: Best Practices for Bridges with Pipe Piles.***

Technical Report Documentation Page

1. Report No. RES2023-04	2. Government Accession No.	3. Recipient's Catalog No.
4. Title and Subtitle *Best Practices for Bridges with Pipe Piles*		5. Report Date July 2024
		6. Performing Organization Code
7. Author(s) Tim Huff, Daniel VandenBerge		8. Performing Organization Report No.
9. Performing Organization Name and Address Tennessee Technological University 1 William L. Jones Drive Cookeville, TN 38505		10. Work Unit No. (TRAIS)
		11. Contract or Grant No.
12. Sponsoring Agency Name and Address Tennessee Department of Transportation 505 Deaderick Street, Suite 900 Nashville, TN 37243		13. Type of Report and Period Covered
		14. Sponsoring Agency Code
15. Supplementary Notes		

16. Abstract

Pipe piles are used extensively for bridge substructures in Tennessee. This research serves to develop a systematic approach to the selection and the design of pipe pile-supported substructures, both piers and abutments. Included are both a design manual and design examples, for the design of three pipe pile-supported pile bents: (1) pipe pile bents with a concrete plug connection to the cap, (2) concrete-filled steel tube (CFST) pile bents with the pile embedded in the cap beam, and (3) reinforced concrete filled steel tube bents with a gap between the top of the pile and the cap beam. Appropriate strain limits are incorporated in accordance with the latest science. Also included is discussion on the implications of modification to current TDOT field verification of pile capacity using dynamic testing rather than static load tests. Updated spring constants for pipe pile-supported integral abutments and updated point-of-fixity estimates are included in the study. Finally, a critical assessment of current corrosion-protection measures has been carried out.

17. Key Words **PIPE PILES, BRIDGES, PILE BENT, SEISMIC DESIGN**	18. Distribution Statement

19. Security Classif. (of this report) Unclassified	20. Security Classif. (of this page) Unclassified	21. No. of Pages xxx	22. Price

Acknowledgement

This research was completed with the assistance of TDOT Research Office personnel Pamela Boy-Walker and Beth Jirik along with the TDOT Technical Advisory Committee composed of Kathleen McLaughlin, Adam Price, Dan Shike, and Eric Slayton, all of the Structures Division. The research team gratefully acknowledges the essential guidance provided by each.

Executive Summary

While pipe pile-supported substructures have been used on bridges in Tennessee for decades, several issues contributed to the need for the research conducted and reported here. Prior to this research, no systematic means of selecting the most appropriate type of installation existed.

Parameters which must be defined to specify and construct a pipe-pile supported foundation include: (1) material requirements for the pile and any concrete fill, (2) the limit of concrete fill, if any, (3) material specification for longitudinal and transverse reinforcing, (4) strain limits for seismic design in the pile and in the concrete core, (5) design methods appropriate for seismic design, (6) point-of-fixity estimates, (7) connection of the pile to the reinforced concrete cap beam, (8) spring constants appropriate for structural analysis under earthquake loading, (9) methods used to verify axial capacity of piles in the field, and (10) corrosion-protection measures.

Three distinct substructure types were identified: (1) pipe pile (PP) bents, with a concrete plug connection to the cap beam and no other concrete, (2) concrete-filled steel tubes (CFST) with the pile embedded into the cap, and (3) reinforced-concrete filled steel tubes (RCFST) with a gap between the pile top and the cap soffit.

Material requirements for both piling and concrete fill were assessed. Current specification requirements are strict but permit alternatives at the Owner's discretion. This study identified the most appropriate material specification for various seismic zones and identified spiral-weld pipe as an acceptable material for all three pipe pile installations.

Concrete fill limits taken from the literature and from standard practice of other state Departments of Transportation have been used in the design methods developed herein. Pipe pile bents require no concrete fill below the connection plug but require much thicker tubes compared to other alternatives.

Reinforcing requirements for pipe pile bent plugs and for reinforced concrete filled steel tubes must align with the AASHTO Guide Specifications for LRFD Seismic Bridge Design. ASTM A 615 Grade 60 reinforcement is appropriate for seismic design categories A and B. ASTM A 706 Grade 60 reinforcing is required for seismic zones C and D in the pipe pile plug and in the RCFST core.

Strain limits from the literature have been incorporated into the design manual. Strain limits for piling at the beginning of this research did not appropriately incorporate local buckling considerations in the piling.

Both force-based and displacement-based design methodologies have been incorporated into the design manual. Rather than resorting to code-based approximations for plastic moments, recommendations have been included for detailed section analysis. A model has been developed which permits the engineer to estimate displacement capacity from simple hand calculations.

Point-of-fixity estimates have historically been based on decades-old rules-of-thumb. Representative borings from bridge projects in Tennessee were evaluated using state-of-the-art science to develop more refined point-of-fixity estimates for bridges in Tennessee.

The connection of the pile to the pile cap, particularly in extended pile construction (PP, CFST, and RCFST pile bents), has been rigorously studied in recent research efforts by others, and these recommendations have been incorporated into the design manual and the design examples.

Spring constants for seismic analysis and design at integral abutments have been historically based on decades-old rules-of-thumb as well. Based on borings from Tennessee bridge sites, refined spring constant estimates for various pipe pile diameters have been developed in this study. It was found that the traditional stiffness values are too high for soft clay and too low for hard clay and dense sand.

TDOT practice for field verification of pile axial load capacity has traditionally been based on use of the Engineering News Record formula in concert with static load testing. As part of this study, a review and commentary on this practice has been included.

Finally, a synthesis of potential alternative corrosion-protection measures for pipe piling in circumstances which warrant such measures has been included.

Key Findings

- Three viable methods for the construction of pile-supported structures were identified.
- A design procedure applicable to any of the three methods was developed.
- Design examples for each of the three substructure types were developed.
- A model for displacement capacity as a multiple of the displacement at first yield was developed
- Specific soil types were identified for which traditional spring constants and depth-to-fixity estimates used for piles in seismic analysis are inappropriate.

Key Recommendations

- Incorporate the recommended design procedure to produce uniformity in the robustness of pile-supported bridges.
- Incorporate design procedure so that details will be similar regardless of whether design is in-house or by consultants.
- Examine soil borings and classify the subsurface as a general soil type to refine spring constants.
- Modify the existing methodology for depth-to-fixity estimates based on the normalized models developed herein.

Table of Contents

List of Tables

List of Figures

Glossary of Key Terms and Acronyms

Capacity Protection: The design of non-ductile elements in the seismic load path to remain essentially elastic during strong ground shaking to ensure that any damage occurs in ductile elements.

Concrete-filled-steel tube (CFST): A steel tube filled with concrete to a specified limit and used as a structural support.

Depth-to-fixity: the distance below ground at which a fixed base structure will behave essentially equal to an embedded pile.

Hollow-Tube-Pile-Bent (HTPB): A pile bent constructed using hollow steel tubes for the piles; the only concrete fill in HTPB construction is the top plug.

Pile bent: A bridge support constructed by driving piles which are left protruding up to a cast-in-place concrete cap.

Plastic moment: the moment at which the entire cross-section of HTPB or CFST has reached the yield stress of the steel tube.

Reinforced Concrete filled steel tube (RCFST): Similar to CFST except the tube is stopped 2 inches below the cast-in-place cap soffit and the concrete is reinforced with longitudinal and transverse bars.

Spring constant: a value of stiffness assigned to a pile at an integral abutment for seismic analysis and design of the bridge.

Yield moment: the smallest moment on HTPB or CFST construction for which combined axial compression and flexure produce a stress equal to the yield stress of the steel tube.

Chapter 1 Introduction

The Tennessee Department of Transportation frequently opts for pipe pile supported bridge structures as an economical and robust solution to transportation needs. The need for uniformity in design procedures and construction practices for pipe pile supported bridges has become paramount, particularly in west Tennessee where the seismic hazard is extreme. The purpose of this report is to summarize the findings for TDOT Research Project RES2023-04: Best Practices for Bridges with Pipe Piles.

This project has included investigations into three distinct methods of construction for pipe pile supported bridges.

1. hollow tube pile bents (HTPB)
2. concrete-filled steel tubes (CFST)
3. Alaska pile bent / reinforced concrete casing (RCFST)

Descriptions of these three construction methods are included in subsequent sub-sections of the current chapter. Also included are subsections for geotechnical aspects of the project, which include:

1. assessment of pile installation procedures
2. assessment of spring stiffness values used in design
3. assessment of depth-to-fixity estimates for pipe piles

Finally, an assessment of corrosion-protection measures available for pipe pile construction has been included in the research project.

1.1 Hollow Tube Pile Bents (HTPB)

The hollow tube pile bent (HTPB) substructure is composed of steel tubes, typically spiral-weld tubes, driven to required bearing. The protruding length of the tubes is such that a bent cap may be poured directly on the tubes, which act as multi-post columns for lateral resistance. Historically, a top, reinforced-concrete plug, approximately 3 feet in length, has been included in the top of the piles as a connection to the reinforced concrete cap. Figure 1 shows typical details for the HTPB method of construction.

Design procedures for HTPB construction and the connection plug are varied and limited. The potential for in-ground hinging (not preferred, but permitted with Owner approval) during strong ground shaking is maximized for this method, given that the plug at the pile top creates the strongest point in the pile anywhere along its length. The lack of design criteria for the plug increases the possibility of plastic hinging at the bottom of the plug in the pile if the plug length is too small. Local buckling of the tube wall is problematic for HTPB construction unless very thick-walled pipe piles are employed. Since the cap soffit is the point of maximum moment in the piles, damage to the cap soffit must be precluded in the connection design procedures.

To summarize concerns for the HTPB method of substructure construction:

- maximum probability for in-ground-hinging
- potential for bottom-of-plug hinging rather than top-of-pile hinging
- design procedures and criteria have not been adequately established

- high potential for local buckling
- high potential for damage to the cap soffit

Of all construction methods, HTPB construction is by far the simplest to achieve in the field. This is the primary advantage of HTPB construction.

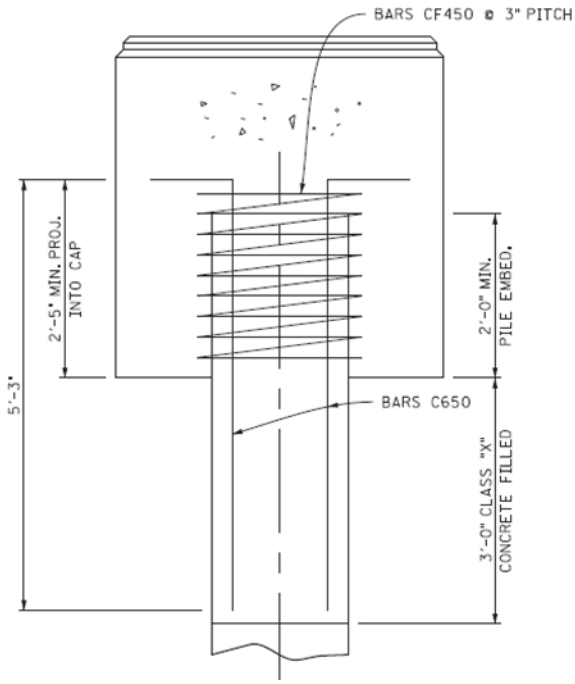

Figure 1. HTPB Plug Connection

1.2 Concrete-Filled Steel Tubes (CFST)

Concrete-filled steel tubes, with or without internal reinforcement, have been the subject of extensive research over the past 15 years or so. CFST construction would seem to have significant advantages over HTPB construction. Three methods of connection to the reinforced concrete cap have been suggested and studied in previous research by others:

(a) the U-bar connection (Figure 2)

(b) the annular ring connection (Figure 3)

(c) simple embedment of the tube into the cap.

Each of these connection methods has been proposed for this type of construction. The detail shown for the annular ring option is for use with a precast bent cap. For the more typical cast-in-place bent cap, the corrugated pipe and the grout would not be required. Figure 2 (Kappes L. R., 2016) depicts a typical CFST bent with the U-Bar connection. Figure 3 (Lehman & Roeder, 2012) shows the general configuration of the embedded annular ring connection.

With CFST construction, the internal concrete fill helps to preclude local buckling of the pipe wall. Hence, thinner tubes may be used in conjunction with CFST pile bents, compared to the HTPB counterpart.

CFST construction has been used extensively in building construction, and in bridge construction in other states (Washington, California). Design procedures and criteria are not well established in the AASHTO LRFD Bridge Design Specifications. It is imperative that the concrete fill extend below ground a distance greater than the expected in-ground point-of-fixity. Similar to the HTPB method, CFST construction does create the potential for damage to the cap soffit when the plastic moment develops at the top of the pile during strong ground shaking.

To summarize concerns with CFST construction:

- design procedures and criteria are not well established
- difficulty in achieving concrete fill to required distance below ground
- potential damage to cap soffit

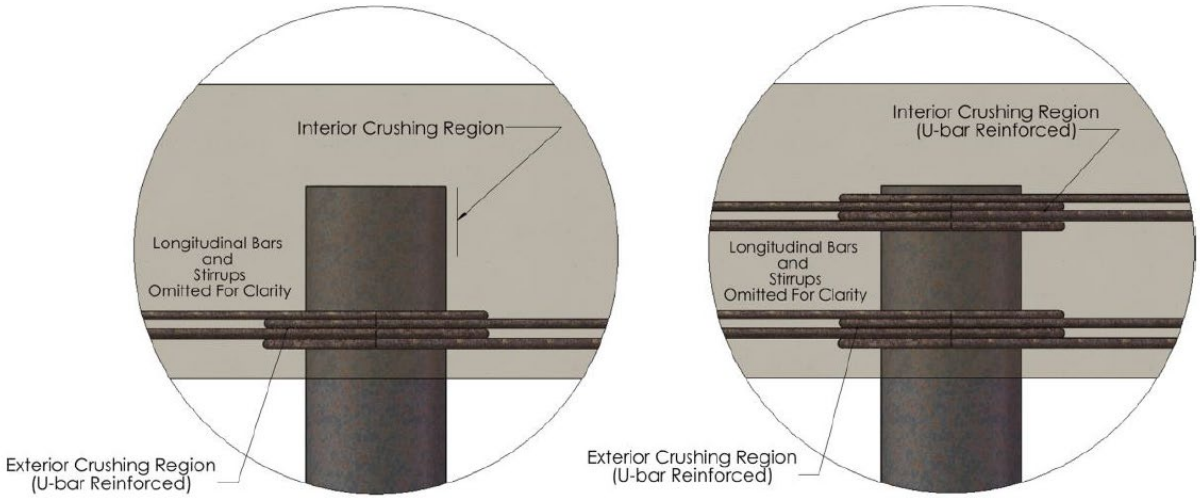

Figure 2. U-Bar Connection for CFST

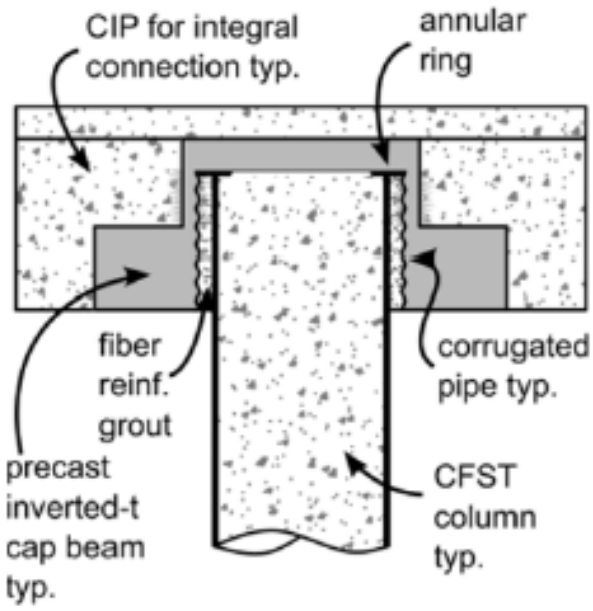

Figure 3. Embedded Ring Connection for CFST

1.3 Alaska Pile Bent / Reinforced Concrete Casing (RCFST)

A method of substructure construction which has been used successfully in the high-seismic-hazard state of Alaska is the RCFST construction method. A small gap of about 2 inches is left between the top of the piles and the cap soffit. This results in a reinforced-concrete circular cross-section, without the added strength of the steel tube, extending into the cast-in-place concrete cap. The top of the pile is the weakest point, but it highly ductile given the confining effect of the steel casing just below. The concrete fill helps to preclude local buckling of the in-ground portion of the pile. Figure 4 shows typical details for RCFST construction.

RCFST construction is likely the most difficult, among the three methods included in this study, to achieve in the field. A small tolerance would be permitted for the top gap at the soffit. Concerns with RCFST construction include:

- lack of historical use in Tennessee and surrounding states
- lack of codified design procedures and criteria
- difficult to achieve in the field

The RCFST method would seem to optimize the protection of the concrete cap and optimize the probability of avoiding in-ground hinging.

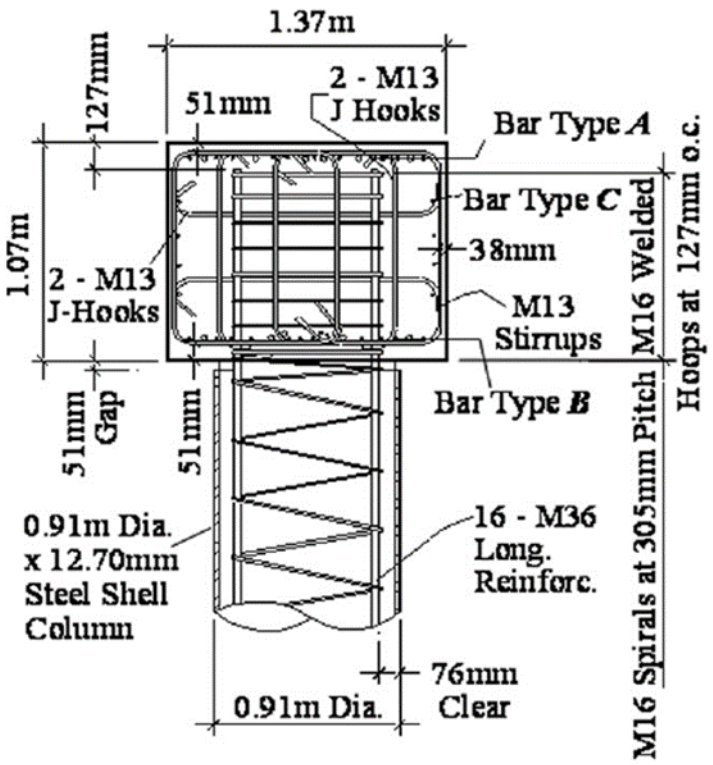

Figure 4. RCFST Pile Bent Construction

1.4 Geotechnical Issues for Pipe Pile Construction

This study serves, not only to propose uniform design methods and criteria for pipe pile supported bridges, but also to assess and possibly recommend changes to (a) point-of fixity estimates for in-ground hinging of pipe piles during strong ground shaking, (b) spring stiffness estimates used at the abutments for the seismic analysis of pipe-pile supported bridges, and (c) pile field installation procedures for pipe piles.

Point-of-fixity estimates are typically taken to be some multiple of the pile diameter, D. Values ranging from 2D to 5D have been proposed in the literature. For soils typically encountered in west Tennessee, the suitability of such estimates needs to be evaluated and, if possible, revised.

Spring stiffness of pile-supported integral abutments is needed to complete the seismic analysis and design of pile-supported bridges. Currently, the Tennessee Department of Transportation (TDOT) uses decades-old "generic" spring stiffness values ranging from 10 kips/inch per pile to 40 kips/inch per pile. One aim of this research project is to attempt a refinement of such spring stiffness estimates to provide more reliable design of west Tennessee, pile-supported bridge substructures.

TDOT currently adopts the Engineering News Record (ENR) formula to estimate pile resistance during driving in the field. The ENR method can be quite inaccurate. While TDOT does use field testing, either static load testing or dynamic analysis, to verify estimated pile resistance, it does

seem appropriate to examine the ENR formula and potential alternatives for field resistance estimates.

1.5 Corrosion Protection Measures for Pipe Pile Construction

Corrosion protection for pipe pile construction on TDOT projects currently consists of concrete collar construction over the pile length subject to wetting and drying. Figure 5, taken from TDOT Standard Drawing STD-5-2, depicts a typical detail for the collar.

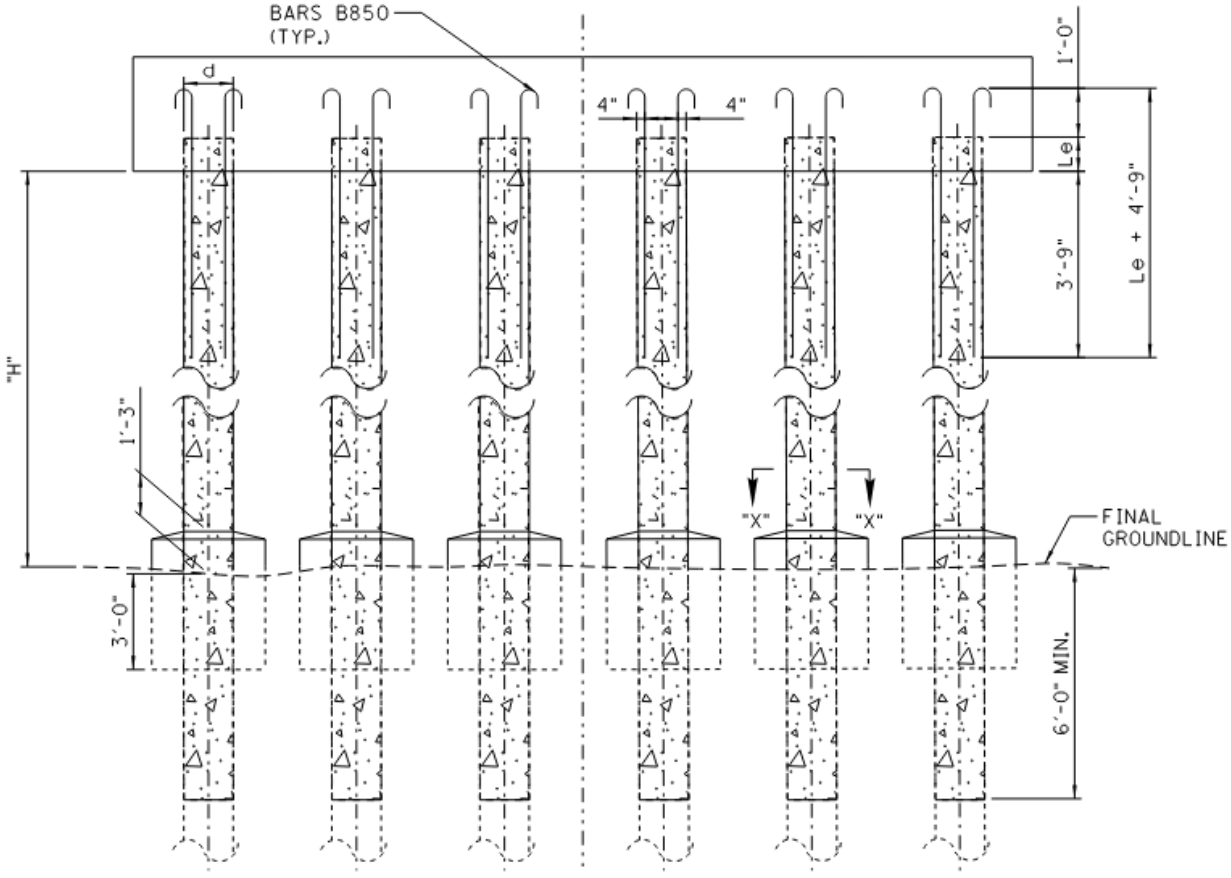

Figure 5. Concrete Collar Corrosion Protection

As part of the research project, alternative corrosion-protection measures have been investigated and conditions under which such alternative measures may be appropriate have been identified.

1.6 Organization of the Report

This report includes discussion of the methods used to establish best practices for bridges with pipe piles and details of the results in the following chapters.

Chapter 2 summarizes the findings from a literature review for current information relevant to the construction of bridges with pipe piles.

Chapter 3 details the details the methodology employed for this research including pushover analysis using fiber-based models. This methodology was used in conjunction with cantilever models to establish factors which may be applied to the yield displacement in order to obtain a lower bound estimate of ultimate displacement, or displacement capacity.

Also, models of pile bents are included to provide comparisons between the simplified cantilever-based displacement capacities and the more refined pile bent displacement capacities. Geotechnical analyses for depth-to-fixity and abutment spring constants are discussed as well.

Chapter 4 presents the results and discussion of each item covered in Chapter 3. Also included in Chapter 4 are discussions on field installation measures and corrosion protection measures.

Chapter 5 presents overall conclusions for the research project.

References are provided immediately after Chapter 5.

Appendix A summarizes the results of cantilever pushover analyses used to develop factors for the amplification of yield displacement to determine displacement capacity. The primary purpose of the analyses presented in Appendix A is to demonstrate that L_c, the distance from points of zero and maximum moment, has negligible effect on displacement capacity as long as slenderness effects are negligible.

Appendix B tabulates the final model for displacement capacity for CFST construction.

Appendix C tabulates the final model for displacement capacity for HTPB construction.

Appendix D includes a descriptive summary of all design examples.

Appendix E provides a description of capabilities for the Excel files generated over the course of the project.

Chapter 2 Literature Review

The literature review includes discussion on historical and current research for each of the five major subsections identified in Chapter 1.

1. HTPB Construction
2. CFST Construction
3. RCFST Construction
4. Geotechnical Issues
5. Corrosion Protection Measures

2.1 HTPB Construction

For hollow tube construction, one of the major concerns regarding extreme seismic loading is the potential for local buckling of the steel shell. A 2020 study (Sadowski, Wong, Li, Malaga-Chuquitaype, & Pachakis, 2020) from the ASCE Journal of structural Engineering recommended the strain-limit given in Equation 2.1-1 for pipe piles, provided the D/t (outside diameter-to-thickness) ratio is with the range of 20 to 60.

$$\varepsilon_s \leq \frac{0.40}{(D/t)^{1.02}} \tag{2.1-1}$$

While not specific to bridge construction, wharf design has historically included provisions for the use of pipe piles similar to those used in bridges. The Port of Long Beach (Port of Long Beach, 2021) includes strain limits as high as 0.035 for deep in-ground hinges in hollow tubes but requires that such tubes have a very restrictive slenderness (D/t no larger than $0.038E_s/F_y$).

While numerical procedures are typically used to perform the necessary cross-section analysis of ductile elements for strong ground shaking, closed form solutions have been developed for hollow, circular tubes. Equations 2.1-2 through 2.1-10 summarize the relationships among axial compression (P), bending moment (M), and neutral axis location (α), for hollow tubes developed by (Rotter & Sadowski, 2017). Equation 2.1-11 for ultimate curvature has been developed in RES2023-04 as a potential aid in moment-curvature analysis of hollow steel tubes. The angle, α, is varied between 0 and $\pi/2$ radians to develop an interaction relationship between P and M. The yield stress of the tube is F_y. R_{mid} is the tube radius to mid-thickness and ε_s is the limiting strain in the tube. Figure 6 defines the angle α.

$$P = P_{C1} + P_{C2} - P_{T1} \tag{2.1-2}$$

$$M = P_{T1}y_{T1} - P_{C1}y_{C1} + P_{C2}y_{C2} \tag{2.1-3}$$

$$P_i = F_y A_i \tag{2.1-4}$$

$$A_{T1} = \alpha D t \tag{2.1-5}$$

$$y_{T1} = D/\pi \tag{2.1-6}$$

$$A_{C1} = \left(\frac{\pi}{2} - \alpha\right) Dt \tag{2.1-7}$$

$$y_{C1} = \left(\frac{1 - \sin\alpha}{\pi - 2\alpha}\right) D \tag{2.1-8}$$

$$A_{C2} = \frac{\pi}{2} Dt \tag{2.1-9}$$

$$y_{C2} = D/\pi \tag{2.1-10}$$

$$\phi_u = \frac{\varepsilon_s}{R_{mid}\left(\frac{1}{2} + \cos\alpha\right)} \tag{2.1-11}$$

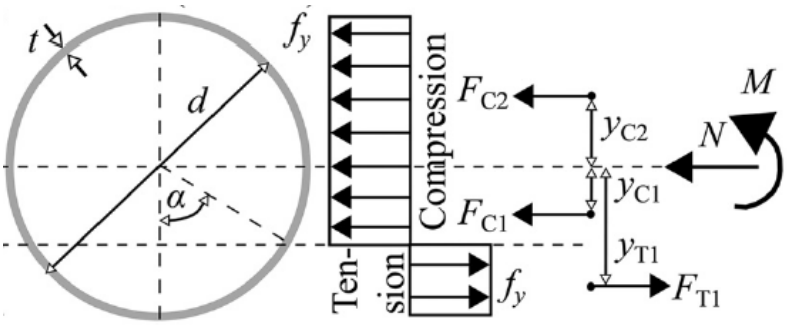

Figure 6. HTPB Cross Section Analysis (Rotter & Sadowski, 2017)

The AASHTO Guide Specifications for LRFD Seismic Bridge Design (LRFD-GS) (AASHTO, 2011) contain limited criteria for the design of hollow tubes. Section 7 of the LRFD-GS specifies that ductile pipe be ASTM A 53 Grade B with an expected yield stress equal to 1.5 times the specified yield stress, but the Commentary does permit other materials with Owner approval. Section 7 also requires stringent limits on D/t ratios for pipe. Equations 2.1-12 and 2.1-13 give the specified limits on D/t ratios for essentially elastic and ductile members, respectively. These limits appear to be among the most restrictive in modern design specifications.

$$\frac{D}{t} \leq \frac{0.09E}{F_y} \tag{2.1-12}$$

$$\frac{D}{t} \leq \frac{0.044E}{F_y} \tag{2.1-13}$$

Research conducted at Brigham Young University (Rollins & Stenlund, 2008) focused on the connection of hollow pipe piles to reinforced concrete caps. The stated goal of the study was to assess the feasibility of eliminating a reinforced connection at the top of the pile and relying on adequate embedment of the pile into the cap. Both filled and hollow pipe piles were studied. Twelve-inch diameter pipe piles were embedded into the cap distances ranging from 6 inches to 24 inches. Test 3 involved 12-inch diameter hollow tube embedment of 12 inches into a reinforced cap. Test 4 used concrete-filled 12-inch diameter pipe piles embedded 24 inches. The research team used previously developed equations to predict the moment capacity of an embedded pile. Equations 2.1-14 and 2.1-15 are two such equations. The width of the pile is b' and the eccentricity, e, is the distance from the point of zero moment in the pile to the center of effective embedment in the cap (actual embedment minus cover depth, c).

$$V_u = \frac{0.85 f_c' b' (L_e - c)}{1 + \frac{3.6e}{L_e - c}} \tag{2.1-14}$$

$$M_p = \frac{f_c' b' L_e^2}{6 + \frac{L_e}{L_e - c}} \tag{2.1-15}$$

Test 3 with the unfilled tube resulted in cracking of the concrete cap. Test 4 with a filled tube and 24-inch embedment was more favorable, with no damage to the cap. The moment capacity was predicted by multiplying the shear resistance from Equation 2.1-14 by the eccentricity, e. This was used to determine a development length needed to produce a connection with higher moment capacity than that of the pile. It is not clear from the BYU study whether the hollow tube would have performed more favorably had the increased 24-inch embedment been employed for Test 3.

Regarding displacement ductility capacity of hollow tubes, research (Fulmer, Kowalsky, & Nau, 2012) has shown that both spirally double submerged arc welded (DSAW) and single seam electric resistance welded (ERW) pipe piles with D/t ratios in the range of 32 to 55 can develop a reliable displacement ductility of 2. Also, for the range of D/t ratios studied, an average tensile strain ductility capacity of 4 prior to any local buckling was observed.

2.2 CFST Construction

Construction methods for CFST applications have been the subject of extensive study for the past 15 years or so. Mush of the research has focused on both strain limits for CFST and on design of the connection between the CFST and the cast-in-place or precast bent cap.

In the previous section on literature review related to hollow tube construction, it was pointed out that the testing at BYU (Rollins & Stenlund, 2008) revealed that a 12-inch diameter filled tube embedded 24 inches in a reinforced concrete cap performed well under lateral loading, relying only on embedment of the pile with no positive connection between the pile and the cap.

A recent NCHRP Report (Murphy, et al., 2020) posed possible future performance level requirements for steel tube strain at various performance goals. Equations 2.2-1, 2.2-2, and 2.2-3 give the possible recommendations for life safety, operational, and fully operational performance goals, respectively, regarding steel tube strains during strong ground shaking.

$$\varepsilon_s \leq 0.025 \tag{2.2-1}$$

$$\varepsilon_s \leq 0.021 - \frac{(D/t)}{9100} \geq \varepsilon_y \tag{2.2-2}$$

$$\varepsilon_s \leq \varepsilon_y \tag{2.2-3}$$

The Port of Long Beach (Port of Long Beach, 2021) strain limits for filled pipe piles at the in-ground hinge in wharf-type structures are significantly higher than those recommended in the NCHRP Report referenced above. POLB strain limits at the three performance goal levels are 0.035, 0.025, and 0.010. POLB strain limits are based on very restrictive D/t limits – $0.038E/F_y$ for hollow tubes and $0.076E/F_y$ for CFST.

CFST construction has been proven more resilient than reinforced concrete construction for certain ranges of materials and geometries (Stephens M. T., 2016). The study cited included CFST-to-cap connections of three types. The embedded ring connection (Figure 3) was found to be superior in terms of stiffness and strength, and comparable to the other two connection types with regard to energy dissipation during cyclic loading. While local buckling of the tube was observed at a drift of 4% during physical testing, such buckling had no detrimental effect on stiffness or moment resistance of the connection. Proposed design expressions were developed for the embedded ring connection for CFST into a reinforced concrete cap. Design provisions were reliant on a tube material specification corresponding to either ASTM 1018 or API 5L requirements. With stricter chemical composition requirements, API 5L tubes were reported to produce drift capacity of 8% prior to tube fracture, while ASTM 1018 tube drift capacity was estimated to be 6%.

The embedded, annular ring connection requires that the ring project a distance equal to 8 times the tube thickness, both into the tube and outside the tube. Either (a) complete joint penetration or (b) fillet welds are required for the ring-to-tube detail. With fillet welds, the minimum size weld is given here by Equation 2.2-4. The weld metal tensile strength is F_{EXX}, the tube tensile strength is F_{us}, and the tube thickness (and also the ring thickness) is t. The ring is to be of material having the same thickness and yield strength as those for the tube. Equation 2.2-5 gives the required embedment of the tube into the cap for the embedded ring connection. The coefficient, n, is 6 for seismic design criteria and 8 otherwise. The concrete strength of the cap, f'_c, must be in units of psi in Equation 2.2-5. To preclude punching through of the pile, the cap depth above the top of the ring, L_{pc}, must be no less than that given by Equation 2.2-6. Cap beam reinforcing must include horizontal bars capable of resisting $1.25M_p$ of the CFST. Vertical reinforcement in the cap beam must include a total area no less than 0.65 times the area of the steel tube and distributed around the CFST within a distance equal to $D/2+L_e$ from the tube center. Horizontal stirrup reinforcement having total area no less than 0.10 times the tube area is also required in the cap beam around the vertical stirrups. Equation 2.2-7 gives the analytical plastic hinge length recommended in the study by Stephens. Equation 2.2-8 gives the displacement capacity. The length, L, is the distance between points of zero and maximum

moment in the CFST. The study recommends an ultimate strain in the tube equal to $0.75\varepsilon_u$ to account for potential low-cycle fatigue.

$$w \geq \frac{1.31 F_{us} t}{F_{EXX}} \tag{2.2-4}$$

$$L_e = \sqrt{\frac{D_o^2}{4} + \frac{D t F_{us}}{n\sqrt{f_c'}}} - \frac{D_o}{2} \tag{2.2-5}$$

$$L_{pc} = \sqrt{\frac{D^2}{4} + \frac{C_c + C_s}{4\sqrt{f_c'}}} - \frac{D}{2} \tag{2.2-6}$$

$$l_p = 0.25D \tag{2.2-7}$$

$$\Delta_u = \Delta_y + (\phi_u - \phi_y) l_p \left(L - \frac{l_p}{2}\right) \tag{2.2-8}$$

The Washington State Department of Transportation Bridge Design Manual (Washington State Department of Transportation, 2022) includes the annular ring detail for CFST design. The WSDOT does permit the tube material to be API 5L, ASTM A 252 Grade 2 or 3, or ASTM A 572. When the CFST is expected to be ductile and develop plastic hinging, the tube is to be "fabricated from steel meeting the mechanical and chemistry requirements of AASHTO M 270 Grade 50" steel, regardless of fabrication method. WSDOT specifies an expected yield strength equal to 1.1 times the minimum specified yield strength. For elastically-responding CFST, WSDOT requires that the D/t ratio be no larger than $0.22E/F_{ys}$. For ductile CFST expected to form plastic hinges, D/t is not to exceed $0.15E/F_{ys}$. For effective stiffness, EI_{eff}, and nominal axial resistance in the absence of moment, P_o, Equations 2.2-9 and 2.2-10 are specified.

Axial load – moment interaction is defined by the relationships given here in Equations 2.2-11 through 2.2-16 for a given distance from the centroid to the neutral axis, y. The outer tube radius is r, the inner tube radius is r_i, and the radius to mid-thickness is r_m. A positive value for P denotes net compression. As an alternative to the equations, strain compatibility analysis may be employed to establish P-M interaction. Equation 2-.2-17 provides an expression for the shear resistance of CFST. In Equation 2.2-17, recommended values for the constants are g_1 = 2.0, g_2 = 0.50, g_3 = 3.0, and g_4 = 1.0. Approximately eight vent holes may be appropriate, based on details provided in the manual. Required embedment of the CFST into the cap in the WSDOT criteria is different from that in the Stephens study (presumably because the units on f'c are different in the two documents), and is given by Equation 2.2-18 when plastic hinging in the CFST is expected, or Equation 2.2-19 when elastically responding CFST is used. In the WSDOT equations, 2.2-18 and 2.2-19, f'_c is to be expressed in ksi. WSDOT recommends an analytical plastic hinge length equal to one diameter for tube fabricated from ASTM A 709 Grade 50 steel, with a reduced ultimate tensile strain equal to 0.13. Equation 2.2-20 gives the required total cap depth, h, necessary to prevent punching failure of the cap. $C_c + C_s$ is the combined compressive forces on the concrete and steel as computed from the plastic stress distribution

interaction equations. Note that $C_c + C_s$ is exactly equal to the applied axial load, P, plus the tensile force, T, on the cross-section.

$$EI_{eff} = E_s I_s + C^{'} E_c I_c \tag{2.2-9}$$

$$P_o = 0.95 f_c^{'} A_c + F_{ys} A_s \tag{2.2-10}$$

$$C^{'} = 0.15 + \frac{P}{P_o} + \frac{A_s}{A_s + A_c} \leq 0.90 \tag{2.2-11}$$

$$r_m = r - \frac{t}{2} \tag{2.2-12}$$

$$\theta = \sin^{-1}\left(\frac{y}{r_m}\right) \tag{2.2-13}$$

$$c = r_i \cos\theta \tag{2.2-14}$$

$$P_n = \left[\left(\frac{\pi}{2} - \theta\right) r_i^2 - yc\right](0.95 f_c^{'}) - 4\theta t r_m F_{ys} \tag{2.2-15}$$

$$M_n = \left[c\left(r_i^2 - y^2\right) - \frac{c^3}{3}\right](0.95 f_c^{'}) + 4ct\frac{r_m^2}{r_i} F_{ys} \tag{2.2-16}$$

$$\phi V_n = \phi g_4\left[g_1\left(0.6 F_{ys} g_2 A_s\right) + 0.0316 g_3 A_c \sqrt{f_c^{'}}\right] \tag{2.2-17}$$

$$L_e = \sqrt{\frac{D^2}{4} + \frac{5.27 D t F_{us}}{\sqrt{f_c^{'}}}} - \frac{D}{2} \tag{2.2-18}$$

$$L_e = \sqrt{\frac{D^2}{4} + \frac{3.95 D t F_{us}}{\sqrt{f_c^{'}}}} - \frac{D}{2} \tag{2.2-19}$$

$$h \geq \sqrt{\frac{D^2}{4} + \frac{1.68(C_c + C_s)}{\sqrt{f_c^{'}}}} - \frac{D}{2} \tag{2.2-20}$$

The WSDOT Bridge Design Manual requires 1" diameter vent holes in the annular ring to "ensure concrete consolidation under the annular ring". A minimum edge distance from the center of the tube to the edge of the concrete cap is to be no less than the diameter of the CFST. Vertical ties similar to those required in the Stephens study are required and are shown graphically in Figure 7. For reinforced concrete connections to a cap (longitudinal rebar cage wit headed bars in lieu of the annular ring) WSDOT also requires that a steel ring be welded to the inside of the steel tube 3 inches below the top of the tube, as shown in Figure 8. The ring need not be continuous but must have a total length no less than 75% of the tube circumference. The ring thickness should be no less than the thickness of the tube but need not exceed 1 inch.

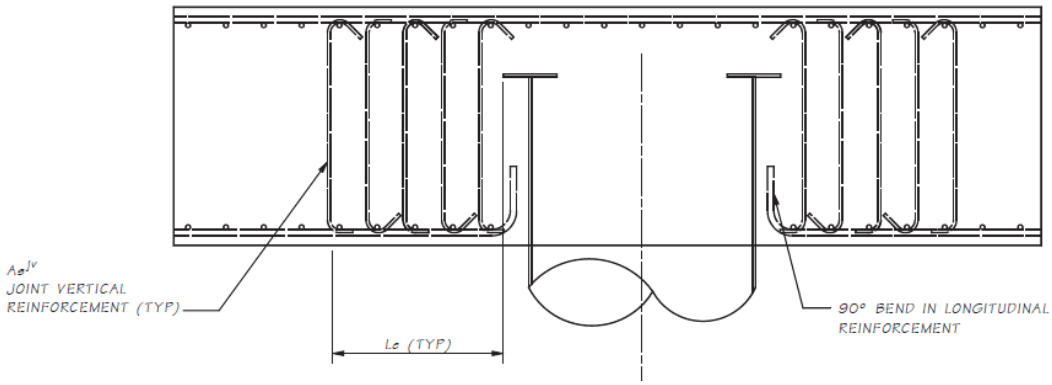

Figure 7. Vertical Ties in CFST Construction (Washington State Department of Transportation, 2022)

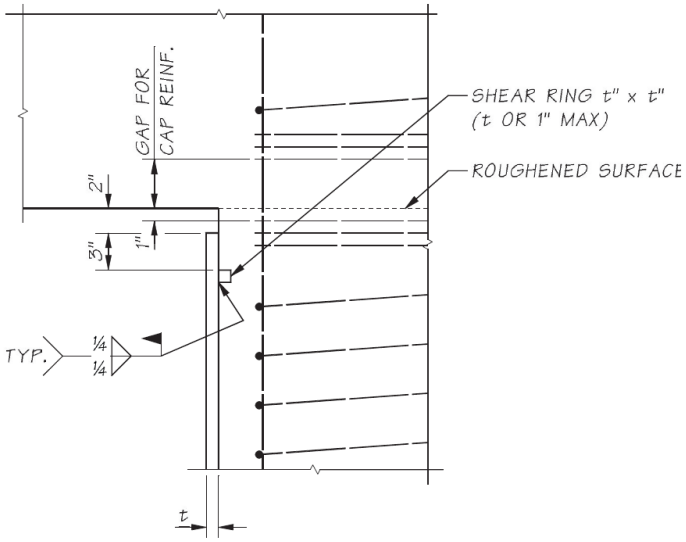

Figure 8. Inside Ring - CFST

Research sponsored by the Montana State Department of Transportation (Kappes L. R., 2016) recommended U-bar connection of CFST to the reinforced concrete cap. Figure 9 shows the arrangement of the proposed bars.

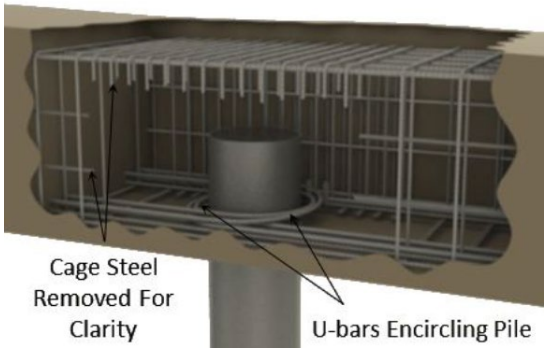

Figure 9. U-Bar Connection Option

The Montana DOT research program identified the importance of (a) adequate embedment and (b) U-bar design criteria. Physical testing from previous research (Stephens & McKittrick, 2005) was combined with new physical testing to develop design guidelines for such connections. The U-bar connection relies on the U-bars to protect the cap. Equation 2.2-21 gives the required embedment of the CFST into the cap as reported in the Montana DOT-sponsored project. The resistance factor, ϕ_b, was recommended to be taken equal to 0.70. The stress block depth, β_1, is 0.85 for concrete strengths up to f'_c = 10 ksi. The factor, a, is intended to account for amplification of the concrete strength in the confined connection region and a value of 1.8 is recommended in the report. The design moment, M_u, is the overstrength plastic moment of the CFST section having diameter, D. Equation 2.2-22 gives the required total area of U-bars, with specified yield stress f_y, in the connection. Transverse reinforcement in the cap around the CFST region was recommended to be taken from the AASHTO LRFD-BDS (AASHTO, 2020) (5.11.4.1.4) as shown in Equations 2.2-23 and 2.2-24 (for a rectangular cap cross-section), with the larger value controlling the required transverse reinforcement. The reinforcement should extend a distance equal to one-half the cap depth beyond the pile in each direction and the maximum spacing, s, should not exceed 4 inches. Given that the requirement for the transverse reinforcement by Equations 2.2-23 and 2.2-24 is for columns expected to experience plastic hinging, it is uncertain why this was recommended for a cap beam intended to remain elastic. In fact, the report stated that "further research is required to more fully characterize this behavior and further develop the proposed design methodology". Figure 10 shows a conceptual cross-section for the U-bar connection scheme.

$$L_e = \sqrt{\frac{2M_u}{D\beta_1\left(1-\frac{\beta_1}{2}\right)\phi_b\alpha f_c^{'}}} \tag{2.2-21}$$

$$A_{u-bars} = \frac{0.3M_u}{L_e\left(1-\frac{\beta_1}{2}\right)f_y} \tag{2.2-22}$$

$$A_{sh} = 0.3sh_c\frac{f_c^{'}}{f_y}\left(\frac{A_g}{A_c}-1\right) \tag{2.2-23}$$

$$A_{sh} = 0.12sh_c \frac{f_c^{'}}{f_y} \quad (2.2\text{-}24)$$

The tubes used in the Montana research program were 219 mm in diameter with wall thickness equal to 6.35 mm and 8.10 mm for the experiments. This results in a D/t ratio of 27-34. There are no tubes locally available in Tennessee with such low D/t ratios. Since the Montana experimental program with U-Bar connections was limited to extremely low D/t ratios, the concept is not recommended for use in Tennessee at this time.

Marcakis & Mitchell (1980) proposed ensuring adequate embedment of the tube into the cap to enable the tube moment to be carried by side couples of bearing forces against the tube-cap interface. The study included a recommendation of filling the tube with concrete to prevent local buckling of the tube wall when the bearing forces develop. Adequately embedded members with no reinforcement behaved in a ductile manner upon lateral testing. The study included a proposed connection capacity given by Equation 2.1-14, which was also reported in (Rollins & Stenlund, 2008).

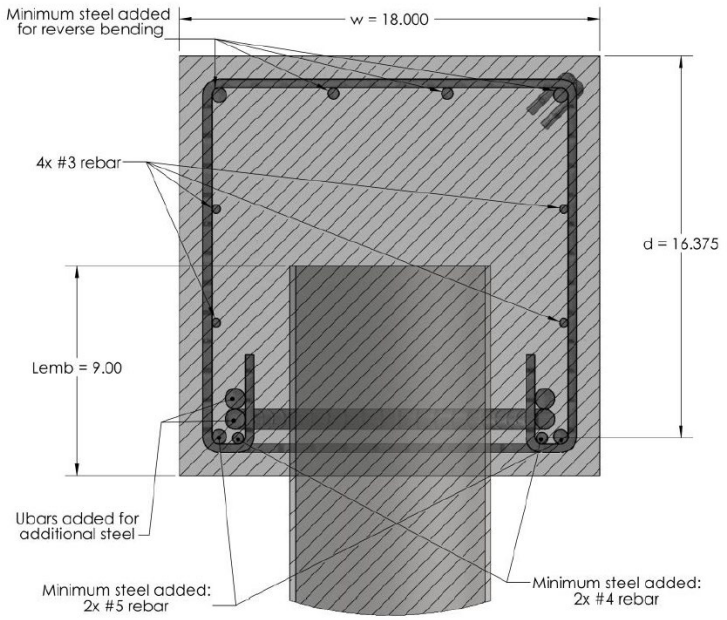

Figure 10. Cap Cross-Section with U-Bars

The U-bar connection does seem to have merit. However, the fact remains that the authors of the U-bar connection strategy do suggest that further research is required in order to fully develop the U-bar connection design in practice.

Regarding minimum cap dimensions, a width no less than two times the outside diameter of the CFST has been recommended (Roeder, Stephens, & Lehman, 2018). This paper also pointed

out that CFST is advantageous over RCFST construction since the latter is more flexible and weaker. In the opinion of the ***RES2023-04*** research team, this is not necessarily a disadvantage where seismic resistance is concerned.

2.3 RCFST Construction

One of the first studies into the feasibility of RCFST construction was conducted for the Alaska Department of Transportation and Public Facilities (Silva & Seible, 1999). Recall that, for purposes of project ***RES2023-04***, RCFST construction refers to a pile bent with a 2-inch gap between the top of the piles and the bottom of the cap, resulting in a short reinforced-concrete section at the top of the piles. Ductile seismic response of RCFST construction was verified in the study. Related research (Silva P. F., Srithiran, Seible, & Priestley, 1999) produced both additional physical testing and a design methodology for RCFST construction. Some of the design considerations for RCFST construction include:

- The cap beam width should be no less than 1.5 times the diameter of the RCFST.
- The cap beam depth should be large enough to permit straight bar development of the RCFST longitudinal reinforcement into the cap. The required development for a bar of diameter d_{bl} and expected yield stress f_{ye} is given in the AASHTO Guide Specification for LRFD Seismic Bridge Design (AASHTO, 2011) (AASHTO-GS) and is given here as Equation 2.3-1.
- A column reinforcement ratio, ρ_l, of no more than 4% was recommended
- Confinement reinforcement in the plastic hinge region at the top of the piles was recommended to be determined in accordance with Equation 2.3-2. The steel shell may be relied upon to provide the confinement.
- A displacement ductility of 8 was obtained for physical tests. The AASHTO-GS limits displacement ductility to no more than 6.
- A two-inch gap between the top of the pile and the cap beam soffit precluded damage to the cap.
- The UCSD shear model was used for the columns and the cap beam. For the RCFST construction tested, special shear reinforcement “will not generally be required” in the columns.
- Cap beam reinforcement should be sufficient to remain elastic even when accounting for strain hardening and expected yield levels in the column longitudinal reinforcing.
- At least 75% of the bottom cap beam reinforcing should be continuous through the column region. This may be accomplished using side bars in the cap.
- Cap beam depth should be in the range of D to (D + 6 inches).
- While the report did recommend joint design procedures, it would seem appropriate to adopt the more current methods available in AASHTO. Joint principal stresses should be evaluated in accordance with the AASHTO-GS, Section 8.13.
- Concrete fill in the pipe piles should extend beyond the in-ground hinge to a depth where the moment is less than 50% of the steel shell yield moment. This is to prevent local buckling in regions where concrete fill below grade has been terminated.
- A maximum displacement ductility of 4 is recommended for design.

$$l_{ac} = \frac{0.79 d_{bl} f_{ye}}{\sqrt{f_c'}} \quad (2.3\text{-}1)$$

$$\rho_s = \frac{4A_{sp}}{D's} = 0.16 \frac{f_{ce}'}{f_{ye}} \left(0.5 + \frac{1.25P}{f_{ce}' A_g} \right) + 0.13(\rho_l - 0.01) \quad (2.3\text{-}2)$$

Figure 11 depicts an example for RCFST construction from the Gakona River Bridge in Alaska. One distinctive feature of RCFST construction lies in the large discrepancy between plastic moments for the top hinge (reinforced concrete section highly confined by the tube) and the in-ground hinge (steel tube with concrete fill). The in-ground hinge will typically have a much larger plastic moment capacity. This means that the top hinge will likely undergo several inelastic cycles while the in-ground structure remains elastic during strong ground shaking.

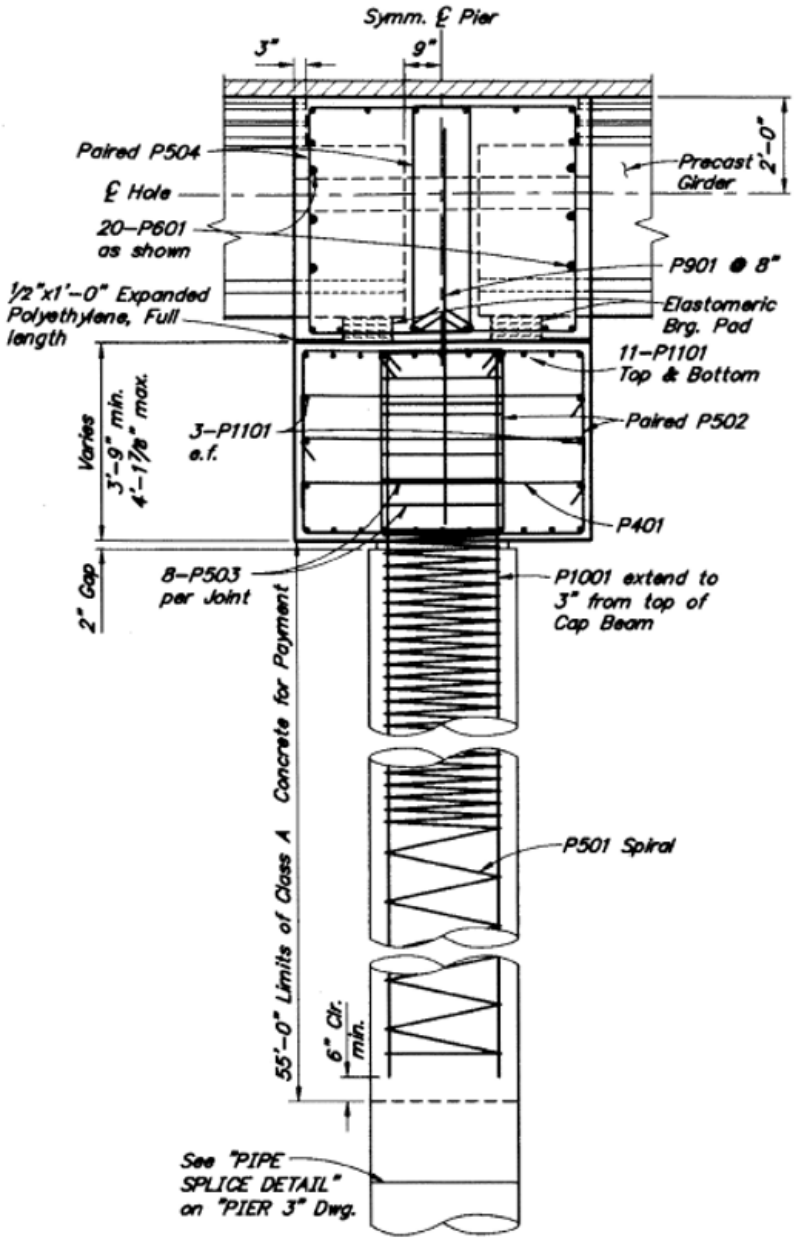

Figure 11. RCFST Pile Detail for the Gakona River Bridge

2.4 Geotechnical Issues

TDOT currently estimates pile stiffness under lateral loading to be in the range of 10-40 kips per inch per pile, based on un-published recommendations from the early 2000's. As noted in the literature, simple methods for the analysis of piles subjected to lateral loading do exist and may be useful for the refinement of assumed values in design.

Broms' method is applicable for lateral analysis of a single pile in either purely cohesive or purely cohesionless soil profiles. Hannigan outlines the method on pages 9-86 through 9-100 in the Reference Manual for NHI Course Nos. 132021 and 132022 (Hannigan, Goble, Likins, & Rausche,

2006). The Broms method is typically appropriate for relatively short piles that rotate near base rather than developing fixity.

For multi-layered soil profiles, the Reese Method, also known as the LPILE method or p-y analysis, is generally recommended. The Reference Manual for the NHI course provides representative values of the required input parameters for both clays and sands. The Manual also provides a step-by-step procedure (pages 9-100 through 9-115) whereby the method may be applied (Hannigan, Goble, Likins, & Rausche, 2006). The numerical p-y approach is the state-of-practice in much of the geotechnical community. The Characteristic Load Method (Duncan, Evans, and Ooi, 1994) provides a closed-form analytical approach based on p-y analyses of many pile sizes and soil conditions.

Pile groups may behave differently from single piles, and such effects may be evaluated using the procedure outlined on pages 9-154 through 9-156 of the NHI Reference Manual (Hannigan, Goble, Likins, & Rausche, 2006).

In addition to stiffness considerations, the matter of depth to fixity for pile bent construction is important. TDOT currently uses 3 to 5 pile diameters below the ground for the estimated depth to fixity, as may be inferred form Figure 4.29, page 215, of Priestley's landmark book on seismic bridge design (Priestley, Seible, & Calvi, 1996).

The AASHTO LRFD Bridge Design Specifications do provide depth-to-fixity equations for preliminary design, and these may be useful in enhancing TDOT analytical procedure for the modeling of pile bents. The Commentary to Section 10.7.3.13.4 provides equations for depth-to-fixity for both sands and clays.

2.5 Corrosion Protection Measures

The LRFD-BDS in Article 10.7.5 provides guidance on corrosion protection measures when required. Consideration of steel pile corrosion is required whenever any of the following conditions are met in soil.

- resistivity less than 2,000 ohm-cm,
- pH less than 5.5,
- pH between 5.5 and 8.5 in soils with high organic content,
- sulfate concentrations greater than 1,000 ppm,
- landfills and cinder fills,
- soils subject to mine or industrial drainage,
- areas with a mixture of high resistivity soils and low resistivity high alkaline soils

For piles in water crossings the following conditions are identified as potentially problematic regarding corrosion.

- chloride content greater than 500 ppm.
- sulfate concentration greater than 500 ppm,
- mine or industrial runoff,
- high organic content,
- pH less than 5.5,

- marine borders, and
- piles exposed to wet/dry cycles.

Several methods, including protective coatings, concrete encasement, cathodic protection, use of special steel alloys, or increased steel area have been suggested for the protection of steel piling when corrosive environments are encountered.

One means of providing corrosion protection is to use galvanized pipe piles. The North Carolina Department of Transportation has developed pipe pile standards which include galvanizing of all pipe piles. The NCDOT standards include details for a top plug similar to the TDOT standard plug. The NCDOT Standard Drawings may be found at the link below.

https://connect.ncdot.gov/resources/Structures/Pages/Structure-Standards.aspx

Another method to mitigate the possible effects of corrosion is to include an allowance in thickness reduction of the steel tube. The WSDOT specifies corrosion allowance rates as shown in Table 1. Definitions of the various zones follow Table 1.

Table 1. WSDOT Corrosion Allowance Rate for Steel Piling

Location	Marine or Non-Marine: Corrosive Environment	Non-Marine: Non-Corrosive Environment
Undisturbed Soil	0.00100 inches per year	0.00050 inches per year
Disturbed Soil or Fill	0.00150 inches per year	0.00075 inches per year
Immersed Zone	0.00300 inches per year	0.00150 inches per year
Tidal Zone	0.00400 inches per year	---
Splash Zone	0.00600 inches per year	---
Atmospheric	0.00200 inches per year	0.00100 inches per year

- Marine – a site is considered a marine environment if the structure is less than 1000 feet measured from the surface or edge of salt or brackish water. Water shall be considered brackish if the chloride concentration is measured at 500 ppm or greater measured at mean tide level or higher.

- Non-Marine: Corrosive – a non-marine site is greater than 1000 feet from salt or brackish water and is considered corrosive if one or more of the following conditions exist based on representative soil and/or water samples:
    1. The chloride concentration is 500 ppm or greater,
    2. The sulfate concentration is 1500 ppm or greater,
    3. The pH is 5.5 or less.

If none of the following conditions exist, the site is considered non-marine: noncorrosive.

- Immersed zone – portion of structural steel element which is continuously immersed or submerged in water. Immersed non-marine: non-corrosive are environments with fresh water or are tested and found not to meet the marine or non-marine: corrosive values.

- Tidal zone – portion of structural steel element in a marine environment between the Mean Lower Low Water (MLLW) and the Mean High Water (MHW) based on the MLLW Datum.

- Splash zone – portion of structural steel element in a marine environment located above the MHW plus five additional feet or as otherwise determined for a specific site.

- Atmospheric - portion of structural steel element above the splash zone or above ground line as applicable.

The Oregon Department of Transportation Bridge Design Manual (Oregon Department of Transportation, 2020) specifies the following as viable corrosion protection measures where required:

- protective coatings: 3-coat system consisting of a zinc-rich primer followed by two coats of cured urethane/urethane-tar
- protective coatings: 4-coat system similar to the 3-coat system but with a top coat
- cathodic protection in conformance with NACE Standard SP0169, requiring regular inspection and maintenance to replace anodes

The Oregon BDM also notes that any corrosion allowance for pipe piles need be applied to the exterior of the pile only, since the interior surface is not exposed to sufficient oxygen to support the corrosion process. For non-marine environments with soil resistivity greater than 2000 ohm-cm and soil pH greater than 5.5, no further evaluation is required by the Oregon DOT and the piling is designed with the following sacrificial thickness values:

- Undisturbed soil: 0.001 inches/year
- Fill or disturbed soil: 0.003 inches/year
- immersed zone (fresh water): 0.002 inches/year

Early research into the corrosion resistance of piling identified the superiority of carbon steel with no less than 0.2% copper.

Such steels have been reported to have corrosion resistance equal to twice that of steels having only 0.01 to 0.02% residual copper. Tests have shown that nickel, chromium, silicon, and phosphorous each are beneficial with regard to corrosion resistance. The ***AISC Steel Structures Design Handbook*** – Volume 1 (AISC, 1986) summarizes in greater detail some of these findings.

The primary concern with piling regarding corrosion potential is in marine environments. According to the same AISC handbook (AISC, 1986), "Generally, steel piles driven into undisturbed soil are not affected by corrosion and therefore no special protection is required." (See Page 7/73 in Chapter 10).

A good summary of potential corrosion problems in piling is provided in a whitepaper by the Pile Driving Contractors Association (2012).

2.6 Summary of Advantages and Disadvantages for Pile Bent Construction

The predominant advantages and disadvantages for each of the three types of construction studied in this project are noted here.

HTPB Construction – Positives and Negatives

- Positive: Reinforcement is required only in the top plug.
- Positive: The HTPB method is the least restrictive with regard to construction requirements for proper installation.
- Negative: Extremely thick tubes are required (D/t no more than $0.044E/F_y$; D/t no more than 36 for F_y = 35 ksi and no more than 25 for F_y = 50 ksi). For F_y = 50 ksi or higher, tubes of the required thickness are not readily available.
- Negative: This is the least ductile of the three methods studied.
- Negative: The concept has never been experimentally verified.

CFST Construction – Positives and Negatives

- Positive: No internal reinforcement is required. Even the top connection requires no reinforcement, only an embedded annular ring at the top of the tube.
- Positive: The flexural resistance is constant throughout the length of the tube. The top and in-ground hinges have similar, if not identical plastic moments. This produces a substructure with the most predictable response. The response has been proven to be ductile in past studies by multiple researchers.
- Positive: Tube D/t ratio may be much higher than that required for HTPB and RCFST construction. For CFST, D/t shall be limited to $0.15E/F_y$.
- Negative: The top connection is strong and stiff, which is disadvantageous with regard to capacity protection of the cap. Cap designs with CFST are likely to be more substantial than those required for RCFST construction.

RCFST Construction – Positives and Negatives

- Positive: With a gap at the top of the pile, this method provides for the most advantageous protection of the cap.
- Positive: The required cap width is no less than 1.5 times the diameter of the tubes, whereas CFST and HTPB construction require a cap width no less than 2 times the tube diameter.
- Positive: The method has been proven in multiple studies and is widely used in Alaska, a state with high seismic hazard.
- Negative: This is the most restrictive method with regard to construction requirements related to the required gap between the top of the tubes and the bottom of the cap.

- Negative: A reinforcing cage is required for the entire length of the tube, extending into the cap, and extending a significant distance beyond the in-ground plastic hinge location.
- Negative: This provides the weakest flexural resistance at the cap interface and thus, may have a significant impact on design for non-seismic forces.
- Negative: This provides the weakest shear resistance at the cap interface and it may be difficult to resist the plastic shear.

Chapter 3 Methodology

3.0 Pushover Analyses

Separate pushover analyses were carried out. First, a series of fiber-based cantilever models were used to estimate the ratio of ultimate displacement to first-yield displacement for a range of parameters. Secondly, full 2D pushover analyses of bridge bents were completed to compare results thusly obtained to those from the simplified models.

The rationale is to use results from the simplified models in routine bridge design and resort to the more detailed models when warranted.

3.1 Fiber-Based Cantilever Pushover Models

A series of simple pushover analyses was completed to identify approximate ratios of ultimate displacement to displacement at first yield. Cantilever fiber-based models were employed and three yield stress levels were included – F_y = 35 ksi, F_y = 52.5 ksi, and F_y = 80 ksi. Two axial load levels were included as well – P_u = 0 and P_u = 0.25 x 35 ksi x A_s. The upper-level axial load was selected based on an assumed maximum driving load equal to 25% of the yield load. Hollow tubes (HTPB) ranging from 12” x 0.375” up to 36” x 1.000” and CFST elements ranging from 12” x 0.375” up to 30” x 0.500” were included.

Post-yield stiffness (stress-strain-based) was taken equal to 0.005 for CFST models and 0.00005 for hollow tube models. The rationale behind this is the anticipated strain limits used. Hollow tube strain limits are lower than CFST strain limits, and it is not expected that hollow tubes will experience significant strain hardening before the strain limit is reached. CFTS elements have higher strain limits with some moderate strain hardening expected (though still well below the strain at ultimate tensile strength).

Figure 12 depicts a sample model in SeismoStruct in part (a) with the associated load deflection curve in part (b) of the figure.

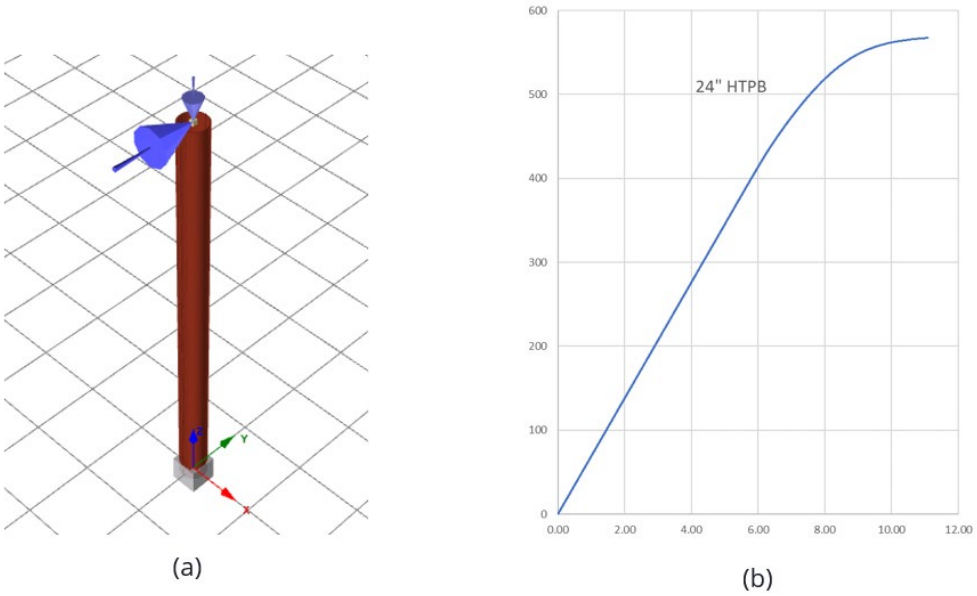

Figure 12. 24-inch HTP (a) Model and (b) Response Curve

P-Delta effects were excluded from the analyses since the AASHTO Guide Specification for LRFD Seismic Bridge Design treats these effects with separate checks.

Cantilever heights, L_c, were varied from 4 feet up to 30 feet. Note that for rigid frame behavior (typical for transverse response), twice the displacement corresponding to a value for L_c equal to one-half of the clear height would be appropriate in estimating displacement capacities.

Strain limits for HTPB elements were determined from Equation 3.1-1 (Sadowski, Wong, Li, Malaga-Chuquitaype, & Pachakis, 2020). This expression was found to be slightly more conservative than that reported elsewhere in the literature (Fulmer, Kowalsky, & Nau, 2012) (Port of Long Beach, 2021). Fulmer's model for critical strain is given here in Equation 3.1-2. Figure 13 provides a comparison between two of the models. Strain limits for CFST tubes were taken equal to 0.025 (Murphy, et al., 2020).

$$\varepsilon_{cr} = \frac{0.40}{\left(D/t\right)^{1.02}} \tag{3.1-1}$$

$$\varepsilon_{cr} = \frac{0.69018}{\left(D/t\right)^{1.0893}} \tag{3.1-2}$$

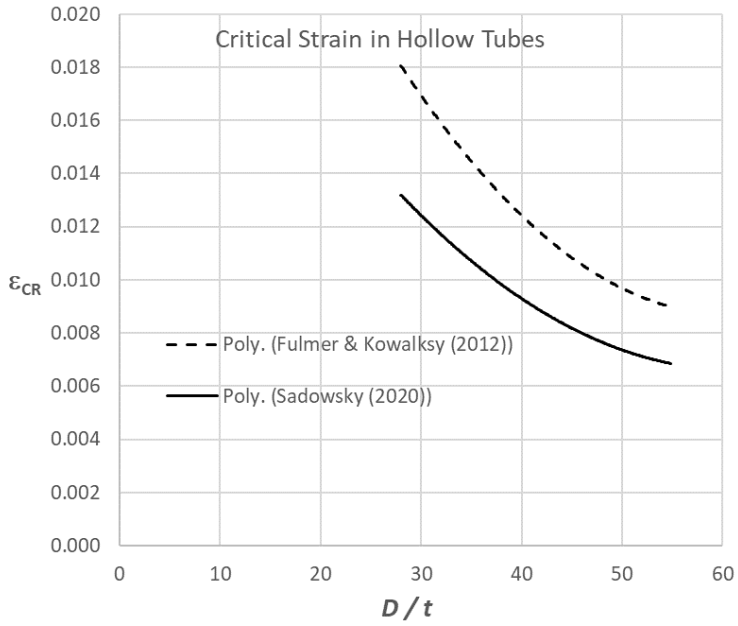

Figure 13. Critical Strain in Hollow Tubes

Table 2 and Table 3 summarize preliminary results from nonlinear analyses using fiber-based models with the strain limits specified. The final column in each row is the average from 10 analyses for various L_c – values. Very little variation in the displacement ratio was observed for a given member as the height was varied.

The recommended method for simplified displacement capacity calculation is the estimate the displacement at first yield using the material properties of the tube alone with no axial load, and multiply by the corresponding tabulated value to obtain the ultimate displacement.

No data is provided for HTPB for yield stress values other than 35 ksi. It is not recommended that HTPB construction be used for yield values larger than 35 ksi.

Figure 14 and Figure 15 depict curve-fitting results for CFST and HTPB respectively.

Table 2. HTPB Ultimate Displacements (P_u = 0, F_y = 35 ksi)

Type	D inches	t inches	D/t	F_y - based $k_\Delta = \Delta_u / \Delta_{y1}$	F_{yE} - based $k_\Delta = \Delta_u / \Delta_{y1}$
HTPB	12	0.375	32.00	2.046	1.799
HTPB	14	0.500	28.00	2.158	1.879
HTPB	16	0.500	32.00	2.042	1.797
HTPB	18	0.500	36.00	1.953	1.734
HTPB	20	0.625	32.00	2.042	1.798

HTPB	24	0.750	32.00	2.042	1.797
HTPB	30	1.000	30.00	2.097	1.835
HTPB	36	1.000	36.00	1.951	1.734

Table 3. CFST Ultimate Displacements (P_u = 0, F_{y1} = 35 ksi, F_{y2} = 52.5 ksi, F_{y3} = 80 ksi)

Type	D, inches	t, inches	D/t	F_{y1} - based $k_\Delta = \Delta_u / \Delta_{y1}$	F_{y2} - based $k_\Delta = \Delta_u / \Delta_{y1}$	F_{y3} - based $k_\Delta = \Delta_u / \Delta_{y1}$
CFST12-0203	12	0.203	59.1	2.788	2.147	1.785
CFST12-0219	12	0.219	54.8	2.804	2.165	1.803
CFST12-0250	12	0.250	48.0	2.829	2.196	1.826
CFST12-0312	12	0.312	38.5	2.916	2.258	1.876
CFST12-0375	12	0.375	32.0	2.977	2.312	1.917
CFST14-0219	14	0.219	63.9	2.777	2.132	1.771
CFST14-0250	14	0.250	56.0	2.799	2.159	1.797
CFST14-0312	14	0.312	44.9	2.849	2.214	1.840
CFST14-0375	14	0.375	37.3	2.925	2.267	1.882
CFST14-0500	14	0.500	28.0	3.037	2.355	1.956
CFST16-0250	16	0.250	64.0	2.777	2.132	1.770
CFST16-0312	16	0.312	51.3	2.816	2.180	1.813
CFST16-0375	16	0.375	42.7	2.870	2.228	1.849
CFST16-0500	16	0.500	32.0	2.976	2.313	1.921
CFST18-0250	18	0.250	72.0	2.751	2.112	1.754
CFST18-0312	18	0.312	57.7	2.793	2.152	1.794
CFST18-0375	18	0.375	48.0	2.828	2.196	1.828
CFST18-0500	18	0.500	36.0	2.936	2.278	1.890
CFST20-0312	20	0.312	64.1	2.774	2.130	1.767
CFST20-0375	20	0.375	53.3	2.809	2.170	1.805
CFST20-0500	20	0.500	40.0	2.897	2.245	1.865
CFST20-0625	20	0.625	32.0	2.976	2.312	1.918
CFST24-0375	24	0.375	64.0	2.776	2.132	1.767
CFST24-0500	24	0.500	48.0	2.828	2.196	1.822
CFST24-0625	24	0.625	38.4	2.915	2.258	1.876
CFST24-0750	24	0.750	32.0	2.977	2.312	1.921
CFST30-0500	30	0.500	60.0	2.786	2.142	1.779
CFST30-0625	30	0.625	48.0	2.828	2.196	1.824
CFST30-0750	30	0.750	40.0	2.895	2.246	1.869
CFST30-1000	30	1.000	30.0	3.011	2.334	1.937
CFST36-0500	36	0.500	72.0	2.750	2.111	1.754
CFST36-0625	36	0.625	57.6	2.793	2.152	1.794
CFST36-0750	36	0.750	48.0	2.828	2.196	1.822
CFST36-1000	36	1.000	36.0	2.936	2.277	1.890

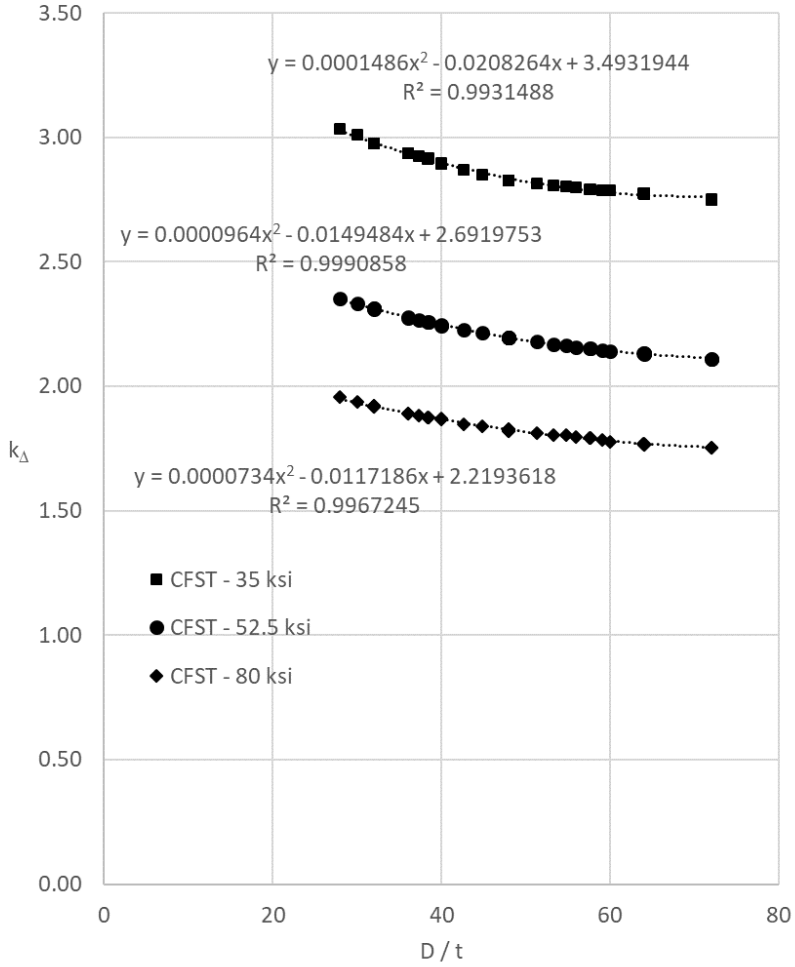

Figure 14. CFST Displacement Ratios

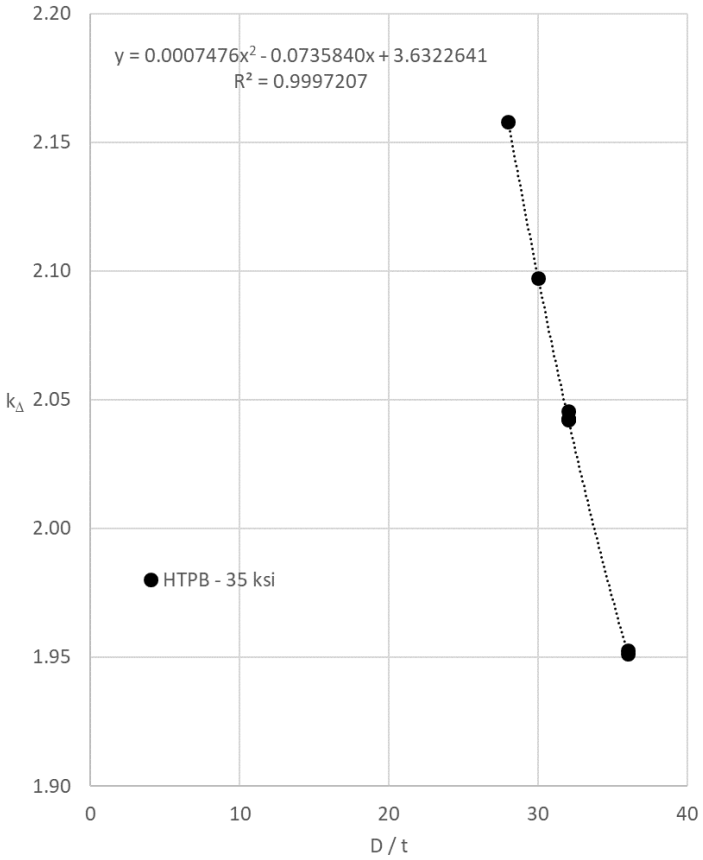

Figure 15. HTPB Displacement Ratios

3.2 2D Bridge Bent Pushover Analyses

In order to compare results from hand calculations to those obtained from pushover analyses using SeismoStruct fiber-based elements with appropriate strain limits, several models of bridge bents were completed. This chapter summarizes the results of those analyses.

In design Example No. 1, CFST construction was adopted using 14" x 0.500" tubes with F_y = 35 ksi and F_{yE} = 52.5 ksi. The proposed bent is shown in Figure 16.

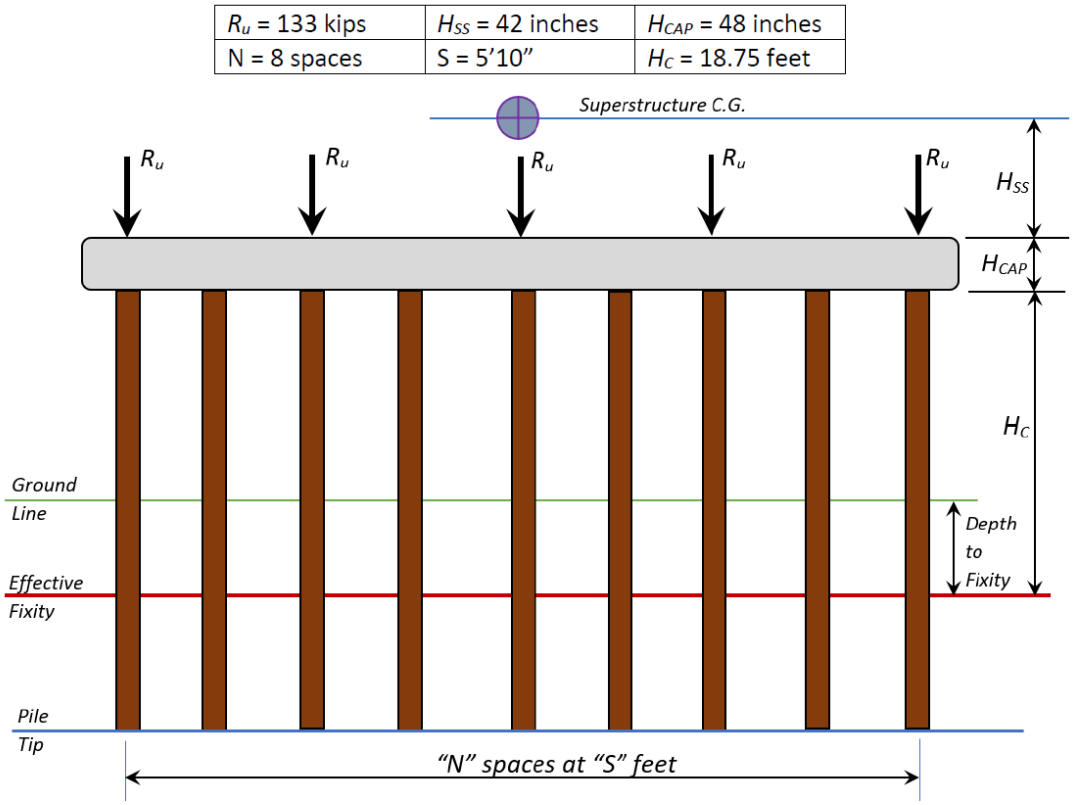

Figure 16. Bridge Bent for Design Example No. 01

- Hand calculated transverse displacement capacity = 5.92 inches
- SeismoStruct transverse displacement capacity = 9.31 inches

For this example, the hand-calculated displacement capacity was considerably less than the presumably more accurate value from SeismoStruct. The tubes for this example are somewhat slender. The SeismoStruct pushover curve is shown in Figure 17.

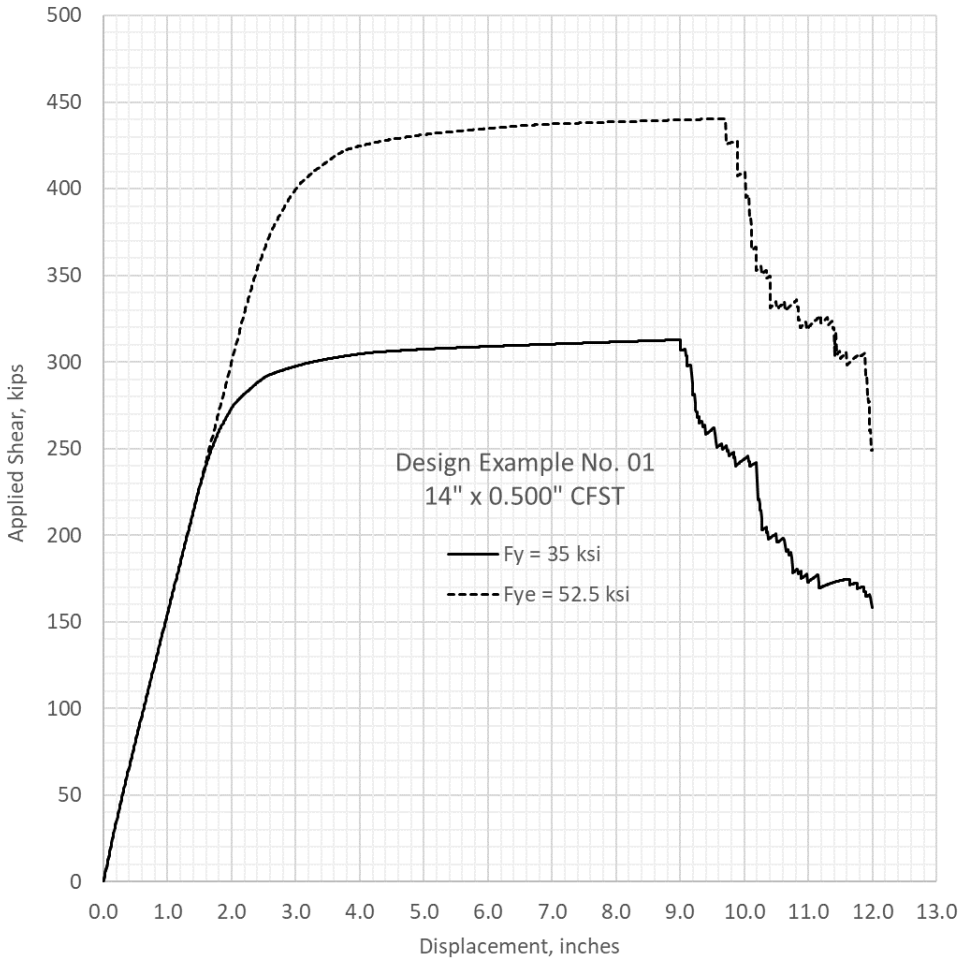

Figure 17. Pushover Curve for Design Example No. 01

In Design Example No. 02, both hand-calculated and rigorous, fiber-based SeismoStruct model transverse displacement capacities were determined for bents resembling that shown in Figure 16, but having different bent heights. Tubes used in the example are 20" x 0.625" with F_y = 35 ksi and F_{yE} = 52.5 ksi. HTPB construction was specified for Design Example No. 02, so the top hinge is CFST while the in-ground hinge is a hollow tube.

Table 4 summarizes the results of Design Example No. 02 for transverse displacement capacity. Once again, the hand-calculated capacities are conservative compared to the rigorous results. However, in this case, with less slender tubes, the results for the two analyses are in closer agreement.

Table 4. Design Example No. 02 Transverse Displacement Capacities

Bent	Height, H_C (feet)	Hand-calculated Δ_u, inches	SeismoStruct Δ_u, inches
1	25	6.35	7.72
2	19	3.67	5.18
3 and 4	12	1.46	2.07

In Design Example No. 03, CFST Pile Bent displacement capacities were determined using the simplified approach developed here as well as the detailed, refined, fiber-based pushover. The geometry is similar to that for Design Example No. 2, but CFST construction is used for Design Example No. 3. Table 35 summarizes the results for Design Example No. 3, again showing conservative estimates from the simplified hand-calculation method as compared to the refined pushover results. In Table 5, the refined results are summarized along with the simplified results, with the simplified results shown in parentheses.

Table 5. Design Example No. 03 Transverse Displacement Capacities

Bent	with F_y = 50 ksi		with F_{yE} = 80 ksi	
	Δ_u, inches	V_P, kips	Δ_u, inches	V_P, kips
Bent No. 1	7.64 (5.75)	893	9.73 (7.74)	1,341
Bent No. 2	4.40 (3.32)	1,172	5.46 (4.47)	1,762
Bent No. 3	1.76 (1.33)	1,847	2.18 (1.78)	2,773
Bent No. 4	1.76 (1.33)	1,847	2.18 (1.78)	2,773

3.3 SeismoStruct Settings for Fiber-based Models

For the fiber-based models created during this project, it is important to retain the proper analytical settings across the models. The following discussion applies to both the simple, cantilever models and the more complex, full-bent pushover models developed for this research.

The default setting with regard to geometric nonlinearities (P-Delta effects) in SeismoStruct is for those effects to be included. Generally speaking, these effects should not be incorporated into the analyses used to develop design guidelines herein since the AASHTO Guide Specification for LRFD Seismic Bridge Design treats those effects separately in Article 4.11.5. The Commentary to this Article states that "typical highway bridges should be designed so that P-Δ effects can be neglected". The specification language for this Article outlines the requirements for these effects to be legitimately neglected. For most of the analyses, geometric nonlinearity was neglected by changing the default setting as shown in Figure 18.

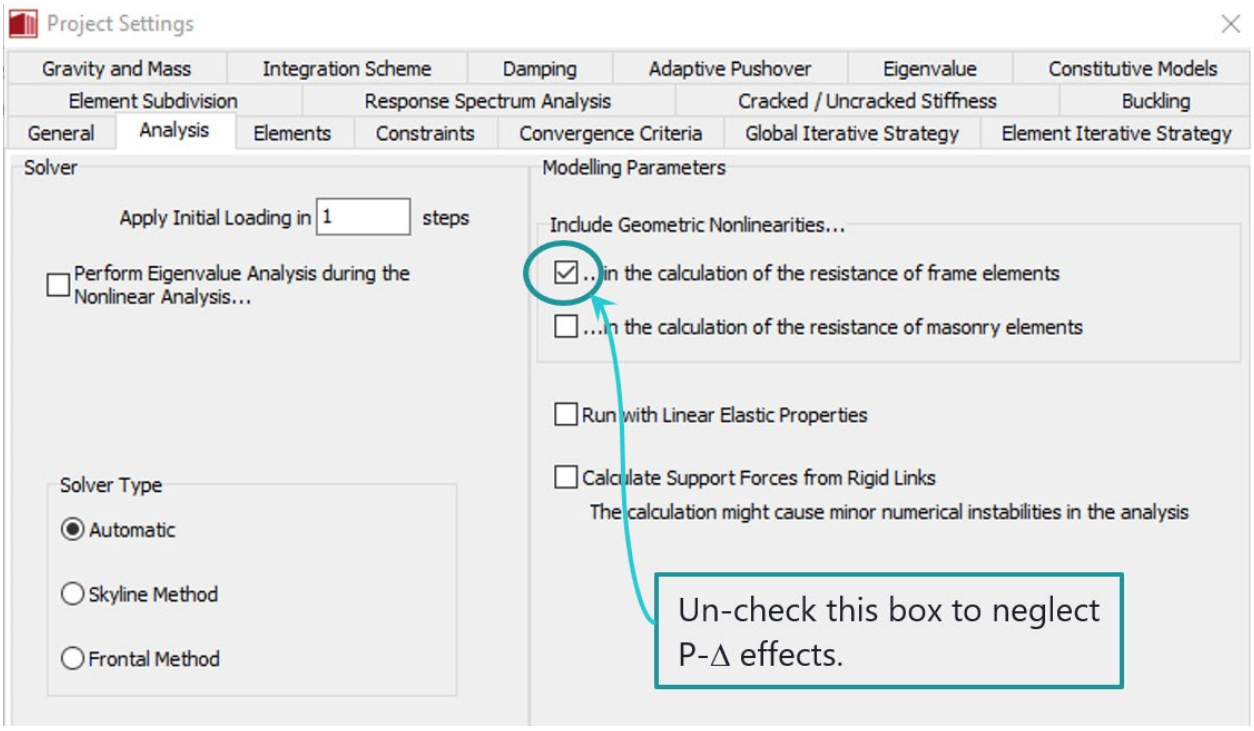

Figure 18. Geometric Nonlinearity in SeismoStruct

While the Guide Specification does claim that "at this time, the only rigorous method for considering P-Δ effects in combination with seismic demands is to use a nonlinear time history analysis", this is not necessarily true today with modern software. In several Design Examples, P-Δ analysis were run to complement the standard 1st-order analyses in the pushover response to demonstrate the effect of slenderness on response. Nonetheless, the Research Team agrees that

bridge bents should generally be designed such that these 2nd-order, geometric nonlinearities have negligible effect.

Pushover analysis used for this research, while generally neglecting geometric nonlinearity, must include material nonlinearity. Nonlinear, force-based inelastic frame elements (*infrmFB* SeismoStruct element type) were used for CFST modeling since the members in CFST construction are prismatic. For HTPB and RCFST construction, nonlinear displacement-based inelastic frame elements (*infrmDB* SeismoStruct element type) were used since the tube elements are not prismatic but vary along the compression member height. Force-based elements require no discretization along the member length (only across the cross-section) while displacement-based elements require discretization along the member length (in addition to cross-sectional discretization) to achieve accuracy. Force-based elements are the preferred choice most any time the inelastic member possesses prismatic properties. The terms "force-based" and "displacement-based" with regard to element type should not be confused with the same terms used for design methodology (force-based design versus displacement-based design). It is perfectly acceptable and, in fact, preferable, to use force-based elements in a displacement-based design.

In SeismoStruct, inelasticity is modeled through the use of cross-sections discretized into a grid of fibers, each possessing the assigned nonlinear stress-strain relationship defined by the user. The default cross-sectional discretization uses 5 integration sections with 150 section fibers. Given that a higher degree of accuracy was desirable for this research, these defaults were modified to 7 integration sections with 300 section fibers as shown in Figure 19.

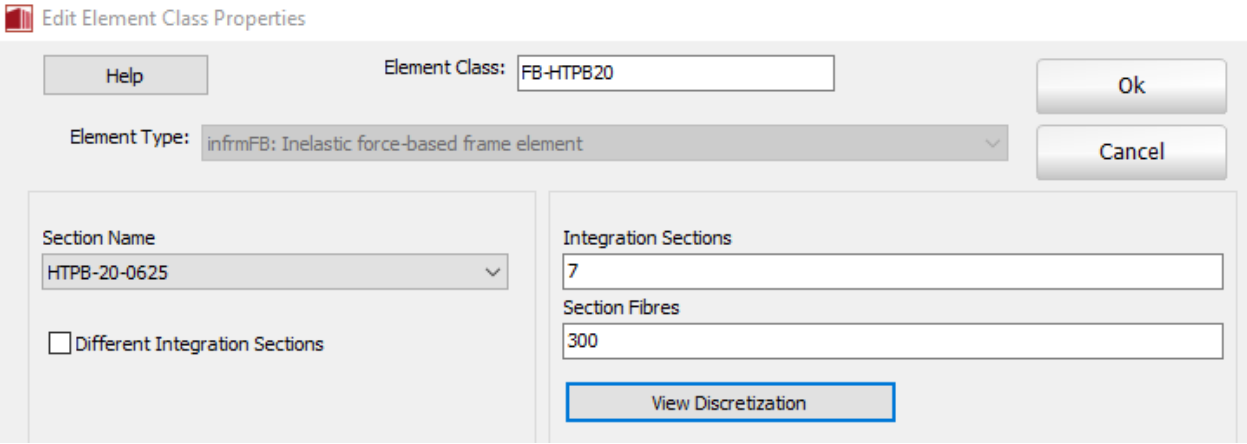

Figure 19. Cross-Section Discretization Parameters

Regarding material nonlinear stress-strain behavior, a bilinear relationship was used for the tubular members in all three types of construction – HTPB, CFST, and RCFST. This requires the specification of a post-yield stiffness ratio. For an elastic, perfectly-plastic material, the post-yield stiffness would be zero. However, for the CFST and RCFST construction, strains are expected to

proceed slightly into the strain-hardening range prior to failure. The steel tube material for CFST and RCFST models was set equal to 0.005 to account for some non-negligible strain hardening. For HTPB construction, local buckling and subsequent fracture of the tube is expected to occur well before any significant strain-hardening takes place. A post-yield stiffness equal to 0.000005 was use for HTPB materials in this project.

Nonlinear pushover analysis typically requires the designation of either load-control, response-control, or automatic-response-control. With load-controlled pushover analysis, the applied lateral force is incremented a specific amount in each step. For material with very low post-yield stiffness, a small increase in force represents a large increment in strain (and subsequently, in displacement). With response-controlled response, the displacement is incremented a specific amount in each step. Constraining the displaced shape of a structure can introduce artificial support reactions. The most common loading strategy, and the one used for this research, is the force-based pushover with response control. With this strategy the incremental lateral force is specified at the center-of-gravity of the superstructure and the displacement response is tracked. In analysis steps where the force increment produces a large displacement increment, the load factor is automatically reduced to achieve convergence. After initially establishing a reasonably close target displacement using initial nonlinear pushover, a number of analytical steps was specified to produce reliable results for the final pushover. Generally speaking, a number of steps equal to one-hundred times the target displacement was used. Figure 20 depicts the dialogue wherein this setting is established for the pushover analysis.

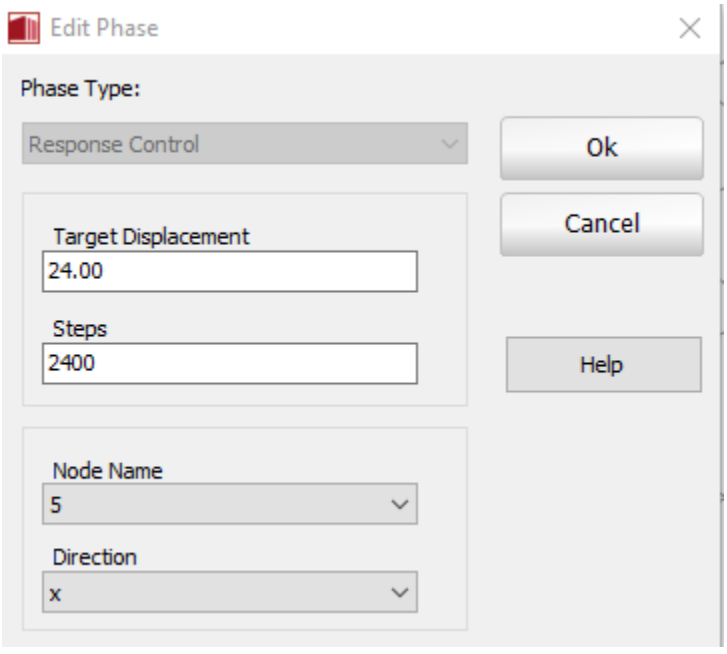

Figure 20. Response Control Pushover Parameters

When possible, it may prove advantageous to specify performance criteria to control the pushover analysis. For this research, the most logical use of performance criteria was in conjunction with the analysis of HTPB elements. For these elements, the analysis should be stopped once the critical strain has been reached. This critical strain is a function of the hollow tube D/t ratio, so specific criteria were applied depending on that ratio. Figure 21 shows a typical performance criteria specification used for a pushover analysis with HTPB elements.

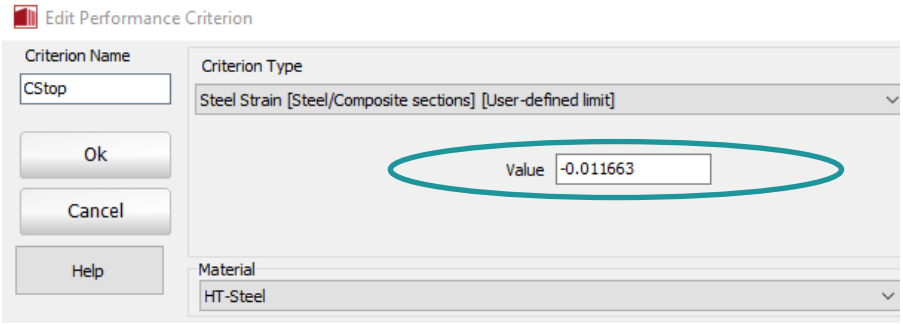

Figure 21. Performance Criteria in SeismoStruct

The maximum permitted strain in the tube is a critical parameter to be used in the analysis of CFST and HTPB elements. The critical strain for CFST may be taken equal to 0.025. The critical strain for HTPB elements is given by equations presented elsewhere in this research report. Hence, for HTPB models with a concrete plug at the top, the critical strain would be 0.025, while the critical strain at the in-ground hinge would be a function of the D/t ratio for the tube. Separate material models require definition for the two hinge locations in SeismoStruct, even though the same physical tube is at both locations. This critical strain is specified by the user in SeismoStruct in the dialogue shown the example in Figure 22.

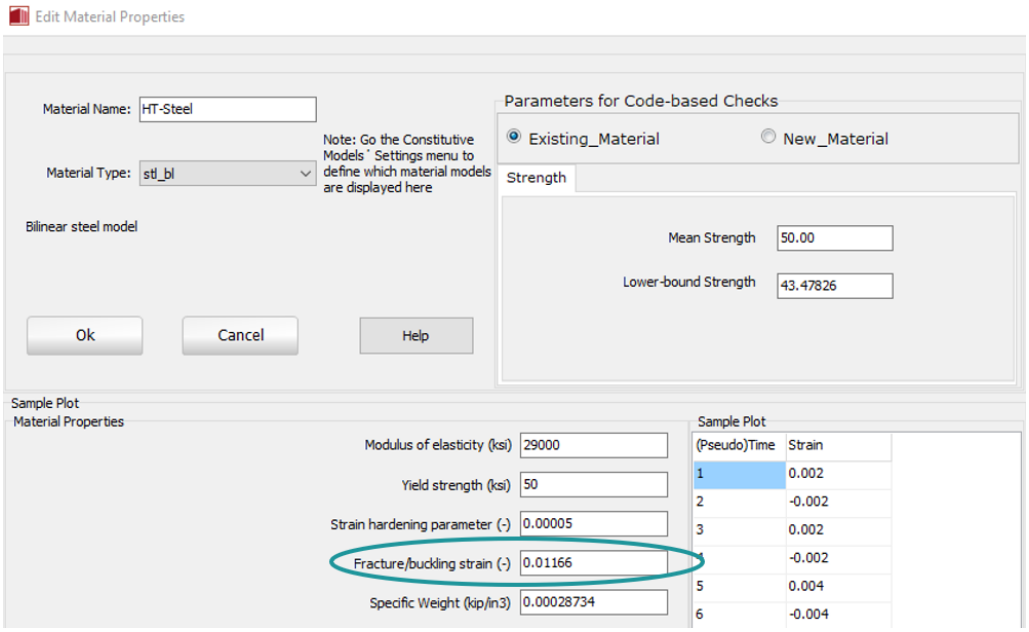

Figure 22. Critical Strain Definition in SeismoStruct Material Models

3.4 Geotechnical Analyses

The three primary study areas for geotechnical aspects of the research are (1) point-of-fixity estimates, (2) spring constant estimates, and (3) field verification of pile capacities.

3.4.1 Spring Constant Estimates

TDOT currently estimates pile stiffness under lateral loading to be in the range of 10-40 kips per inch per pile, based on unpublished recommendations from the early 2000's. As noted in the literature, simple methods for the analysis of piles subjected to lateral loading do exist and may be useful for the refinement of assumed values in design.

Broms' method is applicable for lateral analysis of a single pile in either purely cohesive or purely cohesionless soil profiles. Hannigan outlines the method on pages 9-86 through 9-100 in the Reference Manual for NHI Course Nos. 132021 and 132022 (Hannigan, Goble, Likins, & Rausche, 2006). Broms' method applies to relatively short piles that rotate in a rigid manner.

For longer piles, a method that incorporates pile bending must be considered. The most common approach in current geotechnical practice is the numerical p-y method (FHWA 1984), which represents the soil resistance to lateral movement using discrete springs distributed along the length of the pile. Each spring can have either a linear or nonlinear load-displacement response. The p-y method can easily be used for both uniform and multi-layer soil profiles because of the discretization. The disadvantage of this approach is that specialized software (e.g., LPILE or RSPile) is required to perform the analysis. The Reference Manual for the NHI course provides representative values of the required input parameters for both clays and sands. The Manual also provides a step-by-step procedure (pages 9-100 through 9-115) whereby the method may be applied (Hannigan, Goble, Likins, & Rausche, 2006).

The Characteristic Load Method (CLM) was developed by Evans (1992) and Duncan et al. (1994) using the results from a large number of p-y analyses on a range of pile sizes and soil conditions. The CLM recognized that load-displacement response of the top of a pile can be normalized by the soil and pile properties. Using regression, the CLM defined a characteristic lateral load (or moment) for each combination of soil and pile. The CLM can be used for uniform soil conditions in either sand or clay.

Pile groups may behave differently from single piles, and such effects may be evaluated using the procedure outlined on pages 9-154 through 9-156 of the NHI Reference Manual (Hannigan, Goble, Likins, & Rausche, 2006). However, group effects are limited for piles in a single row.

3.4.1.1 Research Approach

This section seeks to improve on TDOT's methodology for designing piles for lateral loads using the results of p-y pushover analyses performed using the RSPile software. The pushover analyses were performed to determine the lateral load required to produce displacements up to 25% of the pile diameter. The purpose is to provide insight into the usefulness of TDOT's spring stiffness approach and to suggest refinements or alternatives.

Nine soil types were selected for this phase of the project. These soil types encompass the full breadth of soils likely to be encountered. The properties are summarized in Table 6 and Table 7. These properties were selected based on the recommendations of consultant reports to TDOT that were provided to the research team, as well as typical values from references such as Davisson (1970) and (Hannigan, Goble, Likins, & Rausche, 2006). The p-y models used to represent each type of soil are summarized in the tables.

Table 6. Fine-Grained Soil Properties Used for Spring Constant Study

Soil Description	Total unit weight (pcf)	Undrained shear strength, s_u (psf)	Strain factor, ε_{50}	Static soil modulus, k_{py} (pcf)	p-y Model
Soft clay	120	500	0.02	50000	Matlock (1970)
Medium stiff clay	120	1000	0.01	150000	Reese et al. (1975)
Stiff clay	120	2000	0.007	800000	
Very stiff clay	130	4000	0.005	1750000	
Hard clay	130	8000	0.004	3500000	

Table 7. Coarse-Grained Soil Properties Used for Spring Constant Study

Soil Description	Total unit weight (pcf)	Friction angle, ϕ' (deg)	Static soil modulus, k_{py} (pcf)	p-y Model
Very loose sand	110	28	17500	

Loose sand	115	30	35000	Reese et al. (1974)
Medium dense sand	120	35	100000	
Dense sand	125	40	200000	

The pile types considered were twenty-three different concrete-filled steel tube sections and eight hollow-tube piles with diameters ranging from 12 to 36 inches. Combining the 31 pile types and nine soil types, a total of 279 pushover analyses were completed. All of the piles were modeled as hollow tubes with the nominal wall thickness and diameter. RSPile directly calculates the moment of inertia from these dimensions. The effects of the concrete infill were modeled by increasing the pile's effective modulus of elasticity, E_{eff}, by 10%. Thus, the CFST sections used E_{eff} of 31,900 ksi (4,593,600 ksf). The hollow tube sections used E_{eff} of 29,000 ksi (4,176,000 ksf). The method developed in this section can used any method of calculating an equivalent E_{eff} and I.

This approach assumes that the piles are sufficiently long to develop fixity and do not rotate at the base. The minimum pile length to satisfy this constraint ranges from 10 to 20 times the pile diameter, D, (Duncan et al. 1994) depending on pile and soil stiffness. The length of the piles in the model was selected as at 20·D. Piles with smaller length-to-diameter ratios should use numerical analysis or a rigid pile method, such as Broms

3.4.1.2 Pushover Results

Typical results of the pushover analyses are provided in Figure 23 for stiff clay and in Figure 24 for medium dense sand. In the stiff clay, the load-displacement plots for the different piles have the same shape but different magnitude. The strain-softening shape is a result of using the Reese et al. (1975) p-y model for the medium stiff or better clays.

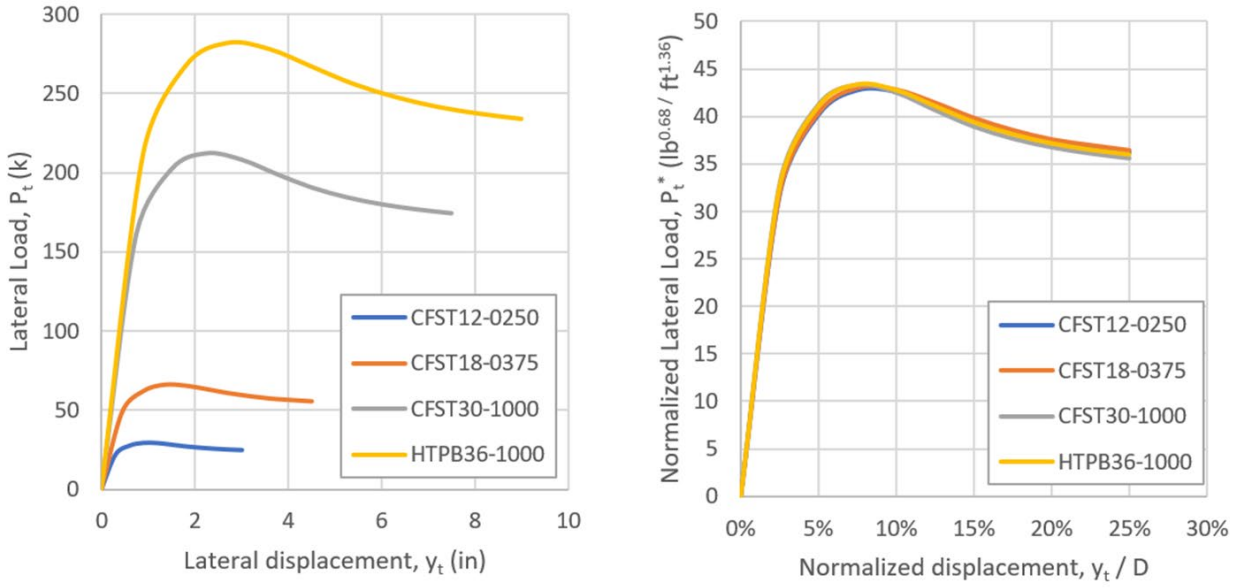

Figure 23. Example pushover results for four piles in stiff clay – (a) actual and (b) normalized

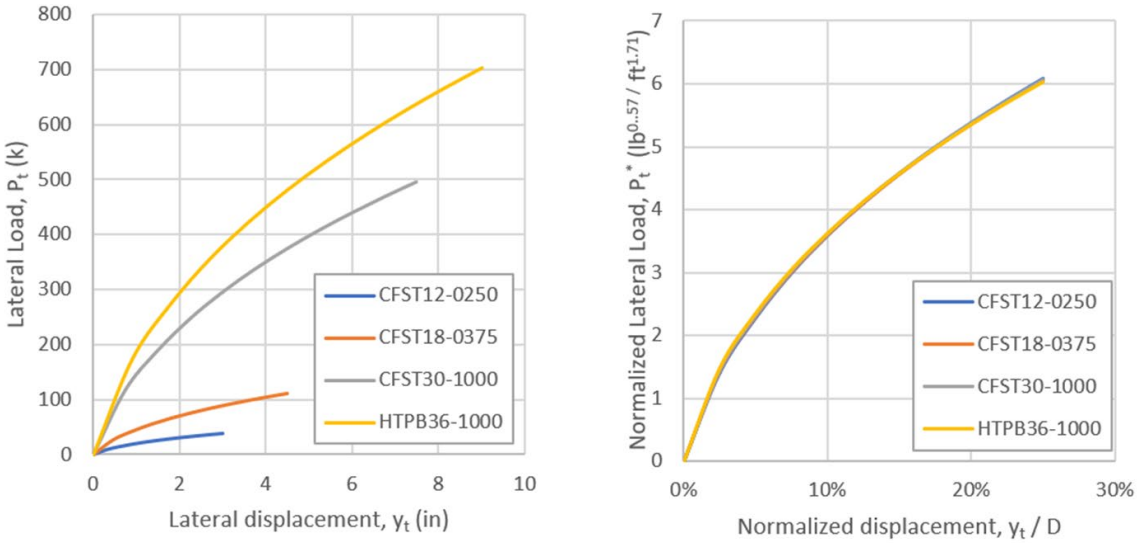

Figure 24. Example pushover results for four piles in medium dense sand – (a) actual and (b) normalized

Similarly, the behavior of the typical piles in sand exhibits the same shape but different magnitude depending on pile size and properties.

Following a similar approach to the CLM, the loads for each analysis were normalized and plotted against y_t/D. The normalized load (P_t*) is calculated as:

$$P_t^* = \frac{P_t}{f^*} \quad (3.4.1.2\text{-}1)$$

$$f^* = D^{2.57}\left(E_{eff}\, R_I\right)^{0.43}, for\ sand \quad (3.4.1.2\text{-}2)$$

$$f^* = D^{2.00}\left(E_{eff}\, R_I\right)^{0.32}, for\ clay \quad (3.4.1.2\text{-}3)$$

where:

- P_t = lateral load applied to the top of the pile and
- f* = normalization variable that depends on pile diameter, modulus, and moment of inertia.
- D = pile diameter
- E_{eff} = effective elastic modulus (in psf) of pile, use E_{steel} for HTPB or $1.1E_{steel}$ for CFST
- R_I = ratio of moment of inertia of the pile to the moment of inertia of a solid circular section of diameter, D.

After normalization in this manner, the normalized load-displacement relationships were very consistent as illustrated by the typical plots (Figure 23b and Figure 24b).

There are two primary differences between the approach presented here and the Characteristic Load Method.

First, the CLM attempts to further normalize the behavior to include other soil parameters, such as undrained shear strength or friction angle into the normalization process. The CLM approach is very useful when used as a standalone method. However, for the purposes of this project, it was not deemed necessary to perform this further fitting. Second, for this project the research team adopted different p-y models from those encountered in CLM, producing similar results for different models.

3.4.1.3 Development of Spring Constants

The lateral resistance predicted by current numerical methods (i.e., p-y analysis via RSPile or LPILE) is nonlinear as illustrated in Figure 25 and Figure 26. Depending on the soil type and p-y model used, the lateral load response may approach a maximum load, may keep increasing, or may experience softening at large displacements. The spring constant concept can still be used if the spring constant (k) is made a function of the normalized displacement (y_t / D). The spring concept can also be applied to the normalized load-displacement curves as shown in Figure 26.

Based on these figures, the normalized spring constant (k*) and the actual spring constant (k) for a particular pile and displacement can be defined as:

$$k^* = \frac{P_t^*}{y_t/D} = \frac{P_t}{f^*(y_t/D)} \qquad (3.4.1.3\text{-}1)$$

$$k = \frac{P_t}{y_t} = \frac{k^*}{D} \times f^* \qquad (3.4.1.3\text{-}2)$$

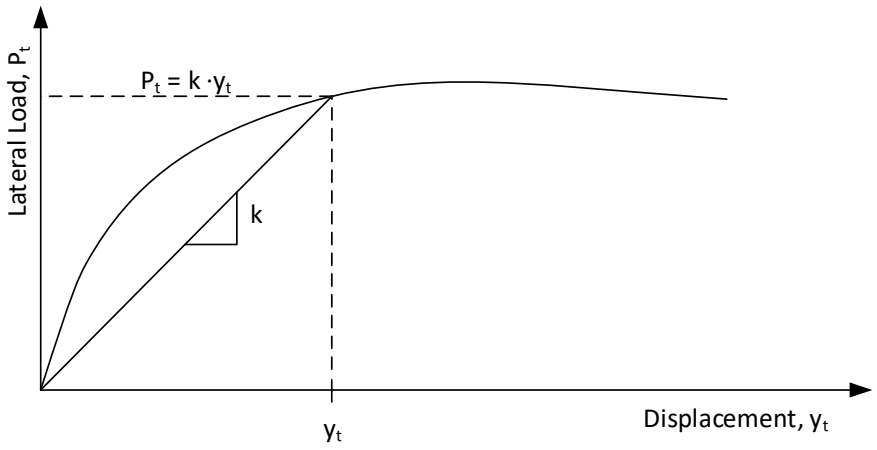

Figure 25. Nonlinear Load-Displacement Relationship

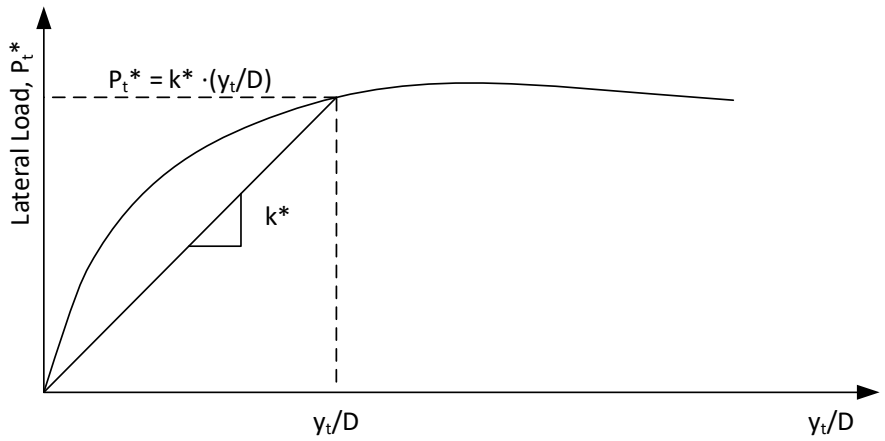

Figure 26. Normalized load-displacement relationship with spring constant

For each of the nine soil types, the normalized lateral load (P_t^*) was calculated for all 31 pile types at displacements up to 25% of the pile diameter. The average P_t^* was determined for each displacement, and values of k* were calculated. Table 8 summarizes the average values of normalized stiffness for each soil type. A simple design procedure follows. Design Examples 14 and 15 illustrate the proper use of the tabulated parameters. A spreadsheet tool has also been developed to assist in the implementation of the approach.

The suggested design process to determine an appropriate stiffness for a given load (P_t) would be:

1. Select an appropriate representative soil type based on the soil borings based on the soil present to a depth of 8·D below the ground surface (Duncan et al. 1994).
2. Determine the required pipe pile size based on axial load requirements and other considerations.
3. Determine the value of f* for the pile.
4. Assume an initial value of relative displacement, y_t/D.
5. Select the value of k* from tabulated values. Interpolation can be used for intermediate values of y_t/D.
6. Calculate the actual spring stiffness, k.
7. Predict the normalized displacement from the applied structural load, P_t.
8. Check the predicted versus assumed normalized displacement. If the assumed displacement is lower, the spring stiffness value may be too high.
9. Iterate by using the calculated value of y_t/D and repeating from Step 4.

Table 8. Displacement-dependent Normalized Spring Stiffness Constants

y_t / D	Normalized Stiffness (k*) = $P_t^*/(y_t/D)$

	Sand ($lb^{0.57}$ / $ft^{1.71}$)				Clay ($lb^{0.68}$ / $ft^{1.36}$)				
	Very Loose sand	**Loose sand**	**Medium Dense sand**	**Dense Sand**	**Soft clay**	**Medium Stiff clay**	**Stiff clay**	**Very Stiff clay**	**Hard Clay**
2.5%	24	36	57	76	298	794	1293	2008	3007
5.0%	24	34	46	60	218	532	815	1202	1764
7.5%	23	30	40	52	181	391	575	819	1197
10.0%	21	27	36	46	158	300	426	596	875
12.5%	20	25	33	42	143	237	328	458	679
15.0%	19	23	30	39	131	191	262	370	553
17.5%	18	21	28	37	122	157	218	310	467
20.0%	17	20	27	34	114	133	186	267	405
22.5%	16	19	25	33	108	115	162	235	359
25.0%	15	18	24	31	103	101	144	211	323

Note: The values of k* have units as indicated and would require conversion for a different unit system.

3.4.1.4 Comparison with Existing Method

In order to understand the implications of this research, the actual spring constants have been calculated for five specific piles and four displacement levels. These are presented in Table 9 for sand and Table 10 for clay.

Values that are in the range of 10 to 40 kips per inch have been highlighted in gray. These indicate cases where TDOT's existing methodology may be approximately correct. The cells left unshaded are values greater than 40 kips/in. In this case, the stiffnesses predicted by the current study are higher than TDOT's typical values, and TDOT's current approach is conservative. A few of the cells are underlined and bold in Table 10. These are values that are below 10 kips/in, indicating situations where TDOT's current approach is unconservative.

Table 9. Spring stiffnesses for select piles and displacements in sand

y_t/D	Pile	Predicted Spring Stiffness (k/in)			
		Very Loose sand	**Loose sand**	**Medium Dense sand**	**Dense Sand**
2.50%	CFST12-0312	14	21	33	45
	CFST20-0500	31	46	73	98

	CFST36-1000	81	121	192	256
	HTPB14-0500	19	29	46	62
	HTPB24-0750	43	65	102	136
5.00%	CFST12-0312	14	20	27	35
	CFST20-0500	31	44	59	77
	CFST36-1000	81	115	155	202
	HTPB14-0500	19	28	37	49
	HTPB24-0750	43	61	83	108
10.00%	CFST12-0312	12	16	21	27
	CFST20-0500	27	35	46	59
	CFST36-1000	71	91	121	155
	HTPB14-0500	17	22	29	37
	HTPB24-0750	38	48	65	83
20.00%	CFST12-0312	10	12	16	20
	CFST20-0500	22	26	35	44
	CFST36-1000	57	67	91	115
	HTPB14-0500	14	16	22	28
	HTPB24-0750	30	36	48	61

The following observations can be made:

- For sand, TDOT's current approach is:
    - Very likely to be safe
    - Somewhat conservative at displacements below 5%, except for small diameter piles
    - More suited to small to moderate diameter piles
- For clay, TDOT's current approach is:
    - Usually, safe
    - Very conservative for displacements below 5%, except for soft clay
    - More suited to soft to medium stiff clay at relatively large displacements

Table 10. Spring stiffnesses for select piles and displacements in clay

y_t/D =	Pile	Predicted Spring Stiffness (k/in)				
		Soft clay	Medium stiff clay	Stiff clay	Very stiff clay	Hard Clay
2.50%	CFST12-0312	18	48	79	122	183
	CFST20-0500	30	79	129	201	301
	CFST36-1000	55	148	240	373	559
	HTPB14-0500	22	60	97	151	227
	HTPB24-0750	37	99	161	250	374
5.00%	CFST12-0312	13	32	50	73	107
	CFST20-0500	22	53	82	120	177
	CFST36-1000	41	99	151	223	328
	HTPB14-0500	16	40	61	91	133
	HTPB24-0750	27	66	101	149	219
10.00%	CFST12-0312	10	18	26	36	53
	CFST20-0500	16	30	43	60	88
	CFST36-1000	29	56	79	111	163
	HTPB14-0500	12	23	32	45	66
	HTPB24-0750	20	37	53	74	109
20.00%	CFST12-0312	**7**	**8**	11	16	25
	CFST20-0500	11	13	19	27	41
	CFST36-1000	21	25	35	50	75
	HTPB14-0500	**9**	10	14	20	31
	HTPB24-0750	14	17	23	33	50

3.4.1.5 Limitations

The primary limitation of the spring constant method presented in Section 4.1.3 is the pile length. This method should not be used for piles that are shorter than 20 times the diameter. Shorter piles are prone to base rotation and may have lower stiffness than that determined by this research.

3.4.2 Depth-to-Fixity Estimates

In structural modeling, engineers typically replace the pile-soil system with a pile that is fixed at the base, as shown in Figure 27. The actual system with an embedded pile is replaced with a purely structural system that produces the same top of pile deflection (y_t) for the same load (P_t). TDOT currently uses 3 to 5 pile diameters below the ground for the estimated depth to fixity.

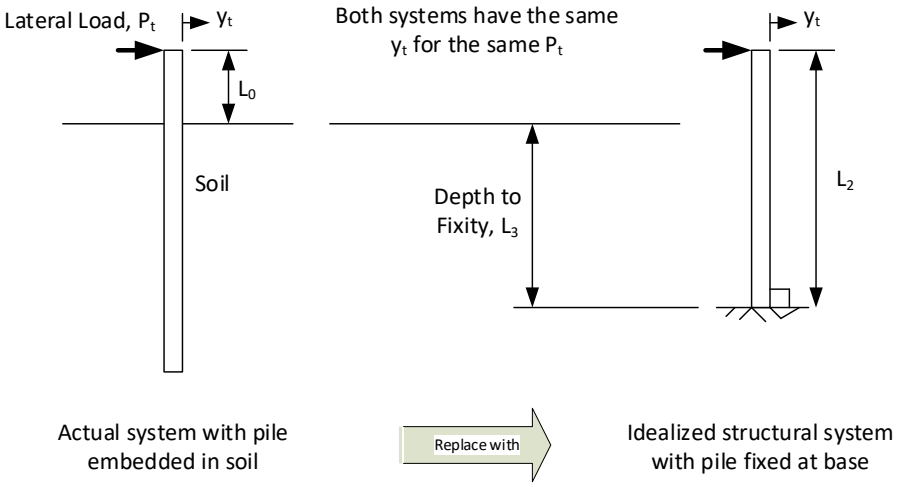

Figure 27. Depth to Fixity for Structural Analysis

If L_0, P_t, and y_t are known as well as the pile properties, then the equivalent fixed base length (L_2) and depth to fixity (L_3) can be found as:

$$L_2 = \sqrt[3]{3E_p I_w \left(\frac{y_t}{P_t}\right)} \qquad (3.4.2\text{-}1)$$

$$L_3 = L_2 - L_0 \qquad (3.4.2\text{-}2)$$

Davisson and Robinson (1965) presented a solution to the bending of partially embedded piles (i.e., piles with $L_0 > 0$). They solved the governing partial differential equation (Hentenyi 1946) using a change of variables for two cases: 1) constant horizontal subgrade modulus, k_h, and 2) linearly increasing horizontal subgrade modulus, $k_h = n_h \cdot z$. The first case is typically used to model clays in undrained conditions while the second case is used for sand and gravel where drained conditions predominate.

The AASHTO LRFD Bridge Design Specifications provide depth-to-fixity equations for preliminary design, which are based on the Davisson and Robinson solution. These may be useful in enhancing TDOT analytical procedure for the modeling of pile bents. The Commentary to Section 10.7.3.13.4 provides equations for depth-to-fixity for both sands and clays.

For Clays:

$$L_3 = 1.4\left[\frac{E_p}{E_s} I_w\right]^{0.25} \quad (3.4.2\text{-}3)$$

For Sands:

$$L_3 = 1.8\left[\frac{E_p}{n_h} I_w\right]^{0.20} \quad (3.4.2\text{-}4)$$

where:

- L_3 = depth below ground to point-of-fixity, feet
- E_p = modulus of elasticity of the pile, ksi
- I_w = moment of inertia for the pile, ft^4
- E_s = soil modulus for clays = $0.465S_u$, ksi
- S_u = undrained shear strength of clays, ksf
- n_h = rate of increase of soil modulus with depth for sands, ksi/ft.

Note that these equations require careful attention to units in order to produce dimensionally correct solutions. The constants are average values recommended by Davisson and Robinson (1965) of slightly more complex behavior.

For clays, the estimate of E_s based on s_u includes a unit conversion (ksf to ksi). It assumes a ratio of undrained modulus to undrained strength of about 67 as recommended by Davisson (1970). According to Duncan and Buchignani (1976), this ratio is more often in the range of 200 to 1000 for moderately overconsolidated clays with plasticity indices less than 50 (i.e., most clays in Tennessee). The effects of underestimating the soil modulus are shown in Table 11. The depths to fixity are substantially lower if a realistic E_s/s_u ratio is used.

Table 11. Effect of E_s/s_u ratio on the calculated L_3/D ratio

s_u (ksf)	Estimated E_s (ksf) for:			Calculated L_3/D for[A]:		
	E_s/s_u=67	E_s/s_u=400	E_s/s_u=800	E_s/s_u=67	E_s/s_u=400	E_s/s_u=800
0.5	33.5	200	400	8.4	5.4	4.5
1	67	400	800	7.1	4.5	3.8
2	134	800	1600	5.9	3.8	3.2
4	268	1600	3200	5.0	3.2	2.7
8	536	3200	6400	4.2	2.7	2.3

[A] Calculated for a 1-foot diameter pile with EI = 43346 $k\text{-}ft^2$

The Davisson and Robinson equations assume soil moduli that are independent of pile displacement. However, the lateral soil spring stiffness is not constant and tends to decrease with pile deflection. This means that the values of L_3/D should be expected to increase as the load magnitude and pile deflection increase.

3.4.2.1 Parametric Analysis of Depth of Fixity

In order to initially investigate the effects of soil type, pile size, pile stickup, and load magnitude on L_3/D, RSPile was used to perform 240 numerical pile analyses. The analyses used the following conditions:

- Pile type: CFST 12-0312, CFST 20-0500, and CFST 36-1000
- Pile extension above ground, L_0: 0, 6, 12, and 18 ft
- Soil type: Very loose sand, dense sand, soft clay, and hard clay (uniform with depth)
- Lateral loading: five pile-soil dependent loads, up to load required for soil displacement of 25% of diameter

After each case was analyzed in RSPile, the displacement and pile rotation were recorded at both the top of the pile and at the ground surface, which were identical for cases with L_0 = 0 ft. The equivalent fixed base length and depth of fixity were calculated from the data for each case.

Representative results from these analyses are plotted in the following figures to illustrate some important trends. Figure 28 and Figure 29 show the variation of L_3/D with shear load for three CFST piles with pile diameters ranging from 12 to 36 inches when the pile extension, L_0, is constant. The figures plot the results soft and hard clay, respectively. The L_3/D ratio ranged from 7 to 12 for the soft clay and from 2 to 5 for the hard clay. For smaller pile diameters, the shear load required is less, and for larger diameter pile the shear load required is higher in order to achieve the same level of deflection. The starting and ending values on the Y-axis (L_3/D) are almost the same for all three piles.

The load required to produce a top of ground displacement equal to 10% of the pile diameter for L_0=0 ft was defined as P_{10}. This is approximately the peak of the lateral resistance for clayey soils and also corresponds to the limit imposed by FHWA (2018) for lateral deflection. P_{10} can be found for a given pile and soil by setting y_t/D to 10% in the spring stiffness method presented in Section 3.4.1. Dividing the shear load by P_{10} produces the normalized results in Figure 28b and Figure 29b, which follow a relatively consistent trend. These two figures also show that the ratio L_3/D is not constant but increases as the magnitude of shear load increases.

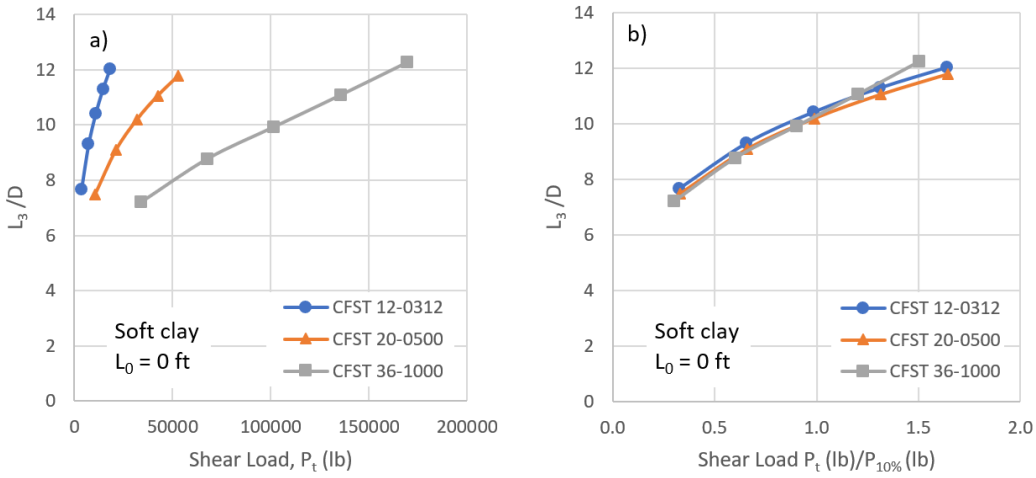

Figure 28. L_3 / D for piles in soft clay - (a) actual and (b) normalized

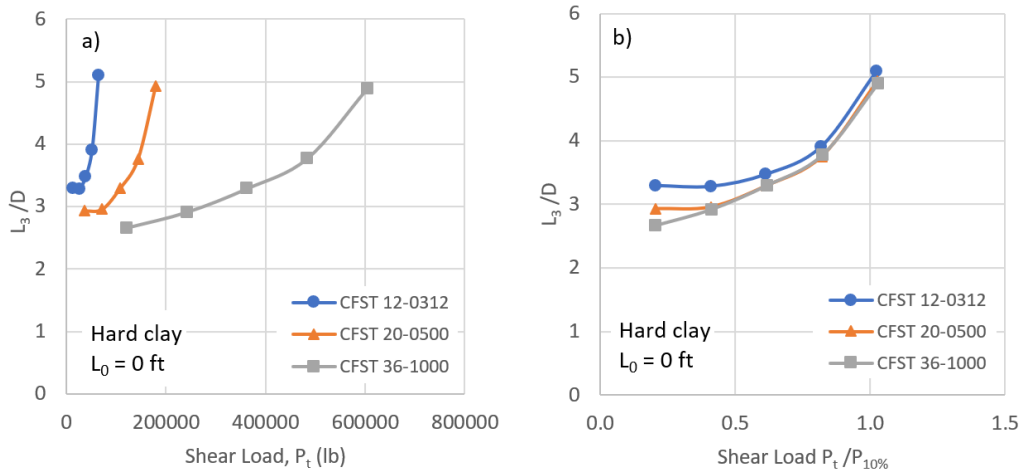

Figure 29. L_3 / D for piles in hard clay - (a) actual and (b) normalized

Figure 30 shows the variation of L_3/D with shear load for a 12-inch CFST pile with different L_0 values. This analysis was done for a dense sand. The L_3/D ratios ranged from 5 to 8. The depth to fixity L_3 is highest when L_0 is minimum (0 ft), and depth to fixity L_3 is lowest when L_0 is maximum (18 ft). The cases with large L_0 are able to sustain much lower lateral loads because of the moment induced by applying the load above the ground surface. Figure 30 illustrates that normalization does not affect the relative trend between piles of the same size because the normalization load is the same for all of the analyses. Both trends show that the value of L_0 has a noticeable but minor effect on the trend in L_3/D with shear load.

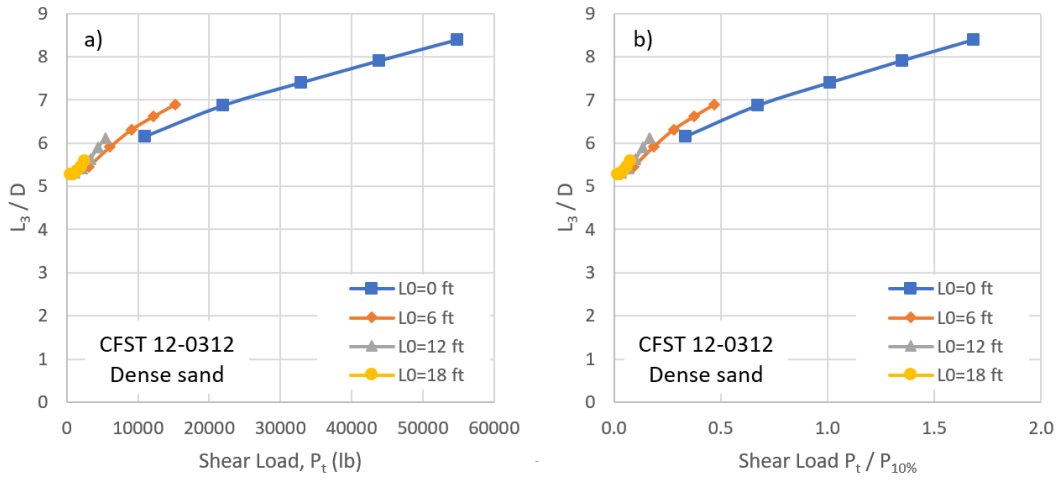

Figure 30. L_3 / D for piles in dense sand for variable L_0 - (a) actual and (b) normalized

Figure 31 shows the effect of soil type on the variation of L_3/D with shear load for a 20-inch CFST pile with L_0 equal to zero. This analysis was done for four different soil types and produced L_3/D ratios ranging from 2 to 12. The depth to fixity increases quickly in soft soil as load is applied, while dense sand and hard clay take more time to respond. For the same magnitude of deflection, the shear load required is larger in dense sand and smaller in soft clay. Dividing the shear load by the shear load required for 10% deflection produces the normalized results in Figure 31. The shape of the hard clay response is different than that of the other soils because of differences in the underlying p-y curves. The p-y curve used for hard clay is strain-softening while those for the soft clay and sands are not. As the stiffness of the clay increases, the depth to fixity (L_3) decreases and vice versa. Similarly, the loose sand has larger L_3/D ratios than the dense sand.

In summary, the lateral load magnitude affects the L_3/D ratio in a manner that depends on the overall lateral load capacity of the system, which includes the pile stiffness, the soil type, and the pile size.

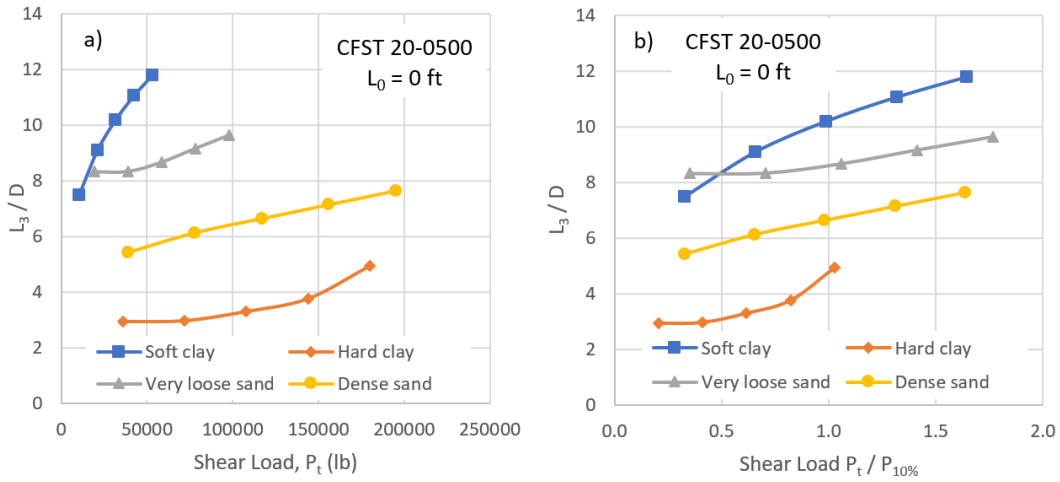

Figure 31. L_3 / D in various soil types - (a) actual and (b) normalized

Figure 32 plots L_3/D against the normalized load for all of the parametric analyses in clay. For the two clay consistencies that were used, relatively consistent trends are shown, regardless of pile size. The L_3/D ratios start in the range of 3 to 5, as typically assumed, but increase as lateral load is applied. The increase in L_3/D occurs because the underlying p-y analysis includes nonlinearity in the soil response. Constant values of L_3/D from Table 11 are plotted for five clay consistencies. These values are constant because they assume a linear soil response that does not change with displacement. Within the band of data for either soil type, the variation appears to be influenced by both pile size and L_0. In general, as L_0 increases from 0 to 18 ft, the depth to fixity increases by up to one diameter for a given level of lateral loading.

The data from the coarse-grained models are shown in Figure 33. Similar to clay, the depth of fixity ratios based on constant n_h tend to be correct only at relatively low loads and are somewhat low at higher loads. Substantially more scatter is present in the results for the sand. However, as indicated in Figure 33, the scatter is mostly explained by the pile size. As the pile diameter increased from 12 to 36 inches, the depth to fixity decreased by about one to two diameters. At low shear load, the 12-inch diameter piles match most closely with the lines based on constant n_h.

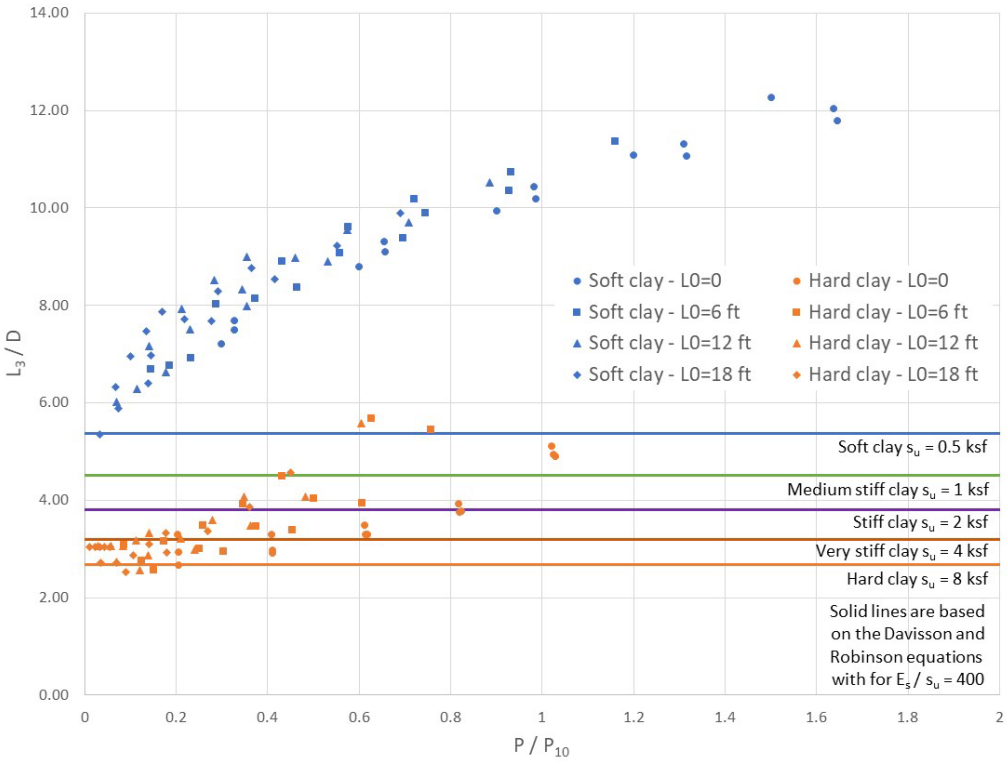

Figure 32. Variation in L_3/D ratio with loading for clay soils

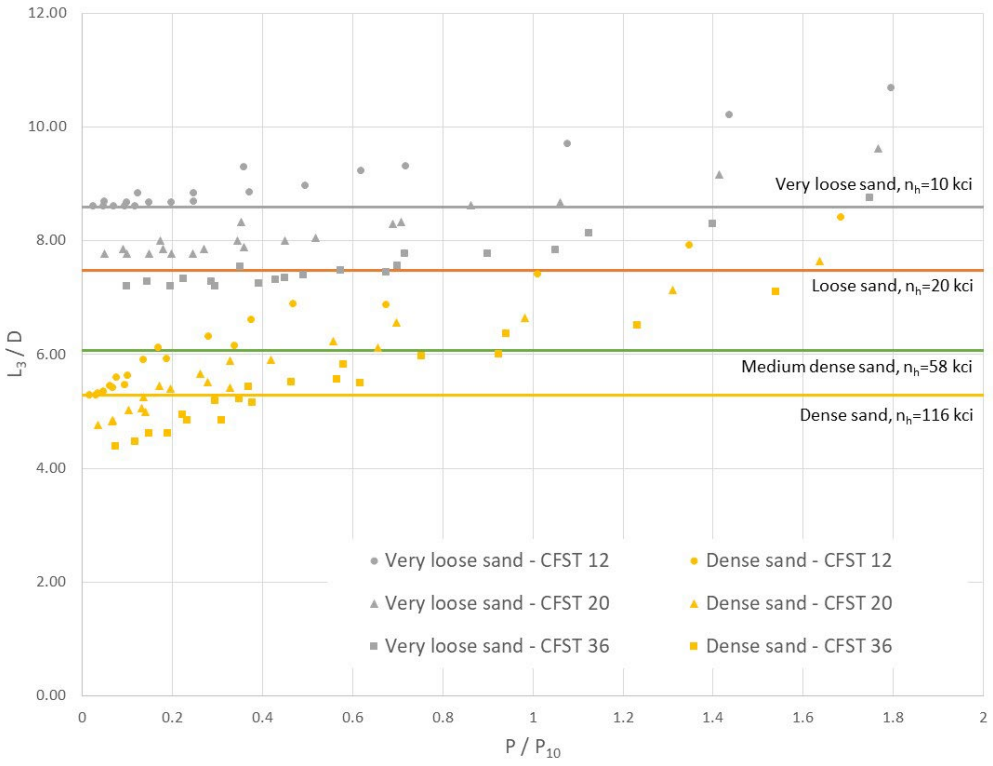

Figure 33. Variation in L_3/D ratio with loading for coarse-grained soils

3.4.2.2 Selection of Depth of Fixity for Design

Based the trends presented in Figure 32 and Figure 33, typical values of L_3/D are summarized in Table 12. For piles in clay, TDOT's current approach of using 3 to 5 pile diameters as the depth to fixity appears to be appropriate only for piles in medium stiff or better clay that experience relatively small loads (< 20% of P_{10}). The analysis in the previous section focused on four soil types that bound the lateral load analysis. Most field situations will fall within these bounds; however greater specificity may be desired.

Table 12. Typical values of L_3 / D for a range of soil types and loads

Soil	Typical Ranges of L_3 / D for Given Load			
	Load < 20% of P_{10}	**Load ≈ 50% of P_{10}**	**Load ≈ P_{10}**	**Load > P_{10}**
Soft clay	6 to 8	9	10 to 11	11 to 12
Hard clay	3	3 to 4	5+	Not studied
Very loose sand	6	7	8 to 9	8 to 10
Dense sand	5	6	7	6 to 8

Note: P_{10} = load required to cause a top of pile displacement of 0.1 × Diameter for the particular pile with L_0 = 0 ft in the indicated soil condition

The parametric analysis in Section 3.4.2.1 suggests that the depth of fixity predicted for the L_0=0 condition can be used to estimate L_3 for other values of L_0. Many analyses with L_0=0 were performed to develop the spring stiffness approach (Section 4.1) and were leveraged to provide a method for selecting the depth of fixity for any of the nine typical soil types.

The spring stiffness study performed RSPile analyses for 31 pile types and all nine soil types with L_0=0 for pile head deflections up to 25% of the pile diameter (i.e., y_t/D up to 0.25). For each of these 279 analyses, the ratio of L_3/D was calculated for each increment of y_t/D and averaged over all 31 pile types. Figure 34 summarizes the average variation in L_3/D with deflection for both sand and clay. Each data point is the mean for all 31 pile types. The ratio of L_3/D fell within arrange of ±1.4 or less from the mean trend. The standard deviation of L_3/D for the trends did not exceed 0.74. The very loose and soft soils exhibited the most variation in L_3/D with pile type. The data plotted in Figure 34 are also provided in Table 13.

The practical use of the ratios in Table 13 was explored by comparing the equivalent fixed based structural model to RSPile pushover analyses for several cases. An example of this comparison is shown in Figure 35. For soft clay and y_t/D = 10%, L_3/D = 10.4 was selected from Table 13. For a 20-inch diameter pile, this results in L_3 of 17.3 ft. The equivalent fixed base length, L_2, was calculated for each value of L_0 studied. Using Equation 3.4.2-1, the lateral load vs. deflection behavior of the structural models was calculated and plotted as the linear trends in Figure 35. The corresponding RSPile analyses are also plotted for comparison.

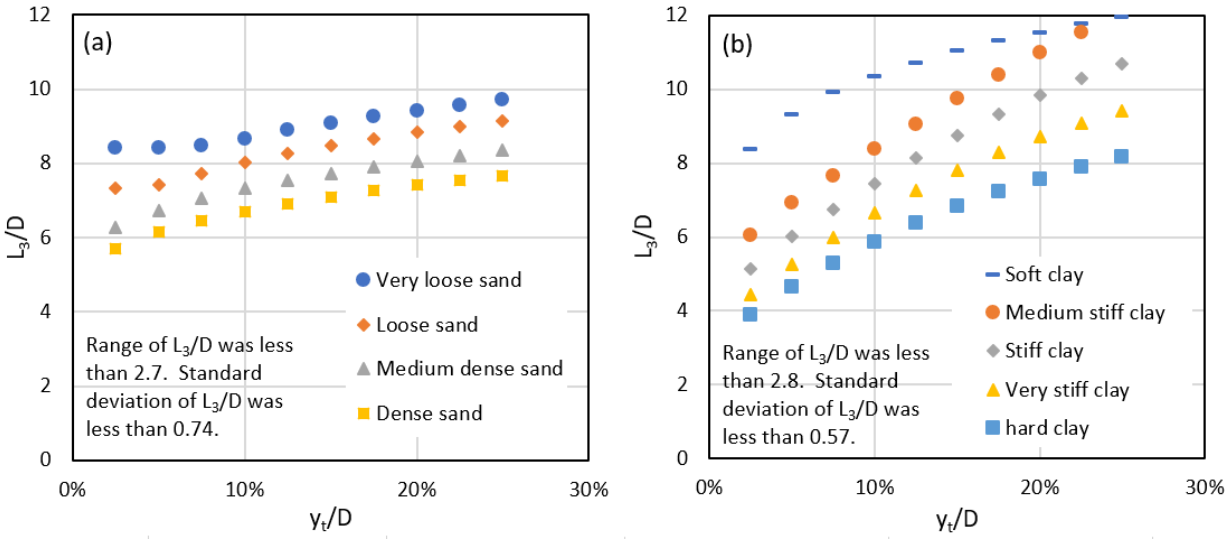

Figure 34. Variation of L_3/D with deflection for pipe piles in (a) sand and (b) clay

Table 13. Average L_3/D for L_0=0 based on 31 pile types

y_t / D	Sand				Clay				
	Very loose	Loose	Medium dense	Dense	Soft	Medium stiff	Stiff	Very stiff	Hard
2.5%	8.4	7.3	6.3	5.7	8.4	6.1	5.1	4.4	3.9
5.0%	8.4	7.4	6.7	6.2	9.3	6.9	6.0	5.3	4.6
7.5%	8.5	7.7	7.1	6.5	9.9	7.7	6.7	6.0	5.3
10.0%	8.7	8.0	7.3	6.7	10.4	8.4	7.5	6.7	5.9
12.5%	8.9	8.3	7.5	6.9	10.7	9.1	8.1	7.3	6.4
15.0%	9.1	8.5	7.7	7.1	11.0	9.7	8.8	7.8	6.8
17.5%	9.3	8.7	7.9	7.3	11.3	10.4	9.3	8.3	7.2
20.0%	9.4	8.8	8.1	7.4	11.6	11.0	9.8	8.7	7.6
22.5%	9.6	9.0	8.2	7.5	11.8	11.5	10.3	9.1	7.9
25.0%	9.7	9.1	8.3	7.7	12.0	12.0	10.7	9.4	8.2

Examining Figure 35a, the equivalent structural model predicts a softer response up to y_t/D = 10%, which was the value assumed in order to pick L_3/D. For other values of L_0, the structural and RSPile models cross over each other at a higher amount of deflection. The structural model is softer for deflections below the crossover point and stiffer at higher deflections. The deflection at the crossover point increases as L_0 increases.

The implications of a softer or stiffer structural model will depend on the characteristics of the structure and cannot be generalized here. The engineer must judge if this difference in stiffness will be detrimental to the design.

The deflection at the crossover point will also depend on the value of y_t/D used to select L_3/D. As the selected deflection increases, the crossover point will increase, regardless of the value of L_0.

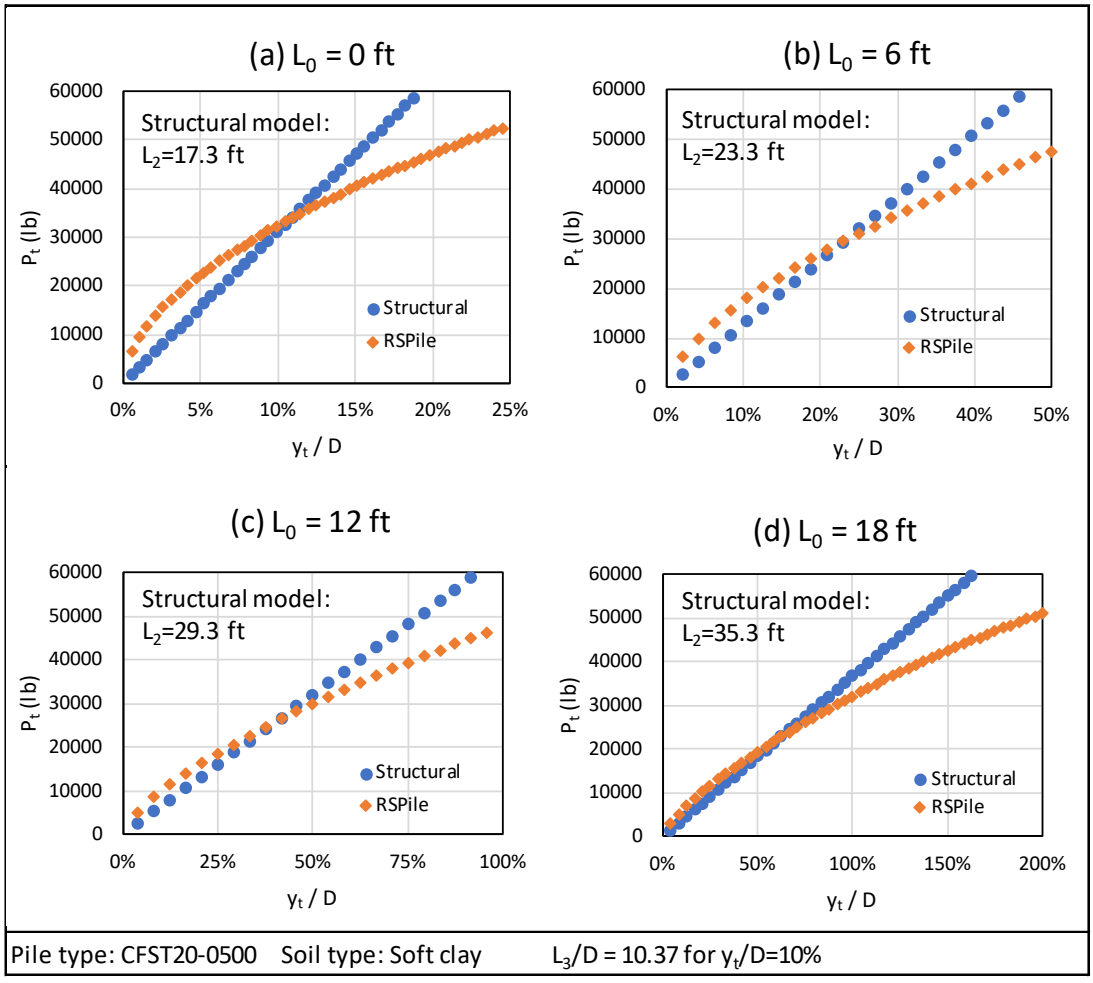

Figure 35. Example comparison of RSPile pushover analysis to structural model with (a) L_0=0 ft, (b) L_0=6 ft,
(c) L_0=12 ft, and (d) L_0=18 ft

The following design methodology is recommended for selecting an L_3/D ratio using Table 13:

1. Estimate the top of pile deflection and calculate y_t/D.
2. Select the appropriate L_3/D ratio from Table 13 for the most applicable soil type based on the soil present in the soil borings to a depth of 8·D below the ground surface.
3. Use L_0, L_3/D, and D to determine L_2.

4. Perform the structural analysis and determine the top of pile deflection.
5. Compare the calculated and estimated values of y_t.
    a. If the value of y_t is higher than estimated in Step 1, the structural model will be too stiff and a higher ratio of L_3/D may be required.
    b. If the value of y_t is lower than estimated in Step 1, the structural model may be too soft and a lower ratio of L_3/D may be required.
    c. Consider returning to Step 2 to 4 to revise L_3/D and repeat the analysis
6. Finalize the analysis when the calculated and estimated values of y_t are similar.

Similar to the spring constant estimates, the typical ratios of L_3/D presented in Table 12 and Table 13, or calculated using the procedure above, only apply to piles that are sufficiently long to prevent rotation. If the pile length is less than 20·D, these methods are not applicable, and it may be difficult to define the depth to fixity because of pile base rotation.

3.4.3 Field Capacity Synthesis and Assessment

Ultimate geotechnical capacity of piles is typically estimated using at least one of the following methods:

- Static capacity analysis using empirical or semi-empirical methods based on the soil conditions at the site,
- Dynamic capacity analysis based on measurements obtained during pile driving, ranging from pile set to strain measurements, or
- Axial load testing of piles following driving.

All of these methods have both advantages and disadvantages, which will be discussed in the following sections. In many parts of Tennessee, piles are driven to practical refusal on relatively shallow bedrock. In this case, the structural capacity of the piles typically governs design. These conditions are not discussed further in this document.

Friction piles develop capacity from load transfer along the side of the pile as a well as some amount of base resistance at the tip of the pile. Side resistance is typically mobilized by small displacements (about ½ inch), while base resistance may require movements of 5 to 10% of the pile diameter to mobilize. Because downward pile movement tends to increase pile capacity, as well as transfer loads to other piles, the typical result of overloading a pile is excessive settlement rather than large-scale bearing capacity failure. While settlement is problematic and expensive, it does not tend to create immediate structural safety concerns. Similar to shallow foundations, the allowable load that a pile can carry is closely tied to the structure's tolerance for settlement.

AASHTO's resistance factors for both static and dynamic capacity analysis methods are summarized in Table 14. The resistance factors communicate the relative uncertainty inherent in the particular testing methodology. In addition, the resistance factors correct for bias in each method in order to maintain a consistent level of risk. In other words, if a method tends to over- or underpredict capacity by a known factor, the resistance factor helps to account for this. While AASHTO specifies these resistance factors, it provides minimal guidance to describe how the results of each testing condition are used to make field decisions regarding pile lengths.

Table 14. Resistance Factors for Pile Foundations (AASHTO, 2020)

Testing condition	**Resistance Factor**
At least one load test + dynamic testing of 2% of production piles or 2 piles, whichever is greater	0.8
At least one load test, no dynamic testing	0.75
Dynamic testing of 100% of production piles	0.75
Dynamic testing of at least 2% of production piles	0.65
Wave equation analysis	0.5
Modified Gates equation	0.4
Static capacity analysis	0.25 to 0.35
ENR equation for use with LRFD	0.1

The following sections describe the different methods for estimating pile capacity followed by a discussion of how these methods can be applied in the field along with the resistance factors. Finally, TDOT's current approach for using static load test data is evaluated.

3.4.3.1 Static Capacity Analysis (SCA)

The primary benefit and usage of static capacity analysis is to estimate the geotechnical capacity of the pile prior to construction. Methods include the α-method for fine-grained soils and the Meyerhof SPT method for coarse-grained soils. Site-specific geotechnical information from soil borings is required to use these approaches. These methods are useful to estimate the required length and diameter of piles to allow for the development of construction drawings.

Static capacity methods for driven piles have AASHTO resistance factors in the range of 0.25 to 0.35. It is uncommon to determine the final length of driven piles solely from static capacity analysis.

3.4.3.2 Axial Load Testing

The axial load test (ASTM 1143, TDOT Article 606.08) is viewed as the "gold standard" for determining the geotechnical capacity of a pile. The axial load test uses a reaction beam and jack to apply an axial load to the top of the pile. The pile head movement is measured as the load is applied, as illustrated in Figure 36. Additional telltale measurements can be made to evaluate pile movement with depth.

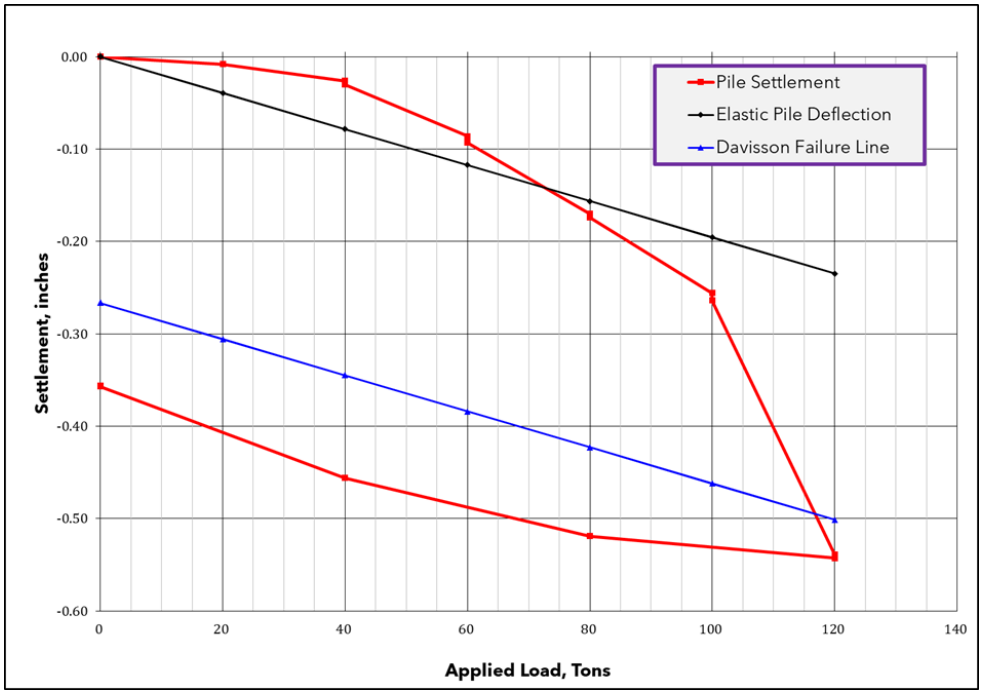

Figure 36. Example Axial Load Test Data

Interpretation of failure or ultimate geotechnical capacity from axial load tests is required and does not usually produce a definitive, unique result. Multiple methods have been proposed (e.g., Davisson 1972, Brinch Hansen 1963, USACE 1991), which each contain assumptions and conservatism. Resistance factors should carefully consider the interpretation method used. Fellenius (2021) and NAVFAC (2024) provide further comparison of the different methods. The Brinch Hansen methods, particularly the 80% method, tend to produce more realistic interpretation of the failure load (Fellenius 2021). For larger piles (B > 24 inches), the Davisson method will under-predict the nominal resistance of the pile.

TDOT follows AASHTO's recommendation to use the Davisson method for piles with a width of 24 inches or less and a modified version of Davisson for larger piles. The Davisson criteria is outlined in ***Design and Construction of Driven Pile Foundations***, FHWA, 2005. According to this method, the point at which the observed load-movement curve intersects the failure criterion line defines the nominal resistance. If the observed load-movement line does not intersect the failure criterion line, then the nominal resistance exceeds the maximum applied test load. The failure criterion line is given by:

$$s_f = \frac{QL}{AE} + 0.15 + \frac{B}{120} \qquad (3.4.3.2\text{-}1)$$

where, s_f = pile top movement (in.), Q = applied load (kips), L = pile length (in.), A = cross-sectional area of the pile (in^2), E = elastic modulus of the pile (ksi), and B = pile width or diameter (in.).

Unless specified otherwise by the Engineer, the nominal bearing resistance is determined from the load test data as follows:

- for piles 24.0 in. or less in diameter (length of side for square piles), the Davisson method;
- for piles larger than 36.0 in. in diameter (length of side for square piles), at a pile top movement, s_f (in.):

$$s_f = \frac{QL}{AE} + \frac{B}{30} \qquad (3.4.3.2\text{-}2)$$

- for piles greater than 24.0 in. but less than 36.0 in. in diameter, criteria to determine the nominal bearing resistance that is linearly interpolated between the criteria determined at diameters of 24.0 and 36.0 in.

Note that s_f is simply the pile elastic deformation with an offset that depends on the pile diameter (0.15 + B / 120 for B < 24 inches and B / 30 for B > 36 inches).

Typically, static load tests will not be completed immediately after driving, and some amount of setup is included in the results, especially if compared to end-of-driving (EOD) dynamic measurements.

3.4.3.3 Dynamic Capacity Analysis – Driving Formulas

Engineers have realized since at least the mid-1800s that the driving resistance of a pile is related to its load carrying capacity. This observation resulted in dynamic formulas that attempt to relate capacity to pile hammer energy and driving resistance. As noted by Likins et al. (2012), at least 30 formulas are catalogued in Chellis's (1951) textbook *Pile Foundations*. Interestingly, the *NCHRP 343 Bridge Foundation Manual*, which is the predecessor to the AASHTO LRFD code makes no mention of dynamic formulae.

TDOT Specifications currently make use of the Engineering News Record formula (originally by Wellington 1892) to estimate pile axial resistance from field driving logs. The formula estimates pile capacity based on the developed hammer energy (E_d), which is the efficiency times the nominal hammer energy, and pile set (s) in inches per blow. The original form of the equation along with the AASHTO (2020) form are presented Table 15. As stated in the commentary to AASHTO (2020) section 10.7.3.8.5, the traditional factor of safety of 6 has been removed from this version of the ENR formula to make it applicable to use with LRFD. Instead, AASHTO requires that a resistance factor of 0.10 be applied to ENR results.

The Gates equation provided in Table 15 was found by Olson and Flaate (1967) to be a more reliable method for predicting pile capacity from pile driving data. They suggested some modification to the original equation, which has evolved to the current form presented by AASHTO (2020). This equation uses the number of blows per inch (N_b) at the end of driving, which is the inverse of the pile set.

Table 15. Dynamic Formulae for Pile Capacity

Method	Original form	AASHTO (2020) form	Comments
ENR	$\left(\frac{2e \cdot E_r}{s+0.1}\right)$	$\left(\frac{12E_d}{s+0.1}\right)$	The results are also affected by the constant in the denominator. Note: E_d in ft-kips, s in inches.
Gates	$0.86\sqrt{e \cdot E_r}\log(10N_b)$	$1.75\sqrt{E_d}\log(10N_b)-100$	Modified based on the work of Olson and Flaate (1967). Gates (1957) publication is not accessible and did not publish the data on which it was based. Note: e = efficiency, E_d in ft-lbs, N_b in blows/inch.

The four equations in Table 15 are plotted in Figure 37 for an assumed hammer energy and a range of pile set values. The original ENR and Gates equations predict similar pile capacities. However, the AASHTO versions predict significantly higher capacities. Figure 38 plots the factored capacity predicted by the AASHTO equations. The Gates equation produces factored capacities that are 1.5 to 3 times higher than ENR.

In general, the AASHTO ENR and Gates formulae do not predict the same nominal capacity. The low resistance factor recommended for the AASHTO ENR equation is partially due to low reliability but also appears to be influenced by an inherent unconservative bias in the ENR formula. The original ENR formula theoretically includes a factor of safety of 6; however, Long, et al. (2009) found that it had an inherent factor of safety slightly over 2.

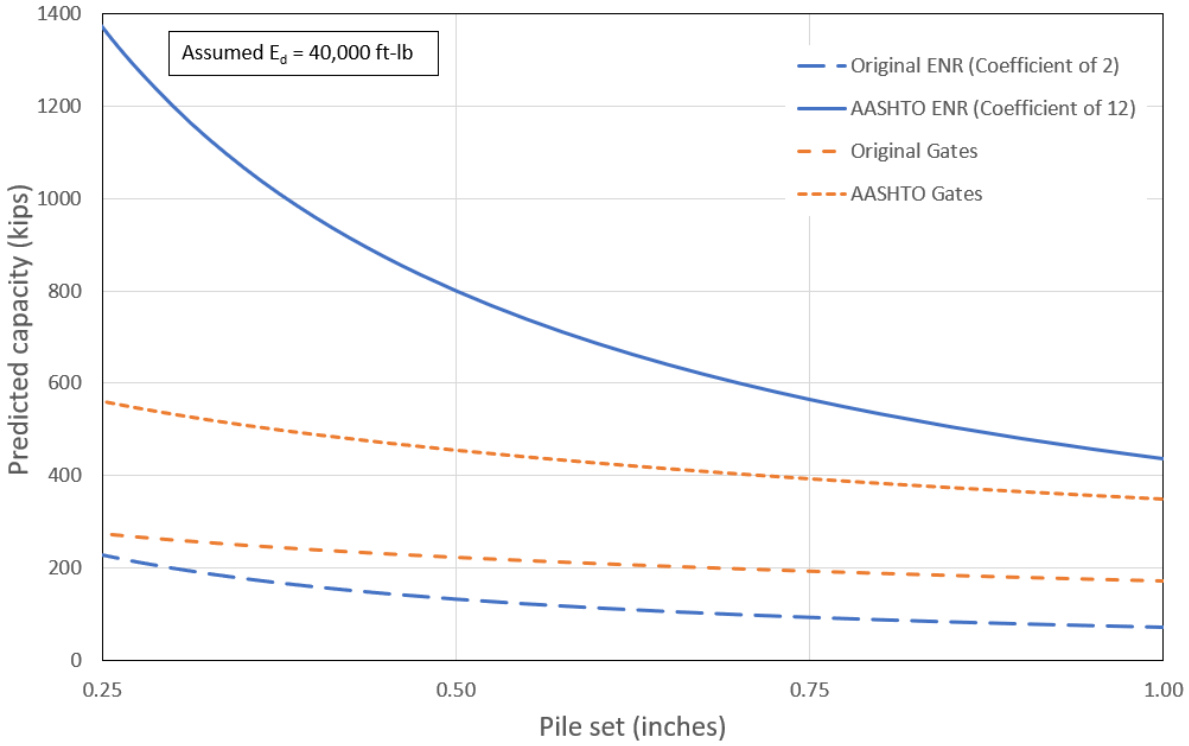

Figure 37. Predicted Nominal Capacity Using the ENR and Gates Pile Driving Formulae

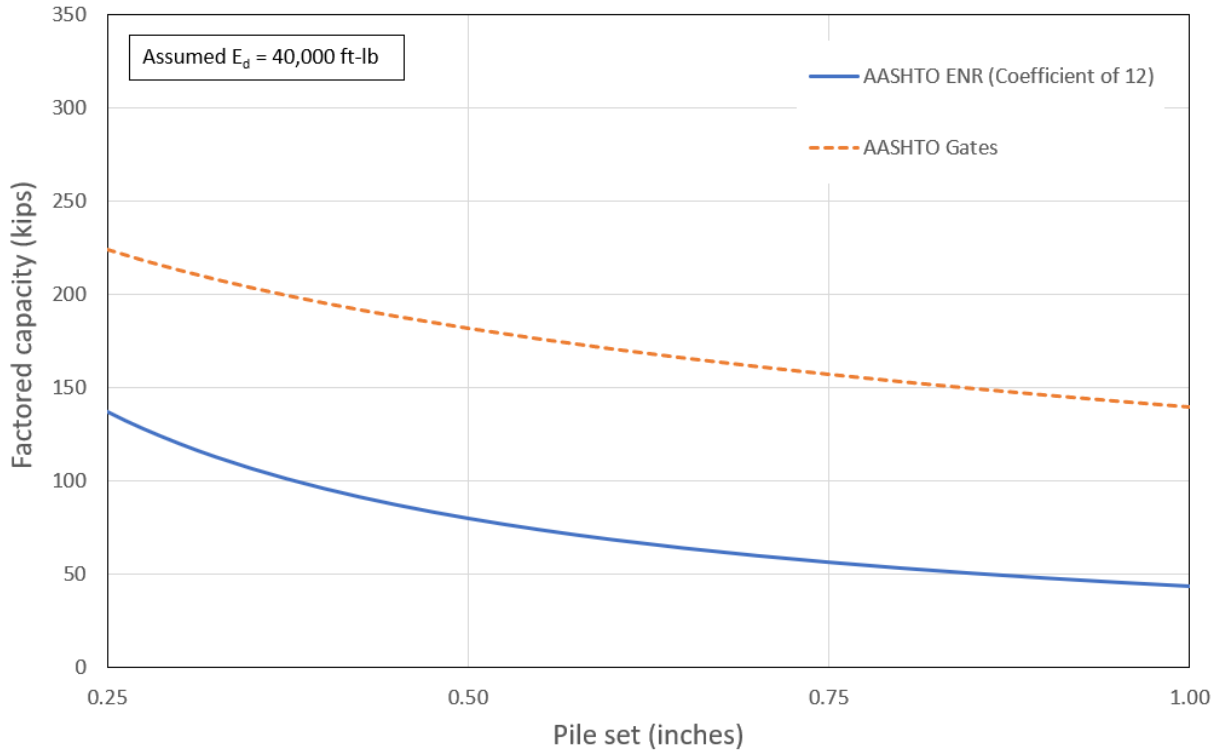

Figure 38. Factored Capacity Using the AASHTO Version of the ENR and Gates Formulae

Appropriate limitations should always be placed on dynamic formulae. These limitations come from the data sets to which the formulae were calibrated. Table 16 lists some important constraints from both the originators of the equations and the codes that apply them. Most importantly, AASHTO (2020) states that dynamic formulae cannot be used as the sole method to measure nominal capacities greater than 600 kips. This translates to maximum factored capacities of 60 kips for the ENR formula and 240 kips for the Modified Gates formula.

Table 16. Limitations of Pile Driving Formulae

Source	Limitation	Implication
Wellington (1892) as quoted in Olson and Flaate	Set should not be less 0.25 inch.	ENR should never be used for nominal capacity greater than 1000 kips and factored capacity greater than 100 kips (assuming $E_d \leq 30$ k-ft).
	Set should preferably greater than 0.5 inch.	ENR should usually be used for nominal capacity less 600 kips and factored capacity less than 60 kips (assuming $E_d \leq 30$ k-ft).

Flaate (1964)	Database of 116 load tests with: • Set: 0.03 to 3 inches • Hammer energy: 8 to 30 k-ft • Load test capacity: 40 to 924 k	Equations based on Flaate's database should not be extrapolated beyond the bounds of the database.
Olson and Flaate (1967), AASHTO Modified Gates	Used same load test data as Flaate (1964) to propose modifications to the Gates formula, which were later adopted into the current form of the Gates equation	Gates should not be used for nominal capacities greater than 900 k and hammer energies greater than about 30 k-ft.
IBC (2018) Section 1810	Do not use *only* dynamic formulae for allowable resistance exceeding 80 kips	Do not use *only* dynamic formulae for nominal capacity exceeding 160 kips (assumes F = 2)
AASHTO (2020) 10.7.3.8.5	Do not use dynamic formulae for nominal resistance exceeding 600 kips.	Do not use the ENR formula for factored resistance exceeding 60 kips or Gates for factored resistance exceeding 240 kips.

3.4.3.4 Dynamic Capacity Analysis – Wave Equation and Instrumentation

Dynamic capacity analysis can also be performed based on the principles of wave propagation as summarized in Table 17. Wave equation analysis (WEAP) is a numerical analysis technique that mimics the physics of the pile driving process. Based on the soil conditions, pile size and type, and hammer properties, the relationship between driving resistance and pile penetration is predicted. WEAP is often used prior to construction to select an appropriate hammer and evaluate drivability. The Case Method uses the results of dynamic force and velocity measurements made on instrumented piles. The resistance of the pile can be estimated in real-time. Signal matching approaches (i.e., CAPWAP) combine the measurements made for the Case Method with WEAP and adjust input parameters until a best-fit to the measured response is obtained.

Table 17. Options for Dynamic Capacity of Driven Piles (NAVFAC, 2024)

Method	**Primarily used…** **during design** **during test installation** **during production installation** **Used to evaluate…**	**Comments**

Wave equation analysis of pile driving (WEAP)	x			Nominal resistance as related to pile penetration	Theoretical behavior based on inputs for the hammer, drive system, pile, and soil
	x			Driveability - evaluating hammer energy and driving stresses	
	x	x	x	Preferred hammer and cushion design	
Case Method with dynamic force and velocity measurements		x	x	Nominal resistance	Output evaluated in real time for every hammer blow
		x	x	Hammer and driving system performance	
		x	x	Driving stresses and pile integrity	
Signal matching with dynamic force and velocity measurements		x	x	Nominal resistance	Involves additional computation based on dynamic measurements. Performed on selected hammer blows for a particular time and penetration. More refined than Case Method
		x	x	Hammer and driving system performance	
		x	x	Driving stresses and pile integrity	

3.4.3.5 Implementation of AASHTO Resistance Factors in the Construction Process

When considering the implementation of different methods for determining pile capacity, the design and construction process must be considered. The implications of AASHTO's methods for estimating nominal pile capacity are compared in Table 18.

Table 18. Implications of Capacity Estimation Method

Timing	**Method**	$\frac{\sum \gamma Q}{n \cdot \eta} \leq$	**Implications**
Before construction	SCA	$(0.25 \text{ to } 0.35) \cdot R_{n,SCA}$	Typically used for initial sizing and constructability considerations but not final installed pile length. Pile length can be
	WEAP	$0.5 \cdot R_{n,WEAP}$	

			adjusted in these methods to obtain the required nominal capacity.
During driving	ENR	$0.1 \cdot R_{n,ENR}$	Pile length can be adjusted during production to obtain the set required by the driving formula to provides the design capacity, $R_{n,PROD}$.
	Gates	$0.4 \cdot R_{n,Gates}$	
	Dynamic testing (2% or 2 piles)	$0.65 \cdot R_{n,DYN}$	Dynamic measurements are used to generate a site-specific driving criterion based on a small number of piles. Pile length can be adjusted per pile to meet the desired $R_{n,DYN}$.
	Dynamic testing (all piles)	$0.75 \cdot R_{n,DYN}$	Dynamic measurements are used to predict the capacity of each production pile. Pile length can be adjusted to meet the desired $R_{n,DYN}$.
After driving test pile	Static load only	$0.75 \cdot R_{n,LT}$	Measured nominal capacity, $R_{n,LT}$, is associated with a particular pile length or set, which cannot be directly used to determine the capacity of piles with different length or set. The number of piles must be changed to satisfy the LRFD inequality, which is problematic for the structural design.
After test pile, during production	Static load + dynamic (2% of piles)	$0.8 \cdot R_{n,LT\&DYN}$	Measured nominal capacity and dynamic measurements are used to generate a site-specific, driving criteria based on a small number of piles. Pile length can be adjusted per pile to meet the desired $R_{n,LT\&DYN}$.

Both static capacity analysis (SCA) and wave equation analysis (WEAP) only use information that is available before construction and are not typically relied upon for final pile length. The driving formulae and dynamic capacity analysis methods allow the pile length to be varied individually in the field in order to meet the minimum nominal pile capacity (total factored load divided by number of piles accounting for group effects). These methods all allow a clear, site-specific driving criterion to be determined that is directly connected to a particular AASHTO φ. The load test *only* approach is allowed by AASHTO but presents practical difficulties because the measured capacity is tied to a particular length and/or pile set, which cannot be directly used to predict capacity of other pile lengths. Finally, as represented by its high resistance factor, the combined use of static load testing and dynamic capacity measurements provides the best method to determine the site-specific driving criterion for a nominal capacity other than $R_{n,LT}$.

3.4.3.6 Current TDOT Approach

TDOT's approach to evaluate the field capacity of piles is summarized in Structural Design Guides 10 and 13 (SDG 10 and SDG13), dated 2023 and 2022 respectively. SDG 10 calculates a required nominal bearing resistance for production piles, $R_{n,prod}$, as:

$$R_{n,prod} = \max \begin{cases} \text{Strength Limit State: } \dfrac{\sum \gamma_i Q_i \text{ per pile}}{0.75} \\ \text{Extreme Event Limit State: } \dfrac{\sum \gamma_i Q_i \text{ per pile}}{1.0} \end{cases} \quad (3.4.3.6\text{-}1)$$

For the strength limit state, the resistance factor of 0.75 comes from the AASHTO case for the static load test only case (see Table 18). The value of $R_{n,prod}$ is listed on the construction drawings as the required bearing resistance for production piles along with estimated pile diameter and length based on static capacity analysis.

At the beginning of construction, a test pile is driven, typically to a depth 10 ft deeper than the design estimate, and the pile set is measured during driving. The final set is used to estimate the nominal resistance of the load test pile as driven using the ENR formula, $R_{n,LT,ENR}$, as:

$$R_{n,LT,ENR} = \frac{2W \cdot H}{s + 0.1} \quad (3.4.3.6\text{-}2)$$

where W is the hammer weight (tons or kips), H is the hammer drop (feet), and s is the set (inches). $R_{n,LT,ENR}$ will have the same units as used for W. This estimate of pile capacity is referred to in SDG 13 as the Driven Load and was originally thought to contain a factor of safety of six.

Next, a static load test is performed on the test pile to allow the use of the 0.75 AASHTO resistance factor. The nominal resistance, $R_{n,LT}$, of the test pile is determined, which is also referred to as the Safe Load.

In SDG 13, a procedure is provided for adjusting the target capacity of the production, as judged using the ENR formula. An adjustment factor, K, is defined as:

$$K = \frac{\text{Safe Load}}{\text{Driven Load}} = \frac{R_{n,LT}}{R_{n,LT,ENR}} \quad (3.4.3.6\text{-}3)$$

The nominal production capacity, as judged using the ENR formula, is then calculated as:

$$R_{n,PROD,ENR} = K\left(\frac{2W \cdot H}{s + 0.1}\right) \qquad (3.4.3.6\text{-}4)$$

In essence, the nominal bearing resistance, $R_{n,PROD}$, is divided by K for use with the ENR formula. SDG 13 indicates that values of K between 0.4 and 1.5 have been observed on TDOT project. The value of K used for the adjustment is limited to a maximum of 1.5 by SDG 13.

For example, suppose that the required nominal capacity on the plans is $R_{n,PROD}$ = 100 tons per pile, which implies that the factored load applied to each pile is 75 tons. Suppose further that the test pile is driven to a set that predicts $R_{n,LT,ENR}$ = 132 tons. Finally assume that the static load test indicates $R_{n,LT}$ = 116 tons using the Davisson method. Using TDOT's approach, the value of K is 0.88 and required nominal capacity for production piles would be estimated by multiplying the value obtained from the ENR formula by 0.88.

In order to evaluate TDOT's approach, published load test data on steel piles was obtained from Long et al. (2009), which includes data from Flaate (1964). This data is plotted in Figure 39. Note that some of the data uses the Wisconsin DOT version of the ENR formula, which produces capacities that are 10 to 20% lower than Equation 3.4.3.6-2.

TDOT's adjustment approach assumes that the load test and ENR equation have a proportional relationship. Such a trend would pass through the origin, as shown by the solid lines in Figure 39. However, the data does not fit a clearly linear trend through the origin. Because the relationship between set and capacity is nonlinear, simply scaling the set is also not likely to produce more accurate results.

The 189 tests plotted in Figure 39 all have values of K greater than 1. This means that ENR formula (as presented in Equation 3.4.3.6-2) was always at or below the capacity predicted by the load test. However, SDG 13 indicates that K may be as low as 0.4, which does not seem to align with the broader experience presented in Figure 39. The plotted data suggest that the required nominal capacity for production piles should never need to be increased based on the comparison between the load test and ENR capacities.

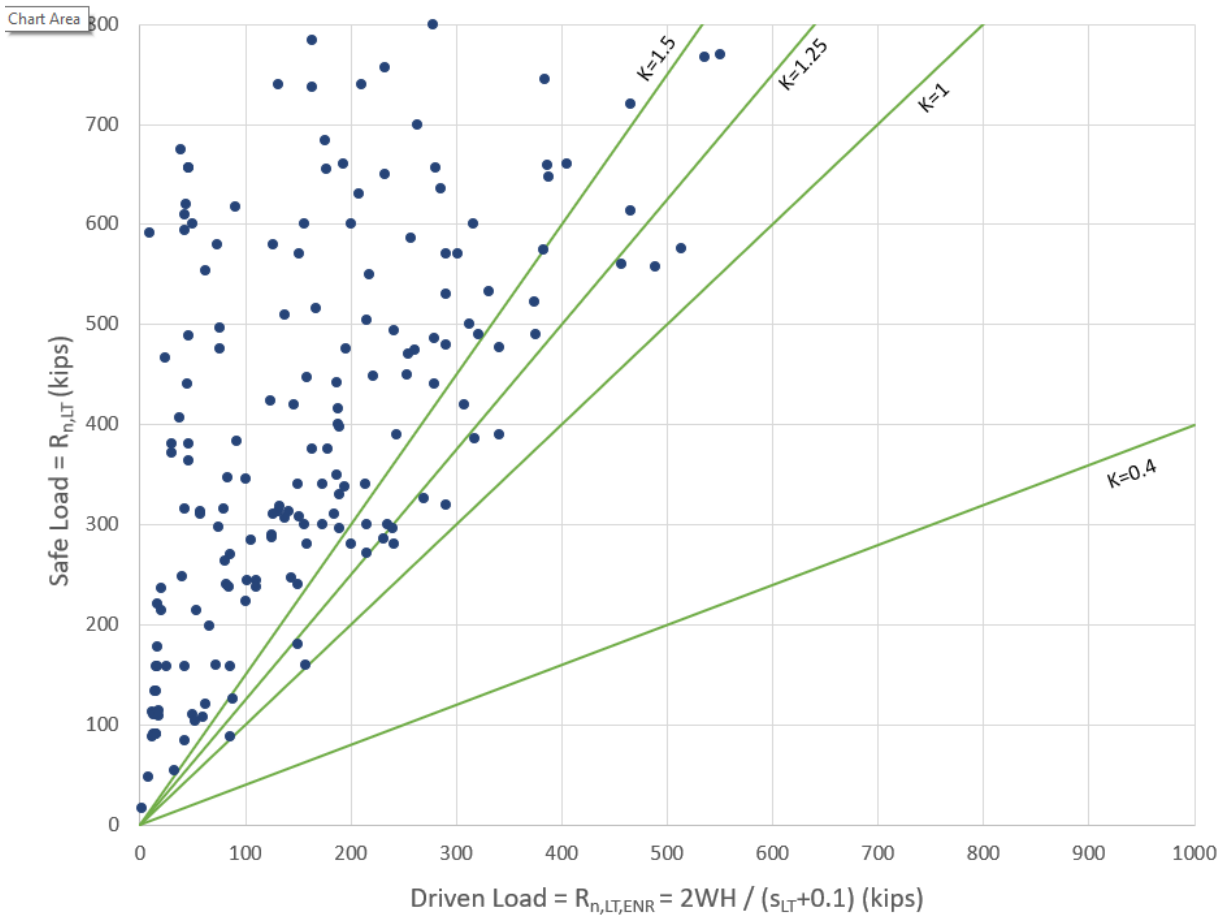

Figure 39. Comparison of Nominal Pile Resistance Measured by Load Tests and the ENR Formula

One explanation for this difference may be evident in the quick load test data presented in SDG 13. The load test data in that example is nearly parallel to the elastic pile deflection lines. This indicates that much of the pile's resistance has not been mobilized during the example load test and the nominal resistance from the load test is much too low. If $R_{n,LT}$ (Safe Load) is under-measured, the value of K will be unrealistically low. This will likely be the case any time that the load-settlement curve from the load test does not intersect with the offset limit line.

As K increases, the nominal capacity for production piles predicted by Equation 3.4.3.6-4 increases. From Figure 39, TDOT's limit on K of 1.5 plots falls near the upper end of the typical data, which means that K values less than 1.5 have rarely been measured in other studies. Thus, the value of 1.5 should be relatively conservative. Long et al. (2009) found that the original ENR formula (Equation 3.4.3.6-2) has a factor of safety of about 2, which would correspond to K = 2, on average.

The following conclusions can be drawn regarding TDOT's current approach:

- Use of the adjustment factor, K, less than or equal to 1.5 may not be theoretically correct. However, this approach should provide predictions of nominal pile resistance that are safe.
- Based on the data from other sources, values of K less than 1 should be questioned. If the resistance measured in the static load test is less than predicted by the ENR formula, the static load test data should be scrutinized. If the static load test does not cross the Davisson offset limit line, then the pile was not loaded to failure and the predicted resistance is too low. The load test should be repeated to higher loads, or a value of K = 1 should be used.
- The adjustment approach may be substantially underestimating pile resistance. In order to determine the degree to which this is true, TDOT's pile load test data would need to be scrutinized more closely, which is beyond the scope of this project.

Chapter 4 Results and Discussion

4.0 Design Recommendations

The following sections summarize design recommendations for each type of substructure:

- Hollow Tube Pile Bents (HTPB)
- Concrete Filled Steel Tube Pile Bents (CFST)
- Reinforced Concrete Filled Steel Tube Pile Bents (RCFST)

For HTPB and CFST construction, the bent cap width shall be no less than twice the outside diameter of the steel tube, D.

The first step in the design process, regardless of which of the three construction methods has been selected, is to obtain an initial estimate for tube size based on the Strength limit state pile axial load. One method of obtaining a first estimate is to select a tube size with:

- an area, A_s, no less than that given by Equation 4-1
- a radius of gyration, r, no less than that given by Equation 4-2
- a D/t value no greater than 36 for HTPB, or 72 for CFST and RCFST

Equation 4-1 is based on a driving load no larger than 35% of 50 ksi. Equation 4-2 is based on the limiting slenderness for flexural-dominant members in the AASHTO Guide Specification for LRFD Seismic Bridge Design (AASHTO, 2011), again assuming a yield stress of 50 ksi.

$$A_s \geq \frac{P_u}{17.5} \tag{4-1}$$

$$r \geq 0.02H_C \tag{4-2}$$

Table 19 (CFST) and Table 20 (HTPB) will prove helpful in this initial estimate. Suppose the estimated Strength limit state pile load is 280 kips and the bent height from cap soffit to in-ground fixity, H_C = 25 feet. The required area is 16.0 in^2. The required radius of gyration is 6.00 inches. For HTPB construction, select a HTPB18-0500 tube (the radius of gyration controls). For CFST or RCFST construction, select a CFST18-0312 tube.

Note that the Extreme Event limit state may eventually control the required driving load and a subsequent adjustment in the tube size.

Driving conditions may at times be so favorable as to require less tube area to achieve the required load. Drivability analyses would generally be required to justify such measures.

Strength limit state axial load and flexural interaction must include resistance factors less than 1.0. Strength limit state resistance factors appropriate for design are found in the AASHTO LRFD Bridge Design Specifications, Section 6.5.4.2:

ϕ = 0.90 for CFST, 0.80 for HTPB

Table 19. CFST Tube Selection Table

Tube	D, inches	t, inches	D / t	A, in^2	r, in.
CFST12-0203	12	0.203	59.1	7.52	4.17
CFST12-0219	12	0.219	54.8	8.11	4.17
CFST12-0250	12	0.250	48.0	9.23	4.16
CFST12-0312	12	0.312	38.5	11.46	4.13
CFST12-0375	12	0.375	32.0	13.70	4.11
CFST14-0219	14	0.219	63.9	9.48	4.87
CFST14-0250	14	0.250	56.0	10.80	4.86
CFST14-0312	14	0.312	44.9	13.42	4.84
CFST14-0375	14	0.375	37.3	16.05	4.82
CFST14-0500	14	0.500	28.0	21.21	4.78
CFST16-0250	16	0.250	64.0	12.37	5.57
CFST16-0312	16	0.312	51.3	15.38	5.55
CFST16-0375	16	0.375	42.7	18.41	5.53
CFST16-0500	16	0.500	32.0	24.35	5.48
CFST18-0250	18	0.250	72.0	13.94	6.28
CFST18-0312	18	0.312	57.7	17.34	6.25
CFST18-0375	18	0.375	48.0	20.76	6.23
CFST18-0500	18	0.500	36.0	27.49	6.19
CFST20-0312	20	0.312	64.1	19.30	6.96
CFST20-0375	20	0.375	53.3	23.12	6.94
CFST20-0500	20	0.500	40.0	30.63	6.90
CFST20-0625	20	0.625	32.0	38.04	6.85
CFST24-0375	24	0.375	64.0	27.83	8.35
CFST24-0500	24	0.500	48.0	36.91	8.31
CFST24-0625	24	0.625	38.4	45.90	8.27
CFST24-0750	24	0.750	32.0	54.78	8.22
CFST30-0500	30	0.500	60.0	46.34	10.43
CFST30-0625	30	0.625	48.0	57.68	10.39
CFST30-0750	30	0.750	40.0	68.92	10.34
CFST30-1000	30	1.000	30.0	91.11	10.26
CFST36-0500	36	0.500	72.0	55.76	12.55
CFST36-0625	36	0.625	57.6	69.46	12.51
CFST36-0750	36	0.750	48.0	83.06	12.47
CFST36-1000	36	1.000	36.0	109.96	12.38

Table 20. HTPB Tube Selection Table

Tube	D, inches	t, inches	D / t	A, in^2	r, in.
HTPB12-0375	12	0.375	32.0	13.70	4.11
HTPB14-0500	14	0.500	28.0	21.21	4.78
HTPB16-0500	16	0.500	32.0	24.35	5.48
HTPB18-0500	18	0.500	36.0	27.49	6.19
HTPB20-0625	20	0.625	32.0	38.04	6.85
HTPB24-0750	24	0.750	32.0	54.78	8.22
HTPB30-1000	30	1.000	30.0	91.11	10.26
HTPB36-1000	36	1.000	36.0	109.96	12.38

4.1 Hollow Tube Pile Bent (HTPB) Design Procedure

Tubes in HTPB construction shall have D/t ratio no larger than 36.5 without approval of the Director of Structures. HTPB construction shall incorporate a top concrete plug for connection to the cap beam. The top plug shall include embedment of the tube and an annular ring. The ring shall be the same thickness as the tube and shall have a width equal to 16 times the tube thickness. The annular ring shall be centered on the tube wall and welded to the top of the tube using a complete joint penetration (CJP) weld.

Step 1. Determine the moment at first yield from Equation 4.1-1.

$$M_{y1} = \left(F_y - \frac{P_u}{A_s}\right) S_s \tag{4.1-1}$$

Step 2. Determine the location of the point of contraflexure in the piles.

Use the over-strength plastic moment of the tube alone, M_{PO2}, for the in-ground hinge. Use the overstrength plastic moment for the tube with concrete fill, M_{PO1}, for the top hinge. Use the expected yield strength of the tube, F_{yE}. Use the confined, expected strength of the concrete fill, f'_{CC}. Locate the contraflexure point, L_{C1}, measured from the top of bottom of the cap. The expressions for α_θ, f'_l, and f'_{CC} are reported in the literature, page 36 (Stephens M. T., 2016).

$$\alpha_\theta = 0.138 - 0.00174(D/t) \tag{4.1-2}$$

$$f_l^{'} = \alpha_\theta F_{yE} \left(\frac{2}{D/t - 2}\right) \tag{4.1-3}$$

$$f_{cc}^{'} = f_{cE}^{'} \left(2.254 \sqrt{1 + \frac{7.94 f_l^{'}}{f_{cE}^{'}}} - 1.254 - 2\frac{f_l^{'}}{f_{cE}^{'}}\right) \tag{4.1-4}$$

$$L_{C1} = H_C\left(\frac{M_{PO1}}{M_{PO1} + M_{PO2}}\right) \tag{4.1-5}$$

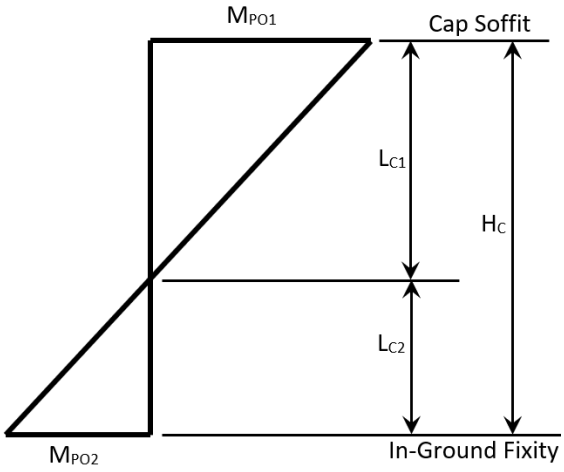

Figure 40. Assumed Moment Diagram - HTPB

Step 4. Determine the transverse plastic shear, V_{PO}, for the bent.

$$V_{PO} = \frac{1.2M_{PO1}}{L_{C1}} \times no.of\ piles \tag{4.1-6}$$

Step 5. Ensure that the shear resistance, V_n, is greater than V_{PO}.

Determine V_n from the AASHTO LRFD-BDS, section 6.12.1.2.3b, as shown in Equation 4.1-7. L_v is to be taken as the larger of L_{C1} and L_{C2} and must be expressed in inches in Equation 4.1-7.

$$V_n = 0.5A_g\left(Max\begin{cases}\dfrac{1.6E}{\sqrt{\dfrac{L_v}{D}}\left(\dfrac{D}{t}\right)^{1.25}} \le 0.58F_{yE} \\ \dfrac{0.78E}{\left(\dfrac{D}{t}\right)^{1.50}} \le 0.58F_{yE}\end{cases}\right) \tag{4.1-7}$$

Step 6. Determine the transverse displacement capacity.

Determine the displacement capacity, δ_{uT1}, between the point of zero moment and the top plastic hinge using Equation 4.1-8 with k_Δ taken from Chapter 3 for the CFST tube in question. Determine the displacement capacity, δ_{uT2}, between the point of zero moment and the in-ground hinge using Equation 4.1-9 with k_Δ taken from Chapter 3 for the HTPB tube in question. Analyses should be performed for both the specified and expected yield stress values. As a lower-bound approximation, take the displacement capacity equal to the least of those obtained. Note that this is based on a pseudo-first-yield displacement for the top hinge (with concrete plug) since the area and section modulus of the tube alone are to be used.

$$\delta_{uT1} = k_{\Delta} \frac{(1/2)\left(M_{y1} + M_{PO1}\right) L_{C1}^2}{3EI_s} \tag{4.1-8}$$

$$\delta_{uT2} = k_{\Delta} \frac{(1/2)\left(M_{y2} + M_{PO2}\right) L_{C2}^2}{3EI_s} \tag{4.1-9}$$

The total displacement capacity in the transverse direction is $\Delta_{uT} = \delta_{uT1} + \delta_{uT2}$.

Step 7. Determine the displacement capacity in the longitudinal direction.

The longitudinal displacement capacity, Δ_{uL}, may be estimated from Equation 4.1-9 with k_{Δ} = taken for the HTPB tube in question and $L_{C2} = H_C$.

Step 8. Determine the displacement capacity ratio for the bent by Equation 4.1-10.

$$\frac{\Delta_{EQ}}{\Delta_u} = \sqrt{\left(\frac{\Delta_{EQ-T}}{\Delta_{uT}}\right)^2 + \left(\frac{\Delta_{EQ-L}}{\Delta_{uL}}\right)^2} \tag{4.1-10}$$

The seismic displacements, $\Delta_{EQ\text{-}T}$ and $\Delta_{EQ\text{-}L}$, shall be transformed to the local bent transverse and longitudinal axes and shall be amplified by R_d when the natural period is short enough to require displacement amplification by the AASHTO-GS Section 4.3.3.

Step 9. Design the cap.

Apply the over-strength plastic shear, V_{PO} from Step 4, as a static load to the model of the cap (most likely, in LEAP). Ensure that the cap reinforcement is capable of resisting the resulting shears and moments as a capacity-protected element.

Step 10. Determine the required embedment, L_e, of the tube and the required cap dimensions.

Equation 4.1-11 gives the required embedment, L_e, of the tube into the cap beam. Equation 4.1-12 gives the required total cap beam depth, h. Equation 4.1-13 gives the required thickness of concrete above the tube, h_{top}. Ensure that details accommodate the required embedment and total depth. In the equations, F_{us} is the tensile strength of the tube steel. In the absence of more reliable data, take $F_{us} = 1.4F_{yE}$. The 5.27 factor in Equation 4.1-11 and the 2.80 factor in Equation 4.1-12 are necessary to accommodate units of ksi for F_{us} and f'_c in the equations. D_o is the outer diameter of the embedded annular ring and is equal to the tube diameter, D, plus 16 times the tube thickness. For this calculation, f'_c is the concrete strength of the cap concrete, not the tube fill. $C_c + C_s$ is the total compressive cross-sectional load from a section analysis at the Extreme Event Limit State. P_{STR} is the Strength Limit State axial load in the pile. b' is the least of the cap width or 2.5 times the tube diameter. The distance from the point of contraflexure in the tube to the center of the embedded portion is e.

$$L_e = Max\begin{Bmatrix} \sqrt{\frac{D_o^2}{4} + \frac{5.27DtF_{us}}{\sqrt{f_c'}}} - \frac{D_o}{2} \\ \frac{(M_{pE}/e)\left(1 + \sqrt{1 + \frac{12.24f_c'b'e^2}{M_{pE}}}\right)}{1.7f_c'b'} + 3" \end{Bmatrix} \quad (4.1\text{-}11)$$

$$h \geq \sqrt{\frac{D^2}{4} + \frac{2.80(C_c + C_s)}{\sqrt{f_c'}}} - \frac{D}{2} \quad (4.1\text{-}12)$$

$$h_{top} \geq 3 + \sqrt{\frac{D^2}{4} + \frac{2.80P_{STR}}{\sqrt{f_c'}}} - \frac{D}{2} \quad (4.1\text{-}13)$$

The cap width shall be no less than 2 times the tube diameter.

Provide joint reinforcement in the cap A_s^{jv} = 0.65 times the tube cross-sectional area. Also note that not all of the cap longitudinal bars need to be interrupted by the tube, as shown in the second figure.

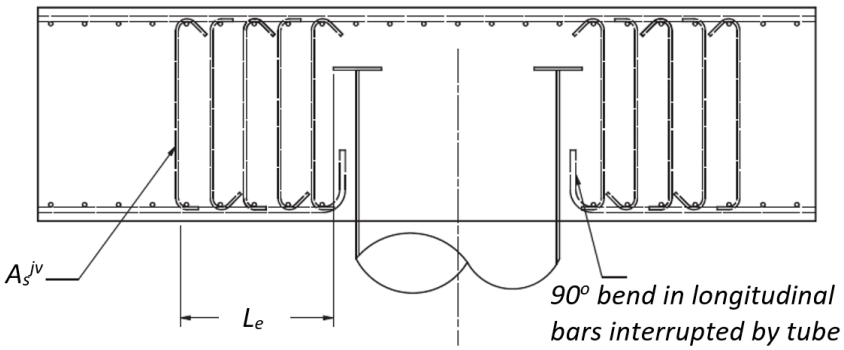

Figure 41. Cap Joint Reinforcement - HTPB

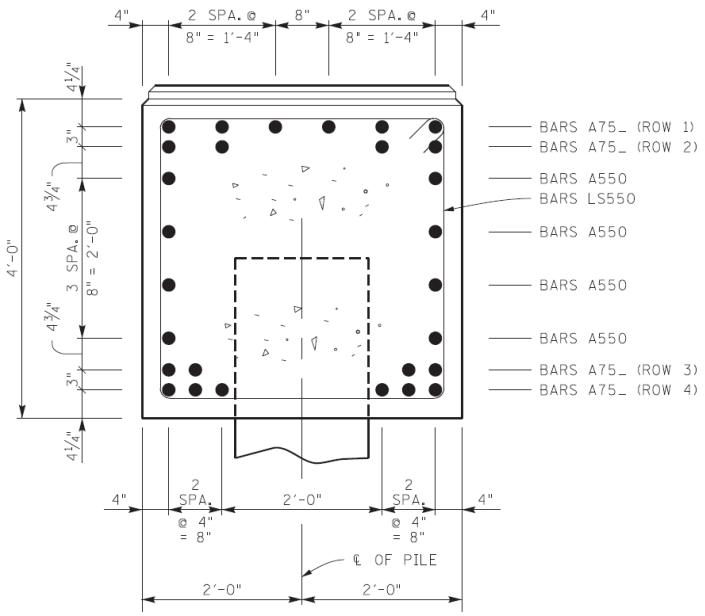

Figure 42. Cap Longitudinal Reinforcement - HTPB

Step 11. Determine the extent of concrete fill in the tubes, x_2.

$$x_2 = L_{C1}\left(1 - \frac{M_{PO2}}{2M_{PO1}}\right) \tag{4.1-14}$$

The plug shall extend to the point at which the flexural demand is one-half of the flexural capacity of the tube alone. Provide a concrete plug which extends to a distance equal to x_2 below the cap soffit.

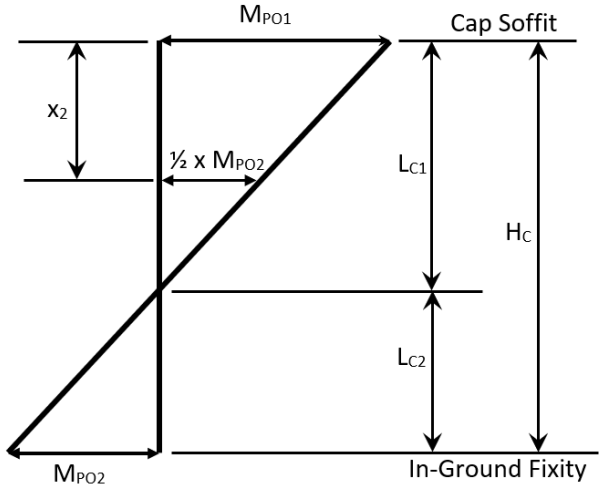

Figure 43. Concrete Fill Limits - HTPB

Step 12. Ensure that Guide Specification Article 4.11.5 P-Delta requirements are satisfied.

$$\Delta_r \leq \frac{0.25M_n}{P_{dl}} \quad (4.1\text{-}15)$$

In Equation 5.1-14, M_n is the nominal resistance of the CFST (top hinge) or HTPB (in-ground hinge) and P_{dl} is the unfactored dead load on the CFST. Δ_r is the relative lateral offset between points of zero moment and maximum moment.

In lieu of Steps 1-11, a detailed analysis may be warranted in some cases to mitigate insufficiencies indicated in Steps 1 through 11. Whenever a detailed pushover analysis by computer is used, determine ε_{cr}, the limiting strain in the hollow tube portion of the piles.

Based on the work of (Rotter & Sadowski, 2017) use Equation 4.1-16a to establish critical buckling strains for pushover analysis when detailed analysis is warranted. A less conservative critical strain limit was proposed by (Fulmer, Kowalsky, & Nau, 2012) in Equation 4.1-16b. Equation 4.1-16(c) (Murphy, et al., 2020) is recommended for critical structures and when design for operational is warranted by the Director of Structures. The buckling strain will be required for the necessary pushover analysis when employed to justify tubes with D/t values larger than 36.5.

$$\varepsilon_{cr} = \frac{0.400}{\left(D/t\right)^{1.02}} \quad (4.1\text{-}16a)$$

$$\varepsilon_{cr} = \frac{0.69018}{\left(D/t\right)^{1.0893}} \quad (4.1\text{-}16b)$$

$$\varepsilon_{cr} = 0.021 - \frac{D/t}{9{,}100} \quad (4.1\text{-}16c)$$

Refer to Section 3.3 for appropriate software settings in a refined analysis by computer.

While not as rigorously tested as the annular ring connection, at the discretion of the Structures Director, the tube may be embedded sufficiently to allow flexure in the tube to be transferred to the cap through bearing couples on the sides of the tube-cap interface, as mentioned in the literature review of studies by Marcakis and Mitchell (1980), and by Rollins and Stenlund (2008). Equation 2-14 is to be used when this method of embedment is employed.

4.2 Concrete Filled Steel Tube (CFST) Design Procedure

The procedure for CFST bents is similar to that outlined for HTPB construction. CFST construction shall be limited to tubes with D/t no greater than 0.15E/F_y. The k_Δ values in Chapter 3 for CFST are more advantageous compared to those for HTPB and the displacement at first yield is not a true yield displacement, but a pseudo-first-yield. This is due to the fact that the reported k_Δ values are based on a hand-calculated yield based on the properties of the tube alone.

Step 1. Determine the average of the moment at first yield, M_{y1}, and the nominal flexural resistance, M_n, from Equation 4.2-1. ***CFST-Analysis.xlsx*** may be used to determine M_n.

$$M = \frac{M_{y1} + M_n}{2} = \frac{\left(F_y - \frac{P_u}{A_s}\right) S_s + M_n}{2} \tag{4.2-1}$$

Step 2. Determine the location of the point of contraflexure in the piles.

Use the overstrength plastic moment of the tube with concrete fill for the top hinge, M_{PO1}, and the in-ground hinge, M_{PO2}. Use the expected yield strength of the tube, F_{yE}. Use the confined, expected strength of the concrete fill, f'_{CC}. Locate the contraflexure point, L_{C1}, measured from the top of bottom of the cap. The expressions for α_θ, f'_l, and f'_{CC} are reported in the literature, page 36 (Stephens M. T., 2016).

$$\alpha_\theta = 0.138 - 0.00174(D/t) \tag{4.2-2}$$

$$f_l^{'} = \alpha_\theta F_{yE} \left(\frac{2}{D/t - 2}\right) \tag{4.2-3}$$

$$f_{cc}^{'} = f_{cE}^{'} \left(2.254 \sqrt{1 + \frac{7.94 f_l^{'}}{f_{cE}^{'}}} - 1.254 - 2\frac{f_l^{'}}{f_{cE}^{'}}\right) \tag{4.2-4}$$

$$L_{C1} = \frac{H_C}{2} \tag{4.2-5}$$

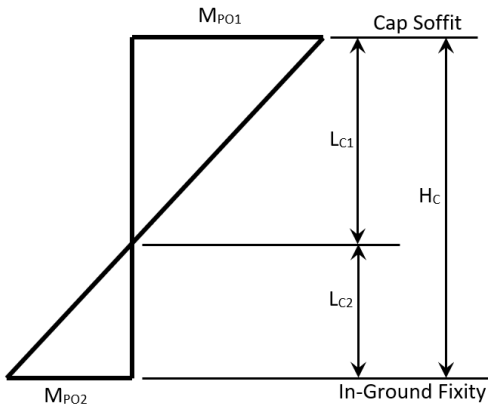

Figure 44. Moment Diagram - CFST

Step 4. Determine the transverse plastic shear, V_{PO}, for the bent.

$$V_{PO} = \frac{1.2M_{PO1}}{L_{C1}} \times no.of\ piles \tag{4.2-6}$$

Step 5. Ensure that the shear resistance, V_n, is greater than V_{PO}.

Determine V_n from the AASHTO LRFD-BDS, section 6.12.3.2, as shown in Equation 4.2-7a. Alternatively, Equation 4.2.7b, from the Washington State Bridge Design Manual, may be used. In Equation 4.2-7b, recommended values for the constants are $g_1 = 2.0$, $g_2 = 0.50$, $g_3 = 3.0$, and $g_4 = 1.0$.

$$\phi V_n = \phi(V_s + V_c) = \phi\left[\frac{2Dt}{\sqrt{3}}F_{yE} + 0.1896\sqrt{f'_{cE}}A_c\right] \tag{4.2-7a}$$

$$\phi V_n = \phi g_4\left[g_1\left(0.6F_{yE}\,g_2A_s\right) + 0.0316g_3A_c\sqrt{f'_{cE}}\right] \tag{4.2-7b}$$

Step 6. Determine the transverse displacement capacity.

Determine the displacement capacity, Δ_{uT}, using Equation 4.2-8 with k_Δ taken from Chapter 3 for the CFST tube in question. Analyses should be performed for both the specified and expected yield stress values. As a lower-bound approximation, take the displacement capacity equal to the least of those obtained. Note that this is based on a pseudo-first-yield displacement for both hinges since the area and section modulus of the tube alone are to be used.

$$\delta_{uT} = k_\Delta \frac{M_{y1}H_C^2}{6EI_s} \tag{4.2-8}$$

Step 7. Determine the displacement capacity in the longitudinal direction.

The longitudinal displacement capacity, Δ_{uL}, may be estimated from Equation 4.2-9 with k_Δ = taken for the CFST tube in question.

$$\delta_{uL} = k_\Delta \frac{M_{y1}H_C^2}{3EI_s} \tag{4.2-9}$$

Step 8. Determine the displacement capacity ratio for the bent by Equation 4.2-10.

$$\frac{\Delta_{EQ}}{\Delta_u} = \sqrt{\left(\frac{\Delta_{EQ-T}}{\Delta_{uT}}\right)^2 + \left(\frac{\Delta_{EQ-L}}{\Delta_{uL}}\right)^2} \tag{4.2-10}$$

The seismic displacements, $\Delta_{EQ\text{-}T}$ and $\Delta_{EQ\text{-}L}$, shall be transformed to the local bent transverse and longitudinal axes and shall be amplified by R_d when the natural period is short enough to require displacement amplification by the AASHTO-GS Section 4.3.3.

Step 9. Design the cap.

Apply the over-strength plastic shear, V_{PO} from Step 4, as a static load to the model of the cap (most likely, in LEAP). Ensure that the cap reinforcement is capable of resisting the resulting shears and moments as a capacity-protected element.

Step 10. Determine the required embedment, L_e, of the tube and the required total cap depth, h.

Equation 4.2-11 gives the required embedment, L_e, of the tube into the cap beam. Equation 4.2-12 gives the required total cap beam depth, h. Equation 4.2-13 gives the required thickness of concrete above the tube, h_{top}. Ensure that details accommodate the required embedment and total depth. In the equations, F_{us} is the tensile strength of the tube steel. In the absence of more reliable data, take F_{us} = 1.4F_{yE}. The 5.27 factor in Equation 4.2-11 and the 7.91 factor in Equation 4.2-12 are necessary to accommodate units of ksi for F_{us} and f'_c in the equations. D_o is the outer diameter of the embedded annular ring and is equal to the tube diameter, D, plus 16 times the tube thickness. For this calculation, f'_c is the concrete strength of the cap concrete, not the tube fill. C_c + C_s is the total compressive cross-sectional load from a section analysis at the Extreme Event Limit State. P_{STR} is the Strength Limit State axial load in the pile. b′ is the least of the cap width or 2.5 times the tube diameter. The distance from the point of contraflexure in the tube to the center of the embedded portion is e.

$$L_e = Max\left\{\begin{array}{l}\sqrt{\frac{D_o^2}{4}+\frac{5.27DtF_{us}}{\sqrt{f_c'}}}-\frac{D_o}{2} \\ \dfrac{\left(M_{pE}/e\right)\left(1+\sqrt{1+\dfrac{12.24f_c'b'e^2}{M_{pE}}}\right)}{1.7f_c'b'}+3"\end{array}\right. \quad (4.2\text{-}11)$$

$$h \geq \sqrt{\frac{D^2}{4}+\frac{2.80(C_c+C_s)}{\sqrt{f_c'}}}-\frac{D}{2} \quad (4.2\text{-}12)$$

$$h_{top} \geq 3+\sqrt{\frac{D^2}{4}+\frac{2.80P_{STR}}{\sqrt{f_c'}}}-\frac{D}{2} \quad (4.2\text{-}13)$$

The cap width shall be no less than 2 times the tube diameter.

Provide joint reinforcement in the cap A_s^{jv} = 0.65 times the tube cross-sectional area in order to justify the dimensional requirements for the cap. Also note that not all of the cap longitudinal bars need to be interrupted by the tube, as shown in the second figure.

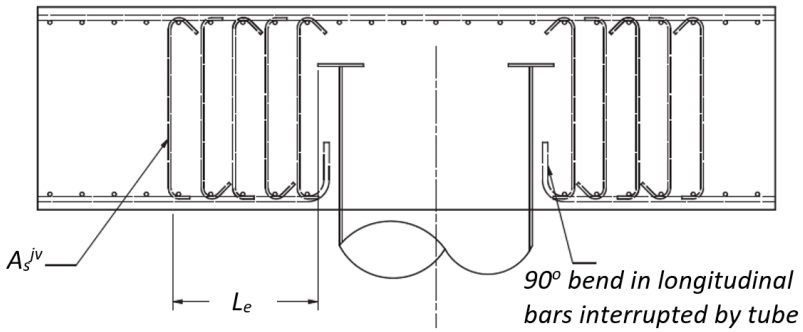

Figure 45. Cap Joint Reinforcement - CFST

While not as rigorously tested as the annular ring connection, at the discretion of the Structures Director, the tube may be embedded sufficiently to allow flexure in the tube to be transferred to the cap through bearing couples on the sides of the tube-cap interface, as mentioned in the literature review of studies by Marcakis and Mitchell (1980), and by Rollins and Stenlund (2008). Equation 2-14 is to be used when this method of embedment is employed.

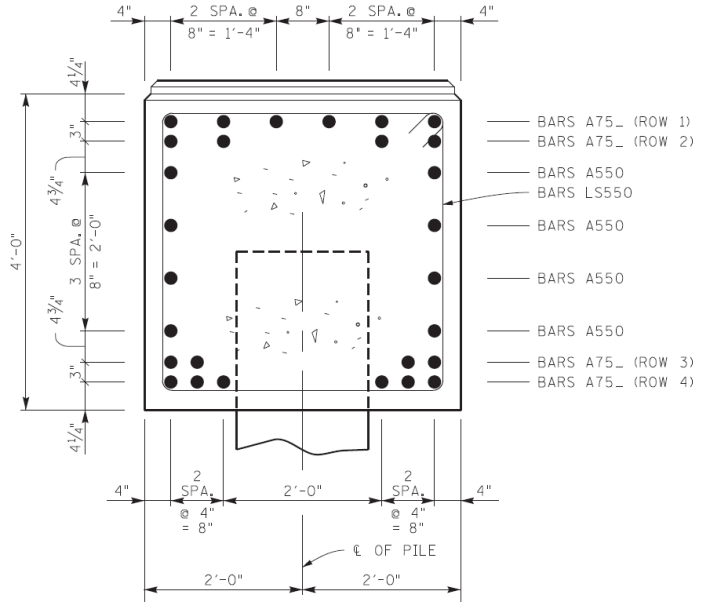

Figure 46. Cap Longitudinal Reinforcement - CFST

Step 11. Determine the extent of concrete fill in the tubes, x_1.

$$x_1 = L_{C2}\left(1 - \frac{M_{PO2}}{2M_{PO1}}\right) \qquad (4.2\text{-}14)$$

Provide concrete fill which extends to a distance equal to x_1 below the equivalent point of fixity below ground. In Equation 4.2-14, M_{PO1} is the plastic moment of the CFST and M_{PO2} is the plastic moment of the tube alone, without fill.

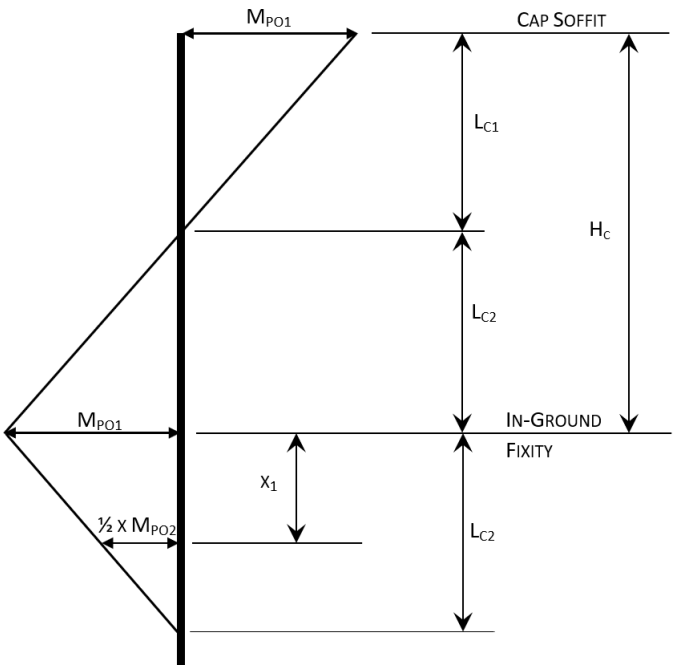

Figure 47. Concrete Fill Limits - CFST

Step 12. Ensure that Guide Specification Article 4.11.5 P-Delta requirements are satisfied.

$$\Delta_r \leq \frac{0.25M_n}{P_{dl}} \qquad (4.2\text{-}15)$$

In Equation 4.2-15, M_n is the nominal resistance of the CFST and P_{dl} is the unfactored dead load on the CFST. Δ_r is the relative lateral offset between points of zero moment and maximum moment.

In lieu of Steps 1-11, a detailed analysis may be warranted in some cases to mitigate insufficiencies indicated in Steps 1 through 11. Whenever a detailed pushover analysis by computer is used, use ε_{cr}, the limiting strain in the tube, equal to 0.025. Use the Mander model for confined concrete.

Refer to Section 3.3 for appropriate software settings in a refined analysis by computer.

4.3 Reinforced Concrete Filled Steel Tubes (RCFST)

RCFST design requires that a section analysis be performed. The cross-section at the bottom of the cap beam is a reinforced concrete section confined by the tube. The following guidelines from the Alaska research shall be followed in RCFST construction.

- The cap beam width shall be no less than 1.5 times the diameter of the RCFST.
- The cap beam depth shall be large enough to permit straight bar development of the RCFST longitudinal reinforcement into the cap. The required development for a bar of diameter d_{bl} and expected yield stress f_{ye} is given in the AASHTO Guide Specification for LRFD Seismic Bridge Design (AASHTO, 2011) (AASHTO-GS) and is given here as Equation 4.3-1.
- A column reinforcement ratio, ρ_l, of no more than 4% shall be used. The column reinforcement should preferably be no more than 2% to prevent congestion.
- Confinement reinforcement in the plastic hinge region at the top of the piles shall be determined in accordance with Equation 4.3-2. The steel shell may be relied upon to provide the confinement.
- A two-inch gap between the top of the pile and the cap beam soffit shall be specified to preclude damage to the cap.
- For the RCFST construction tested, special shear reinforcement "will not generally be required" in the columns.
- Cap beam reinforcement shall be sufficient to remain elastic even when accounting for strain hardening and expected yield levels in the column longitudinal reinforcing.
- At least 75% of the bottom cap beam reinforcing shall be continuous through the column region. This may be accomplished using side bars in the cap.
- Cap beam depth shall be in the range of *D* to (*D* + 6 inches).
- Joint principal stresses shall be evaluated in accordance with the AASHTO-GS, Section 8.13.
- Concrete fill in the pipe piles shall extend beyond the in-ground hinge to a depth where the moment is less than 50% of the steel shell yield moment. This is to prevent local buckling in regions where concrete fill below grade has been terminated.
- A maximum displacement ductility of 4 is recommended for design.

$$l_{ac} = \frac{0.79 d_{bl} f_{ye}}{\sqrt{f_c'}} \tag{4.3-1}$$

$$\rho_s = \frac{4A_{sp}}{D's} = 0.16\frac{f_{ce}'}{f_{ye}}\left(0.5 + \frac{1.25P}{f_{ce}'A_g}\right) + 0.13(\rho_l - 0.01) \tag{4.3-2}$$

Figure 2-6 depicts an example for RCFST construction from the Gakona River Bridge in Alaska.

One distinctive feature of RCFST construction lies in the large discrepancy between plastic moments for the top hinge (reinforced concrete section highly confined by the tube) and the in-ground hinge (steel tube with concrete fill). The in-ground hinge will typically have a much

larger plastic moment capacity. This means that the top hinge will likely undergo several inelastic cycles while the in-ground structure remains elastic during strong ground shaking.

For RCFST construction, the Mander model for confined concrete may be used in conjunction with approximate equations for displacement capacity based on plastic hinge length and strain penetration. Equations 4.3-3 through 4.3-9 summarize the relationships necessary to obtain approximate displacement capacity estimates for RCFST top hinges. Design Example No. 9 illustrates the procedure.

- A_{sp} is the cross-sectional area of the transverse reinforcement
- D' is the core diameter measured to the centerline of the transverse reinforcement
- s is the spacing of the transverse reinforcement
- f'_l is the confining pressure provided by the transverse reinforcement
- f'_{co} is the compressive strength of the unconfined concrete, usually taken as $f'_{ce} = 1.3\,f'_c$
- f_{cc} is the compressive strength of the confined concrete
- D is the outer diameter of the circular reinforced concrete column section
- A_g is the gross cross-sectional area of the concrete column
- c is the distance from the compression face to the neutral axis of the cross-section
- ε_{cu} is the useable strain for confined concrete
- ε_{su} is the maximum permitted steel strain
- ϕ_y is the yield curvature
- ϕ_u is the ultimate curvature
- L_c is the distance from the point of contraflexure to the plastic hinge
- L_p is the analytical plastic hinge length
- L_{sp} is the length of strain penetration
- Δ_y is the yield displacement
- Δ_p is the plastic displacement
- Δ_u is the ultimate displacement (displacement capacity)
- d_{bl} is the diameter of the longitudinal bars in the column
- μ is the displacement ductility capacity

$$\alpha_\theta = 0.138 - 0.00174(D/t) \tag{4.3-3}$$

$$f_l^{'} = \alpha_\theta F_{yE}\left(\frac{2}{D/t-2}\right) \tag{4.3-4}$$

$$f_{cc} = f_{co}^{'}\left(-1.254 + 2.254\sqrt{1+\frac{7.94f_l^{'}}{f_{co}^{'}}} - 2\frac{f_l^{'}}{f_{co}^{'}}\right) \tag{4.3-5}$$

$$L_{SP} = 0.15 f_{ye} d_{bl} \tag{4.3-6}$$

$$L_P = 0.08L_c + L_{SP} \geq 2L_{SP} \tag{4.3-7}$$

$$\Delta_y = \frac{1}{3}\phi_y (L_c + L_{SP})^2 \tag{4.3-8}$$

$$\Delta_u = 4\Delta_y \tag{4.3-9}$$

It may be difficult to provide a shear resistance greater than the overstrength plastic shear in RCFST construction. The shear resistance will be controlled by the short segment at the gap, comprised of the concrete fill in combination with the hoop or spiral reinforcement used within the joint region. Equation 4.3-10 through 4.3-15 from the AASHTO Guide Specification for LRFD Seismic Bridge Design provide the resistance.

$$f_s = \rho_s f_{yh} \tag{4.3-10}$$

$$\alpha' = \frac{f_s}{0.15} + 3.67 - \mu_D \tag{4.3-11}$$

$$v_c = 0.032\alpha'\left(1 + \frac{P}{2A_g}\right)\sqrt{f'_c} \le Min\left\{0.11\sqrt{f'_c}, 0.047\alpha'\sqrt{f'_c}\right\} \tag{4.3-12}$$

$$V_c = v_c\left(0.8A_g\right) \tag{4.3-13}$$

$$V_s = \frac{\pi}{2}\left(\frac{A_h f_y D'}{s}\right) \le 0.25 f'_c\left(0.8A_g\right) \tag{4.3-14}$$

$$\phi V_n = 0.90(V_c + V_s) \tag{4.3-15}$$

Step 1. Using section analysis software, determine the expected plastic moment resistance, M_{PE1}.

For the top hinge, comprised of the concrete core and 2% longitudinal reinforcement.

Step 2. Using ***CFST-Analysis.xlsx***, determine M_{PE2} for the CFST in-ground hinge.

Other appropriate software may be used if approved by the Director of Structures.

Step 3. Using ***CONSEC*** or other section analysis software, determine the expected resistance of the reinforced concrete top hinge, M_{PE1}, and the idealized yield curvature, ϕ_y.

Step 4. Locate the point of contraflexure in the piles.

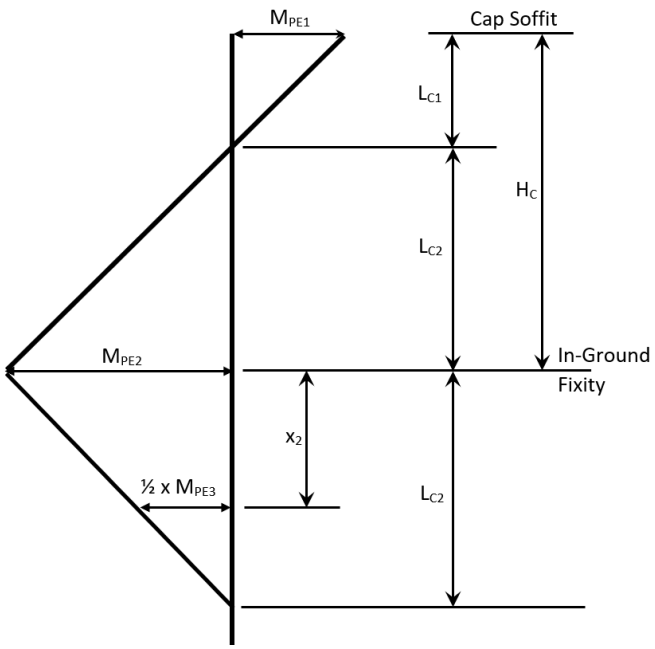

Figure 48. Point of Contraflexure - RCFST

Step 5. Determine the displacement capacity, δ_{uT1}, for the top segment.

This analysis is for the concrete core without the tube. The longitudinal bars have diameter, d_{bl}, and expected yield stress, f_{yE}. E_s is the elastic modulus for steel, 29,000 ksi. D' is the diameter of the concrete core, equal to the tube diameter minus twice the tube thickness minus 4 inches.

$$\delta_{uT1} = 4\delta_{y1} = 6\left[\frac{1}{3}\phi_y (L_{C1} + L_{SP})^2\right] \tag{4.3-16}$$

$$L_{SP} = 0.15 f_{yE} d_{bl} \tag{4.3-17}$$

Step 6. Determine the transverse displacement capacity, δ_{uT2}, for the bottom segment.

$$\delta_{uT2} = k_\Delta \frac{ML_{C2}^2}{3EI_s} \tag{4.3-18}$$

$$M = \frac{\left(F_{yE} - \frac{P_u}{A_s}\right) S_s + M_{PE2}}{2} \tag{4.3-19}$$

Step 7. Determine the transverse displacement capacity, Δ_{uT}.

The total displacement capacity in the transverse direction is $\Delta_{uT} = \delta_{uT1} + \delta_{uT2}$.

Step 8. Determine the longitudinal displacement capacity, Δ_{uL}.

The longitudinal displacement capacity, Δ_{uL}, may be estimated from Equation 4.3-20 with k_Δ = taken for the CFST tube in question.

$$\delta_{uL} = k_{\Delta}\frac{MH_C^2}{3EI_s} \tag{4.3-20}$$

Step 9. Determine the displacement capacity ratio for the bent by Equation 4.3-21.

$$\frac{\Delta_{EQ}}{\Delta_u} = \sqrt{\left(\frac{\Delta_{EQ-T}}{\Delta_{uT}}\right)^2 + \left(\frac{\Delta_{EQ-L}}{\Delta_{uL}}\right)^2} \tag{4.3-21}$$

The seismic displacements, $\Delta_{EQ\text{-}T}$ and $\Delta_{EQ\text{-}L}$, shall be transformed to the local bent transverse and longitudinal axes and shall be amplified by R_d when the natural period is short enough to require displacement amplification by the AASHTO-GS Section 4.3.3.

Step 10. Determine the shear resistance of the piles.

A longitudinal reinforcement ratio, $\rho_l = A_{sr} / A_g$, of about 2% is recommended.

$$f_s = \rho_s f_{yh} \tag{4.3-22}$$

$$\rho_s = \frac{4A_{sp}}{D's} = 0.16\frac{f'_{ce}}{f_{ye}}\left(0.5 + \frac{1.25P_u}{f'_{ce}A_g}\right) + 0.13(\rho_l - 0.01) \tag{4.3-23}$$

$$\alpha' = \frac{f_s}{0.15} + 3.67 - \mu_D \tag{4.3-24}$$

$$v_c = 0.032\alpha'\left(1 + \frac{P}{2A_g}\right)\sqrt{f'_c} \le Min\left\{0.11\sqrt{f'_{c'}}, 0.047\alpha'\sqrt{f'_c}\right\} \tag{4.3-25}$$

$$V_c = v_c\left(0.8A_g\right) \tag{4.3-26}$$

$$V_s = \frac{\pi}{2}\left(\frac{A_h f_y D'}{s}\right) \le 0.25f'_c\left(0.8A_g\right) \tag{4.3-27}$$

$$\phi V_n = 0.90(V_c + V_s) \times no.of\ piles \tag{4.3-28}$$

Step 11. Calculate the overstrength plastic shear for the bent.

$$V_{PO} = \frac{1.2M_{PE1}}{L_{C1}} \times no.of\ piles \tag{4.3-29}$$

Step 12. Ensure that the shear resistance is adequate.

$$V_{PO} \le \phi V_n \tag{4.3-30}$$

Step 13. Determine the required embedment of longitudinal bars into the cap.

$$l_{ac} = \frac{0.79 d_{bl} f_{ye}}{\sqrt{f_c'}} \quad (4.3\text{-}31)$$

Step 14. Apply the overstrength plastic shear to design the cap reinforcing.

This may be done in LEAP or other software. The cap is to be designed to remain elastic when subjected to the over-strength plastic shear.

Step 15. Design the joint reinforcing.

See the AASHTO Guide Specification for LRFD Seismic Bridge Design, Section 8.13.

4.4 Abutment Spring Stiffness

Refer to the discussion in Section 3 for guidance in estimating spring constants for all types of construction.

4.5 Depth to Fixity for Displacement Analysis

Refer to the discussion in Section 3 for guidance in estimating depth-to-fixity for all types of construction.

4.6 Corrosion Protection Measures

Refer to Sections 1.5 and 2.5 for guidance on alternatives proposed for corrosion protection of steel tubes used in any of the three types of construction covered in this report.

4.7 Recommended Plans Notes

Tubes may be either straight seam or spiral welded and must conform to either ASTM 1018 or API 5L requirements.

Spiral welded tubes must be fabricated using a double submerged arc welding process. Weld metal properties must match the properties of the base metal and must meet minimum toughness requirements of demand critical welds.

The Contractor shall ensure that the inside of all tubes is clean for the entire tube length to which concrete fill is to be applied.

Chapter 5 Conclusions

The research project "***Best Practices for Bridges with Pipe Piles***" (RES2023-04) includes both structural and geotechnical recommendations regarding Concrete-Filled-Steel-Tube (CFST), Hollow-Tube-Pile-Bent (HTPB), and Reinforced-Concrete-Filled-Steel-Tube (RCFST) bridge substructures.

The recommendations for structural design include:

1. Select only tube diameter and thickness combinations as listed in the tables found in Chapter 3. Tubes with D/t ratio outside these limits are not recommended for bridges in Tennessee.
2. For a majority of normal bridge designs, estimate displacement capacity as the appropriate multiple, k_{Δ}, of the displacement at first yield. Note that this is a pseudo-yield displacement for CFST since the properties of the tube alone are to be used.
3. For complex bridges, use a pushover analysis to establish displacement capacity. The pushover analysis settings appropriate for this type of procedure are summarized in Chapter 3.
4. The procedures outlined in Chapter 4 for capacity protection and for limits of concrete fill in tubes should be followed for all types of construction: CFST, HTPB, and RCFST.

The geotechnical recommendations are:

1. For soft clays, reduce the traditional spring constant value in accordance with Chapter 4 of this report.
2. For hard clays and dense sands, increase the traditional spring constant values in accordance with Chapter 3 of this report.
3. In lieu of the use of a single depth-to-fixity estimate across all projects, incorporate the normalized curves from Chapter 3 to obtain more refined estimates for seismic analysis.
4. In lieu of pile driving criteria based on static load tests and the ENR formula, use dynamic testing methods or consider revisions to the current scaling process.

References

AASHTO. (2011). *Guide Specifications for LRFD Seismic Bridge Design (2nd edition).* Washington, D.C.: American Association of State Highway and Transportation Officials.

AASHTO. (2020). *LRFD Bridge Design Specifications (9th editiion).* Washington, D.C.: American Association of State Highway and Transportation Officials.

Brinch Hansen, J. (1963). Discussion of “Hyperbolic stress-strain response: cohesive soils". *Journal for Soil Mechanics and Foundation Engineering, 89*(SM4), 241-242.

Brown, N. K., Kowalsky, M. J., & Nau, J. M. (2015). Impact of D/t on Seismic Behavior of Reinforced Concrete Filled Steel Tubes. *Journal of Constructional Steel Research, 107*, 111-123.

Bruneau, M., & Marson, J. (2004). Seismic Design of Concrete-Filled Circular Steel Bridge Piers. *ASCE Journal of Bridge Engineering, 9*(1), 24-34.

Bruneau, M., Kenarangi, H., & Murphy, T. P. (2018). *Contribution of Steel Casing to Single Shaft Foundation Structural Resistance.* Washington, D. C.: National Cooperative Highway Research Program.

California Department of Transportation. (2003). *Corrosion Guidelines v 1.0.* Sacramento: CALTRANS Division of Engineering Services.

Chellis, R. D. (1951). *Pile Foundations.* McGraw Hill Book Company.

Davisson, M. T. (1970). *Lateral Load Capacity of Piles.* Washington, D. C.: Highway Research Record.

Davisson, M. T. (1972). High Capacity Piles. *Soil Mechanics Lecture Series on Innovations in Foundation Construction*, (pp. 81-112). Chicago, IL.

Davisson, M. T., & Robinson, K. E. (1965). Bending and Buckling of Partially Embedded Piles. *International Conference Soil Mechanics and Foundation Engineering*, (pp. 243-246). Montreal, Canada.

Duncan, J. M., & Buchignani, A. L. (1987). *Engineering Manual for Settlement Studies - CGPR #2.* Center for Geotechnical Practice and Research.

Duncan, J. M., Evans Jr., L. T., & Ooi, P. S. (1994). Lateral load analysis of single piles and drilled shafts. *Journal of geotechnical engineering, 120*(6), 1018-1033.

Elchalakani, M., Zhao, X., & Grzebieta, R. H. (2001). Concrete-Filled Circular Steel Tubes Subjected to Pure Bending. *Journal of Constructional Steel Research, 57*, 1141-1168.

Evans Jr., L. T. (1982). *Simplified Analysis of Laterally Loaded Piles.* Berkeley: University of California.

Fellenius, B. H. (2021). *Basics of Foundati on Design, Electronic Editi on*. Retrieved May 1, 2021, from http://www.fellenius.net

FHWA. (2018). *Drilled Shafts: Construction Procedures and Design Methods, Geotechnical Engineering Circular No. 10. FHWA-NHI-18-024.* Washington, DC: U.S. Department of Transportation, Federal Highway Administration.

Flaate, K. S. (1964). *An Investigation of the Validity of Three Pile-driving Formulae in Cohesionless Material.* Norwegian Geotechnical Insti tute Publicati on No. 56.

Fujikura, S., & Bruneau, M. (2008). *Experimental and Analytical Investigation of Blast Performance of Seismically Resistant Bridge Piers.* Buffalo: Multidisciplinary Center for Earthquake Engineering Research (MCEER).

Fujikura, S., Bruneau, M., & Lopez-Garcia, D. (2007). *Experimental Investigation of Blast Performance of Seismically Resistant Concrete-Filled Steel Tube Bridge Piers.* Buffalo: Multidisciplinary Center for Earthquake Engineering Research (MCEER).

Fulmer, S. J., Kowalsky, M. J., & Nau, J. M. (2012). Reversed Cyclic Flexural Behavior of Spiral DSAW and Single Seam ERW Steel Pipe Piles. *ASCE Journal of Structural Engineering, 138*(9), 1099-1109.

Fulmer, S. J., Kowalsky, M. J., & Nau, J. M. (2013). *Seismic Performance of Steel Pipe Pile to Cap Beam Moment Resisting Connections.* Fairbanks: Alaska Department of Transportation & Public Facilities.

Goel, R. K. (2010). *Simplified Procedures for Seismic Analysis and Design of Piers and Wharves in Marine Oil and LNG Terminals.* San Luis Obispo, CA: California Polytechnic State University.

Hannigan, P. J., Goble, G. G., Likins, G. E., & Rausche, F. (2006). *Design and Construction of Driven Pile Foundations - Volume 1.* Washington, D.C.: Federal Highway Administration.

Harn, R., Ospina, C. E., & Pachakis, D. (2019). Proposed Pipe Pile Strain Limits for ASCE 61-19. Pittsburgh: PORTS.

Hetenyi, M. (1946). *Beams on Elastic Foundations.* Ann Arbor: University of Michigan Press.

Hyzak, M., Galvan, M., Fisk, M., Smith, A., Johnson, D., Caldwell, D., & Miller, J. (2014). *Guidelines for the Use of Steel Piling for Bridge Foundations.* Austin: Texas Department of Transportation - Bridge Division.

Kappes, L. R. (2016). *Performance and Design of Steel Pipe Pile to Concrete Cap Connections Subject to Seismic or High Transverse Loading.* Bozeman: Montana State University.

Kappes, L., Berry, M., & Stephens, J. (2013). *Performance of Steel Pipe Pile to Concrete Cap Connections Subject to Seismic or High Transverse Loading.* Bozeman: Montana State University - Western Transportation Institute.

Kappes, L., Berry, M., Murray, F., Stephens, J., & Barnes, K. (2016). Seismic Performance of Concrete-Filled Steel Tube to Concrete Pile-Cap Connections. *ASCE Journal of Bridge Engineering, 21*(7), 1-17.

Kappes, L., Berry, M., Stephens, J., & Matteson, K. (2021). Simple Moment–Rotation Methodology for Predicting the Capacity of Concrete-Filled Steel Pipe Piles to Concrete Cap Connections. *ASCE Journal of Bridge Engineering, 26*(10), 1-11.

Kenarangi, H., & Bruneau, M. (2019). Experimental Study on Composite Action in Reinforced Concrete-Filled Steel-Tube Shaft Foundations. *ASCE Journal of Bridge Engineering, 24*(7), 1-15.

Lehman, D. E., & Roeder, C. W. (2012). *An Initial Study into the use of Concrete Filled Steel Tubes for Bridge Piers and Foundation Connections.* Seattle: University of Washington.

Lehman, D. E., & Roeder, C. W. (2012). *Rapid Construction of Bridge Piers with Improved Seismic Performance.* Seattle: University of Washington.

Li, P., Zhang, T., & Wang, C. (2018). Behavior of Concrete-Filled Steel Tube Columns Subjected to Axial Compression. *Advances in Materials Science and Engineering*, 1-16.

Likins, G. E., Fellenius, B. H., & Holtz, R. D. (2012). Pile Driving Formulas: Past and Present. In *Full-ScaleTesti ng and Foundati on Design: Honoring Bengt H. Fellenius* (pp. 737-753).

Long, J. H. (2009). *Comparison of Five Different Methods for Determining Pile Bearing Capacities.* Wisconsin Highway Research Program.

Mamaghani, I. H. (2004). Seismic Design and Retrofit of Thin-Walled Steel Tubular Columns. *13th World Conference on Earthquake Engineering* (pp. 1-15). Vancouver, B.C., Canada: Canadian Association for Earthquake Engineering.

Mamaghani, I. H., & Packer, J. A. (2002). Inelastic Behavior of Partially Concrete-Filled Steel Hollow Sections. *4th Structural Specialty Conference* (pp. 1-10). Montreal, Quebec, Canada: Canadian Society for Civil Engineering.

Marcakis, K., & Mitchell, D. (1980, July-August). Precast Concrete Connections with Embedded Steel Members. *PCI Journal*, 88-116.

Marsh, M. L., & Stringer, S. J. (2013). *NCHRP Synthesis 440: Performance-Based Seismic Bridge Design.* Washingtom, D.C.: Transportation Research Board.

Montana Department of Transportation. (2002, August). *Montana Structures Manual - Part II: Chapter 19.* Retrieved January 21, 2022, from https://www.mdt.mt.gov/other/webdata/external/bridge/structures-manual/part_II/chp-19-final.pdf

Montejo, L. A., Gonzalez-Roman, L. A., & Kowalsky, M. J. (2012). Seismic Performance of Reinforced Concrete-Filled Steel Tube Pile/Column Bridge Bents. *Journal of Earthquake Engineering, 16*(3), 401-424.

Moon, J., Lehman, D. E., Roeder, C. W., & Lee, H.-E. (2013). Strength of Circular Concrete-Filled Tubes with and without Internal Reinforcement under Combined Loading. *ASCE Journal of Structural Engineering, 139*(12), 1-12.

Murphy, T. P., Bennion, S., Marsh, L., Buckle, I. G., Luco, N., Anderson, D., . . . Restrepo, J. (2020). *NCHRP Research Report 949: Proposed AASHTO Guidelines for Performance-Based Seismic Bridge Design.* Washington, DC: The National Academies of Sciences, Engineering, and Medicine.

NAVFAC. (2024 (in press)). *Foundations and Earth Structures (DM 7.2).* Washington, DC: United States Department of Defense.

North Carolina Department of Transportation. (2005). *Standard Drawings.* Retrieved January 21, 2022, from https://connect.ncdot.gov/resources/Structures/Pages/Structure-Standards.aspx

Olson, R. E., & Flaate, K. S. (1967). Pile-driving Formulas for Friction Piles in Sand. *Journal of the Soil Mechanics and Foundations Division, 93*(6), 279-296.

Oregon Department of Transportation. (2020). *Bridge Design Manual.* Salem: Bridge Engineering Section.

Pile Driving Contractors Association. (2012). *Dealing with Piling Corrosion.* Orange Park, FLA: Lester Publications, LLC.

Port of Long Beach. (2021). *Wharf Design Criteria Version 5.0.* Long Beach CA: POLB.

Priestley, M. J., Seible, F., & Calvi, G. M. (1996). *Seismic Design and Retrofit of Bridges.* New York: Wiley-Interscience.

Reese, L. C., Cox, W. R., & Koop, F. D. (1975). Field Testing and Analysis of Laterally Loaded Piles in Stiff Clay. *Proceedings of the VII Annual Offshore Technology Conference*, (pp. 672-690). Houston, Texas.

Roeder, C. W., Cameron, B., & Brown, C. B. (1999). Composite Action in Concrete Filled Tubes. *ASCE Journal of Structural Engineering, 125*(5), 477-484.

Roeder, C. W., Lehman, D. E., & Thody, R. (Fourth Quarter 2009). Composite Action in CFT Components and Connections. *Engineering Journal*, 229-242.

Roeder, C. W., Stephens, M. T., & Lehman, D. E. (2018). Concrete Filled Steel Tubes for Bridge Pier and Foundation Construction. *International Journal of Steel Structures, 18*(1), 39-49.

Roeder, C., Lehman, D., Heid, A., & Maki, T. (2016). *Shear Design Expressions for Concrete Filled Steel Tube and Reinforced Concrete Filled Tube Components.* Washington State Department of Transportation.

Rollins, K. M., & Stenlund, T. E. (2008). *Laterally Loaded Pile Cap Connections.* Provo, Utah: Brigham Young University.

Rotter, J. M., & Sadowski, A. J. (2017). Full Plastic Resistance of Tubes Under Bending and Axial Force: Exact Treatment and Approximations. *Structures, 10*, 30-38.

Sadowski, A. J., Wong, W. J., Li, S. C., Malaga-Chuquitaype, C., & Pachakis, D. (2020). Critical Buckling Strains in Thick Cold-Formed Circular Hollow Sections under Cyclic Loading. *ASCE Journal of Structural Engineering, 146*(9), 1-13.

Shama, A. A., Mander, J. B., & Aref, A. J. (2002). Seismic Performance and Retrofit of Steel Pile to Concrete Cap Connections. *ACI Structural Journal, January-February*(2002), 1-12.

Silva, P. F., & Seible, F. (1999). *Design Example of a Multiple Column Bridge Bent Under Seismic Loads Using the Alaska Cast-in-Place Steel Shell.* San Diego: University of California.

Silva, P. F., & Srithiran, S. (2011). Seismic Performance of a Concrete Bridge Bent Consisting of Three Steel Shell Columns. *Earthquake Spectra, 27*(1), 107-132.

Silva, P. F., Srithiran, S., Seible, F., & Priestley, M. J. (1999). *Full-Scale Test of the Alaska Cast-in-Place Steel Shell Three Column Bridge Bent.* University of California, San Diego.

Stephens, J. E., & McKittrick, L. R. (2005). *Performance of Steel Pipe Pile-to-Concrete Bent Cap Connections Subject to Seismic or High Transverse Loading: Phase II.* Montana Department of Transportation.

Stephens, M. T. (2016). *Design Expressions and Dynamic Evaluation of CFST Bridges Subjected to Seismic Hazards.* Seattle: The University of Washington.

Stephens, M. T., Berg, L. M., Lehman, D. E., & Roeder, C. W. (2016). Seismic CFST Column-to-Precast Cap Beam Connections for Accelerated Bridge Construction. *ASCE Journal of Structural Engineering*, 1-14.

Stephens, M. T., Lehman, D. E., & Roeder, C. W. (2015). *CALTRANS Report CA15-2417: Concrete-Filled Tube Bridge Pier Connections for Accelerated Bridge Construction.* California Department of Transportation.

Stephens, M. T., Lehman, D. E., & Roeder, C. W. (2018). Seismic Performance Modeling of Concrete-Filled Steel Tube Bridges: Tools and Case Study. *Engineering Structures, 165*, 88-105.

USACE. (1991). *Design of Pile Foundations: Engineer Manual: EM 1110-2-2906.* Washington, DC: Department of the Army.

Washington State Department of Transportation. (2022). *Bridge Design Manual (LRFD).* Bridge and Structures Office.

Appendix A Cantilever Pushover: Detailed Results

Appendix A presents the results of all cantilever fiber-based model pushover analyses. The results given here were used to establish lower-bound ratios for ultimate to yield displacement for both CFST and HTPB construction. The results show that the ratio of displacement capacity to displacement at first yield is primarily a function of D/t and that the distance from the point of contraflexure to the point of maximum moment has negligible effect.

Table 21. Cantilever Pushover - 12-inch HTPB, P = 0, Fy = 52.5 ksi

Type		D, inches	t, inches	F_y, ksi	ε_{limit}
HTPB		12	0.375	52.5	0.011663
		A_s, in^2	I_s, in^4	S_s, in^3	P, kips
		13.695	231.6	38.60	0.0

L_C, ft	Displacements, inches			SeismoStruct Ratio	Theoretical Ratio
	Theoretical 1st Yield	SeismoStruct 1st Yield	SeismoStruct Ultimate		
4	0.232	0.239	0.412	1.724	1.778
6	0.521	0.539	0.927	1.720	1.778
8	0.927	0.958	1.648	1.720	1.778
10	1.448	1.495	2.490	1.666	1.719
12	2.086	2.152	3.709	1.724	1.778
14	2.839	2.930	5.033	1.718	1.773
16	3.708	3.829	6.594	1.722	1.779
18	4.692	4.846	8.421	1.738	1.795
20	5.793	5.982	10.303	1.722	1.778
30	13.034	13.467	23.183	1.721	1.779

Table 22. Cantilever Pushover - 14-inch HTPB, P = 0, Fy = 52.5 ksi

Type		D, inches	t, inches	F_y, ksi	ε_{limit}
HTPB		14	0.5	52.5	0.013365
		A_s, in^2	I_s, in^4	S_s, in^3	P, kips
		21.206	483.8	69.11	0.0

L_C, ft	Displacements, inches			SeismoStruct Ratio	Theoretical Ratio
	Theoretical 1st Yield	SeismoStruct 1st Yield	SeismoStruct Ultimate		
4	0.199	0.206	0.366	1.777	1.843
6	0.447	0.463	0.834	1.801	1.866
8	0.794	0.824	1.440	1.748	1.813
10	1.241	1.288	2.290	1.778	1.845
12	1.788	1.854	3.314	1.787	1.854
14	2.433	2.525	4.454	1.764	1.831
16	3.178	3.297	5.892	1.787	1.854
18	4.022	4.172	7.457	1.787	1.854
20	4.966	5.151	9.001	1.747	1.813
30	11.172	11.589	20.253	1.748	1.813

Table 23. Cantilever Pushover - 16-inch HTPB, P = 0, Fy = 52.5 ksi

Type		D, inches	t, inches	F_y, ksi	ε_{limit}
HTPB		16	0.5	52.5	0.011663
		A_s, in^2	I_s, in^4	S_s, in^3	P, kips
		24.347	731.9	91.49	0.0

L_C, ft	Displacements, inches			SeismoStruct Ratio	Theoretical Ratio
	Theoretical 1st Yield	SeismoStruct 1st Yield	SeismoStruct Ultimate		
4	0.174	0.179	0.325	1.816	1.870
6	0.391	0.404	0.730	1.807	1.867
8	0.695	0.718	1.298	1.808	1.867
10	1.086	1.121	2.029	1.810	1.868
12	1.564	1.615	2.921	1.809	1.867
14	2.129	2.199	3.957	1.799	1.859
16	2.781	2.871	5.193	1.809	1.868
18	3.519	3.636	6.535	1.797	1.857
20	4.345	4.488	8.114	1.808	1.868
30	9.776	10.103	18.258	1.807	1.868

Table 24. Cantilever Pushover - 18-inch HTPB, P = 0, Fy = 52.5 ksi

Type		D, inches	t, inches	F_y, ksi	ε_{limit}
HTPB		18	0.5	52.5	0.010343
		A_s, in^2	I_s, in^4	S_s, in^3	P, kips
		27.489	1053.2	117.02	0.0

L_C, ft	Displacements, inches			SeismoStruct Ratio	Theoretical Ratio
	Theoretical 1st Yield	SeismoStruct 1st Yield	SeismoStruct Ultimate		
4	0.154	0.159	0.276	1.736	1.787
6	0.348	0.357	0.622	1.742	1.789
8	0.618	0.636	1.106	1.739	1.790
10	0.966	0.994	1.728	1.738	1.790
12	1.390	1.430	2.489	1.741	1.790
14	1.892	1.947	3.368	1.730	1.780
16	2.472	2.543	4.399	1.730	1.780
18	3.128	3.220	5.576	1.732	1.782
20	3.862	3.979	6.913	1.737	1.790
30	8.690	8.939	15.554	1.740	1.790

Table 25. Cantilever Pushover - 20-inch HTPB, P = 0, Fy = 52.5 ksi

Type		D, inches	t, inches	F_y, ksi	ε_{limit}
HTPB		20	0.625	52.5	0.011663
		A_s, in^2	I_s, in^4	S_s, in^3	P, kips
		38.043	1787.0	178.70	0.0

L_C, ft	Displacements, inches			SeismoStruct Ratio	Theoretical Ratio
	Theoretical 1st Yield	SeismoStruct 1st Yield	SeismoStruct Ultimate		
4	0.139	0.143	0.260	1.818	1.870
6	0.313	0.323	0.585	1.811	1.870
8	0.556	0.574	1.037	1.807	1.865
10	0.869	0.897	1.623	1.809	1.868
12	1.251	1.292	2.333	1.806	1.864
14	1.703	1.758	3.171	1.804	1.862
16	2.225	2.296	4.132	1.800	1.857
18	2.815	2.907	5.265	1.811	1.870
20	3.476	3.587	6.494	1.810	1.868
30	7.821	8.074	14.540	1.801	1.859

Table 26. Cantilever Pushover - 24-inch HTPB, P = 0, Fy = 52.5 ksi

Type		D, inches	t, inches	F_y, ksi	ε_{limit}
HTPB		24	0.75	52.5	0.011663
		A_s, in^2	I_s, in^4	S_s, in^3	P, kips
		54.782	3705.5	308.79	0.0

L_C, ft	Displacements, inches			SeismoStruct Ratio	Theoretical Ratio
	Theoretical 1st Yield	SeismoStruct 1st Yield	SeismoStruct Ultimate		
4	0.116	0.120	0.216	1.800	1.864
6	0.261	0.269	0.487	1.810	1.868
8	0.463	0.479	0.866	1.808	1.869
10	0.724	0.747	1.354	1.813	1.870
12	1.043	1.076	1.948	1.810	1.868
14	1.419	1.465	2.653	1.811	1.869
16	1.854	1.914	3.464	1.810	1.869
18	2.346	2.422	4.369	1.804	1.862
20	2.897	2.990	5.400	1.806	1.864
30	6.517	6.729	12.167	1.808	1.867

Table 27. Cantilever Pushover - 30-inch HTPB, P = 0, Fy = 52.5 ksi

Type		D, inches	t, inches	F_y, ksi	ε_{limit}
HTPB		30	1.00	52.5	0.012457
		A_s, in^2	I_s, in^4	S_s, in^3	P, kips
		91.106	9588.9	639.26	0.0

L_C, ft	Displacements, inches			SeismoStruct Ratio	Theoretical Ratio
	Theoretical 1st Yield	SeismoStruct 1st Yield	SeismoStruct Ultimate		
4	0.093	0.096	0.178	1.854	1.920
6	0.209	0.216	0.400	1.852	1.918
8	0.371	0.383	0.710	1.854	1.915
10	0.579	0.599	1.110	1.853	1.916
12	0.834	0.863	1.598	1.852	1.916
14	1.135	1.174	2.172	1.850	1.913
16	1.483	1.534	2.842	1.853	1.916
18	1.877	1.941	3.596	1.853	1.916
20	2.317	2.397	4.439	1.852	1.916
30	5.214	5.393	9.973	1.849	1.913

Table 28. Cantilever Pushover - 36-inch HTPB, P = 0, Fy = 52.5 ksi

Type		D, inches	t, inches	F_y, ksi	ε_{limit}
HTPB		36	1.00	52.5	0.010343
		A_s, in^2	I_s, in^4	S_s, in^3	P, kips
		109.956	16850.7	936.15	0.0

L_C, ft	Displacements, inches			SeismoStruct Ratio	Theoretical Ratio
	Theoretical 1st Yield	SeismoStruct 1st Yield	SeismoStruct Ultimate		
4	0.077	0.079	0.134	1.696	1.735
6	0.174	0.179	0.301	1.682	1.732
8	0.309	0.318	0.535	1.682	1.732
10	0.483	0.496	0.833	1.679	1.726
12	0.695	0.715	1.205	1.685	1.733
14	0.946	0.973	1.638	1.683	1.731
16	1.236	1.271	2.142	1.685	1.733
18	1.564	1.609	2.707	1.682	1.731
20	1.931	1.986	3.334	1.679	1.727
30	4.345	4.468	7.518	1.683	1.730

Table 29. Cantilever Pushover - 12-inch HTPB, P = 120, Fy = 52.5 ksi

Type		D, inches	t, inches	F_y, ksi	ε_{limit}
HTPB		12	0.375	52.5	0.011663
		A_s, in^2	I_s, in^4	S_s, in^3	P, kips
		13.695	231.6	38.60	119.8

L_C, ft	Displacements, inches			SeismoStruct Ratio	Theoretical Ratio
	Theoretical 1st Yield	SeismoStruct 1st Yield	SeismoStruct Ultimate		
4	0.193	0.200	0.390	1.950	2.020
6	0.434	0.448	0.873	1.949	2.009
8	0.772	0.798	1.536	1.925	1.989
10	1.207	1.247	2.416	1.937	2.002
12	1.738	1.795	3.516	1.959	2.023
14	2.366	2.445	4.742	1.939	2.005
16	3.090	3.193	6.176	1.934	1.999
18	3.910	4.035	7.773	1.926	1.988
20	4.828	4.986	9.596	1.925	1.988
30	10.862	11.219	22.106	1.970	2.035

Table 30. Cantilever Pushover - 14-inch HTPB, P = 186, Fy = 52.5 ksi

Type		D, inches	t, inches	F_y, ksi	ε_{limit}
HTPB		14	0.5	52.5	0.013365
		A_s, in^2	I_s, in^4	S_s, in^3	P, kips
		21.206	483.8	69.11	185.6

L_C, ft	Displacements, inches			SeismoStruct Ratio	Theoretical Ratio
	Theoretical 1st Yield	SeismoStruct 1st Yield	SeismoStruct Ultimate		
4	0.166	0.172	0.349	2.029	2.109
6	0.372	0.386	0.780	2.021	2.094
8	0.662	0.686	1.396	2.035	2.109
10	1.034	1.072	2.152	2.007	2.080
12	1.490	1.544	3.141	2.034	2.109
14	2.028	2.103	4.275	2.033	2.108
16	2.648	2.745	5.583	2.034	2.108
18	3.352	3.477	7.067	2.032	2.108
20	4.138	4.289	8.607	2.007	2.080
30	9.310	9.646	19.400	2.011	2.084

Table 31. Cantilever Pushover - 16-inch HTPB, P = 213, Fy = 52.5 ksi

Type		D, inches	t, inches	F_y, ksi	ε_{limit}
HTPB		16	0.5	52.5	0.011663
		A_s, in^2	I_s, in^4	S_s, in^3	P, kips
		24.347	731.9	91.49	213.0

L_C, ft	Displacements, inches			SeismoStruct Ratio	Theoretical Ratio
	Theoretical 1st Yield	SeismoStruct 1st Yield	SeismoStruct Ultimate		
4	0.145	0.150	0.305	2.033	2.106
6	0.326	0.337	0.684	2.030	2.099
8	0.579	0.598	1.212	2.027	2.092
10	0.905	0.934	1.899	2.033	2.098
12	1.303	1.347	2.735	2.030	2.098
14	1.774	1.834	3.688	2.011	2.079
16	2.317	2.392	4.847	2.026	2.092
18	2.933	3.034	6.068	2.000	2.069
20	3.621	3.738	7.479	2.001	2.066
30	8.147	8.405	16.454	1.958	2.020

Table 32. Cantilever Pushover - 18-inch HTPB, P = 240, Fy = 52.5 ksi

Type		D, inches	t, inches	F_y, ksi	ε_{limit}
HTPB		18	0.5	52.5	0.010343
		A_s, in^2	I_s, in^4	S_s, in^3	P, kips
		27.489	1053.2	117.02	240.5

L_C, ft	Displacements, inches			SeismoStruct Ratio	Theoretical Ratio
	Theoretical 1st Yield	SeismoStruct 1st Yield	SeismoStruct Ultimate		
4	0.129	0.132	0.261	1.977	2.027
6	0.290	0.298	0.585	1.963	2.020
8	0.515	0.526	1.043	1.983	2.025
10	0.805	0.828	1.626	1.964	2.021
12	1.159	1.194	2.325	1.947	2.007
14	1.577	1.621	3.186	1.965	2.020
16	2.060	2.118	4.133	1.951	2.007
18	2.607	2.680	5.249	1.959	2.014
20	3.218	3.314	6.503	1.962	2.021
30	7.241	7.445	14.199	1.907	1.961

Table 33. Cantilever Pushover - 20-inch HTPB, P = 333, Fy = 52.5 ksi

Type		D, inches	t, inches	F_y, ksi	ε_{limit}
HTPB		20	0.625	52.5	0.011663
		A_s, in^2	I_s, in^4	S_s, in^3	P, kips
		38.043	1787.0	178.70	332.9

L_C, ft	Displacements, inches			SeismoStruct Ratio	Theoretical Ratio
	Theoretical 1st Yield	SeismoStruct 1st Yield	SeismoStruct Ultimate		
4	0.116	0.120	0.244	2.033	2.106
6	0.261	0.269	0.550	2.045	2.110
8	0.463	0.478	0.976	2.042	2.106
10	0.724	0.748	1.520	2.032	2.099
12	1.043	1.077	2.189	2.032	2.099
14	1.419	1.465	2.989	2.040	2.106
16	1.854	1.914	3.904	2.040	2.106
18	2.346	2.424	4.949	2.042	2.109
20	2.897	2.991	6.080	2.033	2.099
30	6.517	6.724	13.222	1.966	2.029

Table 34. Cantilever Pushover - 24-inch HTPB, P = 479, Fy = 52.5 ksi

Type		D, inches	t, inches	F_y, ksi	ε_{limit}
HTPB		24	0.75	52.5	0.011663
		A_s, in^2	I_s, in^4	S_s, in^3	P, kips
		54.782	3705.5	308.79	479.3

L_C, ft	Displacements, inches			SeismoStruct Ratio	Theoretical Ratio
	Theoretical 1st Yield	SeismoStruct 1st Yield	SeismoStruct Ultimate		
4	0.097	0.100	0.204	2.040	2.113
6	0.217	0.224	0.459	2.049	2.113
8	0.386	0.399	0.815	2.043	2.110
10	0.603	0.623	1.269	2.037	2.103
12	0.869	0.897	1.834	2.045	2.111
14	1.183	1.222	2.485	2.034	2.101
16	1.545	1.596	3.237	2.028	2.095
18	1.955	2.018	4.104	2.034	2.099
20	2.414	2.494	5.077	2.036	2.103
30	5.431	5.604	11.027	1.968	2.030

Table 35. Cantilever Pushover - 30-inch HTPB, P = 797, Fy = 52.5 ksi

Type		D, inches	t, inches	F_y, ksi	ε_{limit}
HTPB		30	1.00	52.5	0.012457
		A_s, in^2	I_s, in^4	S_s, in^3	P, kips
		91.106	9588.9	639.26	797.2

L_C, ft	Displacements, inches			SeismoStruct Ratio	Theoretical Ratio
	Theoretical 1st Yield	SeismoStruct 1st Yield	SeismoStruct Ultimate		
4	0.077	0.080	0.167	2.088	2.162
6	0.174	0.180	0.375	2.083	2.158
8	0.309	0.320	0.667	2.084	2.159
10	0.483	0.499	1.042	2.088	2.158
12	0.695	0.719	1.499	2.085	2.156
14	0.946	0.979	2.039	2.083	2.155
16	1.236	1.278	2.670	2.089	2.160
18	1.564	1.618	3.375	2.086	2.158
20	1.931	1.997	4.169	2.088	2.159
30	4.345	4.493	8.990	2.001	2.069

Table 36. Cantilever Pushover - 36-inch HTPB, P = 962, Fy = 52.5 ksi

Type		D, inches	t, inches	F_y, ksi	ε_{limit}
HTPB		36	1.00	52.5	0.010343
		A_s, in^2	I_s, in^4	S_s, in^3	P, kips
		109.956	16850.7	936.15	962.1

L_C, ft	Displacements, inches			SeismoStruct Ratio	Theoretical Ratio
	Theoretical 1st Yield	SeismoStruct 1st Yield	SeismoStruct Ultimate		
4	0.064	0.066	0.127	1.924	1.973
6	0.145	0.149	0.285	1.913	1.968
8	0.257	0.265	0.505	1.906	1.961
10	0.402	0.414	0.791	1.911	1.966
12	0.579	0.596	1.140	1.913	1.968
14	0.789	0.811	1.547	1.908	1.962
16	1.030	1.059	2.021	1.908	1.962
18	1.303	1.341	2.550	1.902	1.956
20	1.609	1.655	3.149	1.903	1.957
30	3.621	3.726	7.091	1.903	1.958

Appendix B Final k_Δ Model for CFST

Table 37. Final kΔ Model for CFST

		F_y = 35 ksi	F_y = 52.5 ksi	F_y = 80 ksi
CFST	D/t	k_Δ	k_Δ	k_Δ
CFST12-0203	59.1	2.788	2.147	1.785
CFST12-0219	54.8	2.804	2.165	1.803
CFST12-0250	48.0	2.829	2.196	1.826
CFST12-0312	38.5	2.916	2.258	1.876
CFST12-0375	32.0	2.977	2.312	1.917
CFST14-0219	63.9	2.777	2.132	1.771
CFST14-0250	56.0	2.799	2.159	1.797
CFST14-0312	44.9	2.849	2.214	1.840
CFST14-0375	37.3	2.925	2.267	1.882
CFST14-0500	28.0	3.037	2.355	1.956
CFST16-0250	64.0	2.777	2.132	1.770
CFST16-0312	51.3	2.816	2.180	1.813
CFST16-0375	42.7	2.870	2.228	1.849
CFST16-0500	32.0	2.976	2.313	1.921
CFST18-0250	72.0	2.751	2.112	1.754
CFST18-0312	57.7	2.793	2.152	1.794
CFST18-0375	48.0	2.828	2.196	1.828
CFST18-0500	36.0	2.936	2.278	1.890
CFST20-0312	64.1	2.774	2.130	1.767
CFST20-0375	53.3	2.809	2.170	1.805
CFST20-0500	40.0	2.897	2.245	1.865
CFST20-0625	32.0	2.976	2.312	1.918
CFST24-0375	64.0	2.776	2.132	1.767
CFST24-0500	48.0	2.828	2.196	1.822
CFST24-0625	38.4	2.915	2.258	1.876
CFST24-0750	32.0	2.977	2.312	1.921
CFST30-0500	60.0	2.786	2.142	1.779
CFST30-0625	48.0	2.828	2.196	1.824
CFST30-0750	40.0	2.895	2.246	1.869
CFST30-1000	30.0	3.011	2.334	1.937
CFST36-0500	72.0	2.750	2.111	1.754
CFST36-0625	57.6	2.793	2.152	1.794
CFST36-0750	48.0	2.828	2.196	1.822
CFST36-1000	36.0	2.936	2.277	1.890

Appendix C Final k_Δ Model for HTPB

Table 38. Final kΔ Model for HTPB

		F_y = 35 ksi	F_y = 52.5 ksi	F_y = 80 ksi
HTPB	D/t	k_Δ	k_Δ	k_Δ
HTPB12-0375	32.0	2.046	1.799	Do Not Use
HTPB14-0500	28.0	2.158	1.879	
HTPB16-0500	32.0	2.042	1.797	
HTPB18-0500	36.0	1.953	1.734	
HTPB20-0625	32.0	2.042	1.798	
HTPB24-0750	32.0	2.042	1.797	
HTPB30-1000	30.0	2.097	1.835	
HTPB36-1000	36.0	1.951	1.734	

Appendix D Design Example Summary

Design Example No. 01. A CFST pile bent is analyzed by hand and by computer for displacement capacity and plastic shear. Required embedment of the tube into the cap and required cap dimensions are determined. The analysis is carried out for three yield strength values: 35 ksi, 50 ksi, and 80 ksi.

Design Example No. 02. A HTPB pile bent is analyzed by hand and by computer for displacement capacity and plastic shear. Required embedment of the tube, required cap dimensions, and tube shear resistance are all included.

Design Example No. 03. A CFST pile bent is analyzed by hand and by computer for displacement capacity and plastic shear. Displacement capacity is compared to displacement demand for the bridge located in Lake County. Options for mitigating inadequate displacement capacity are identified.

Design Example No. 04. A CFST pile bent is analyzed for displacement capacity by hand and by computer. The pile bent is for a bridge which results in extremely low pier heights. A proposed location in Dyer County is used to establish displacement demands. Difficulties in designing extremely short piers are identified and a methodology is developed whereby the piles remain elastic during strong ground shaking.

Design Example No. 05. Both CFST and HTPB options for a pile bent are considered and the required extent of concrete fill in the tubes is determined for each option.

Design Example No. 06. A CFST pile bent is analyzed by hand for plastic shear and compared to results from a computer analysis. Tube embedment, cap dimensions, and tube shear resistance are included.

Design Example No. 07. CFST, HTPB, and RCFST options are considered for a pile bent located in Shelby County.

Design Example No. 08. A CFST pile bent is analyzed for displacement capacity and plastic shear. P-Delta analysis by computer is performed for comparison purposed. Tube embedment and cap dimensional requirements are included.

Design Example No. 09. A RCFST pile bent is analyzed for displacement capacity and plastic shear. Reinforcing requirements for the top hinge in the RCFST tubes is included.

Design Example No. 10. CFST pile bents of varying height are analyzed by hand for three different proposed locations: Madison County, Shelby County, and Lake County. The proposed

pile bent incorporates tubes only directly underneath the girder lines to demonstrate the potential use of fewer tubes provided driving load requirements can be met.

Design Example No. 11. As displacement capacity calculations by hand for previous examples were in some cases overly conservative, an alternate (recommended) approach was developed and used to perform hand and computer analyses for a CFST pile bent. A wide range of tubes was considered. The proposed method provided much closer agreement with computer results. In two cases, however, hand-calculated displacement capacity results were actually larger (< 3%) than results obtained from the computer analysis.

Design Example No. 12. Design by hand calculation using the proposed alternative methodology was compared to results from computer analysis for a RCFST bent. The proposed methodology was shown to produce satisfactory prediction of displacement capacity (still below that predicted by computer).

Design Example No. 13. CFST designs for a six-span bridge were completed using both displacement-based and force-based design procedures in accordance with AASHTO provisions. Four different locations were considered for the bridge: Madison County, Shelby County, Dyer County, and Lake County. The proposed methodology was shown to produce excellent predictions for both displacement capacity and plastic shear. Calculations for required driving loads to satisfy Extreme Event criteria were included.

Design Example 14. The refined spring constant for a 14-inch CFST embedded in medium-dense sand is calculated.

Design Example 15. The refined spring constant for a 30-inch CFST embedded in soft clay is calculated.

Appendix E Excel Spreadsheets

The following spreadsheets were developed in Microsoft Excel over the course of project RES2023-04. The spreadsheets have been validated against hand-calculated design examples. Nonetheless, continued validation must be a part of the spreadsheet usage in design to identify possible scenarios for which spreadsheets may not provide the correct solution.

All worksheets within the spreadsheets are password-protected to prevent inadvertent modification of calculated cells. The password for all worksheets is "quake". In general, shaded cells are input parameters to be entered by the engineer. Non-shaded cells are calculated and should only be modified (by un-protecting the worksheet) if errors are found or adjustments are needed to comply with changes in the theory or code requirements.

Transverse-Analysis.xlsx – seismic displacement and demand calculations, primarily in the transverse direction, but with longitudinal analysis included as well for pile-bent piers (both HTPB and CFST); plastic shear computations for pile-bent piers; shear resistance determination

CFST-Analysis.xlsx – axial load – moment (P-M) interaction for concrete-filled steel tubes; shear resistance of CFST

HTPB-Analysis – axial load – moment (P-M) interaction for hollow tube members used in pile bents; shear resistance of HTPB

CFST-Embed.xlsx – required embedment of concrete-filled tubes into reinforced concrete pier caps; used for both CFST and HTPB since HTPB is identical to CFST at the top plug; multiple criteria are available in the literature and are included in the worksheet

Final-K-Delta-Model.xlsx – coefficients from curve-fitting to be used in estimating displacement capacity of CFST and HTPB construction; plots included as are coefficients for both CFST (35 ksi, 52.5 ksi, and 80 ksi yield strength) and HTPB (35 ksi and 52.5 ksi yield strength)

RCFST-Analysis.xlsx – transverse and longitudinal displacement capacities for RCFST construction; RCFST is the most difficult of the three methods (HTPB, CFST, RCFST) to predict in a spreadsheet-type environment; generally, this worksheet is useful in obtaining a first estimate; detailed analysis using CONSEC or other software adopted by the Structures Division is highly recommended for final design

CFST-IEFF.xlsx – estimation of the effective flexural stiffness (EI_{EFF}) for CFST construction; demonstrates that for typical axial load levels, an increase of approximately 10% over that of the steel tube alone is a reasonable estimate in many cases

Geotech-k-and-L3.xlsx – estimation of abutment pile spring stiffness and pile depth-to-fixity

More detailed descriptions of each spreadsheet follow.

Transverse-Analysis.xlsx

This spreadsheet may be used for preliminary design and includes calculations for seismic displacement demand and displacement capacity in the transverse direction. Up to ten spans may be defined. The spreadsheet is based on the assumptions of:

a) symmetric distribution of lateral stiffness about the center of the bridge; i.e., symmetric span arrangement and symmetric pier heights

b) equal stiffness for each of the two bridge abutments (may be zero, so expansion abutments may be modeled)

c) rigid block behavior of the bridge deck when subjected to ground shaking; this is typically a reasonable assumption when the span length is short relative to the bridge width

d) the three-point design response spectrum

e) short-period displacement amplification in accordance with the AASHTO LRFD Guide Specification

Displacement demand estimates are approximate. Final displacement demand should be determined using *WinSeisab* or other software currently adopted by the Structures Division. Displacement capacity calculation is in accord with the research findings from RES2023-04.

The spreadsheet consists of three worksheets:

1. *Rigid-Block-Bridge*: This is the primary worksheet. Input includes the three-point design response spectrum, the abutment pile stiffness, the span arrangement, the number of tubes (either CFST or HTPB) per pier, the superstructure weight, the pier weight (cap plus diaphragm), the abutment weight, the tube designation, the various pier heights, and the anticipated displacement ductility. The primary output from this worksheet is the **displacement demand** in both the transverse and longitudinal directions.

2. *VP-Sheet*: The input for this worksheet is similar to that for the *Rigid-Block-Bridge* worksheet. Additional input includes the initial axial load per pile, the spacing of tubes, the pier dimensions, and the expected concrete strength for the tube fill. This worksheet is useful in determining the **plastic shear** for a pile bent (either HTPB or CFST). The other primary output from this worksheet is the **transverse displacement capacity**.

3. P-M-Data: Additional input includes the strength limit state pile load, which is used in determining the required depth of cap above the top of the tube. This spreadsheet may be used to determine **displacement capacities** in both the **longitudinal and transverse directions**. Output also includes the **shear resistance** for CFST and HTPB tubes, the required **tube embedment** into the pier cap, and the required **cap depth** above the top of the tube. This worksheet also summarizes the coefficients which are derived from curve-fitting during the research and used to determine nominal flexural resistance and displacement capacity.

CFST-Analysis.xlsx

This spreadsheet may be used to develop axial load-moment (P-M) interaction curves and results for concrete-filled steel tubes (CFST). In developing the spreadsheet, use has been made of the equations found in the Washington State Bridge Design Manual (WSDOT, 2022). The equations are based on the plastic stress distribution method (PSDM). As an alternative to this spreadsheet, section analysis software may be used to determine P-M relationships.

The spreadsheet requires the user to define the limiting strains for compression and tension. Recommended values are e_{uc} = 0.025 in/in for compression and e_{ut} = 0.130 in/in for tension.

P-M interaction curves may be plotted and nominal moment capacities may be determined for any given neutral axis location. Examples of each are shown in the subsequent figures.

Results include the plastic axial load (P_n) and moment (M_n) for a given neutral axis location (q), effective moment of inertia, EI_{EFF}, and nominal shear resistance, V_n.

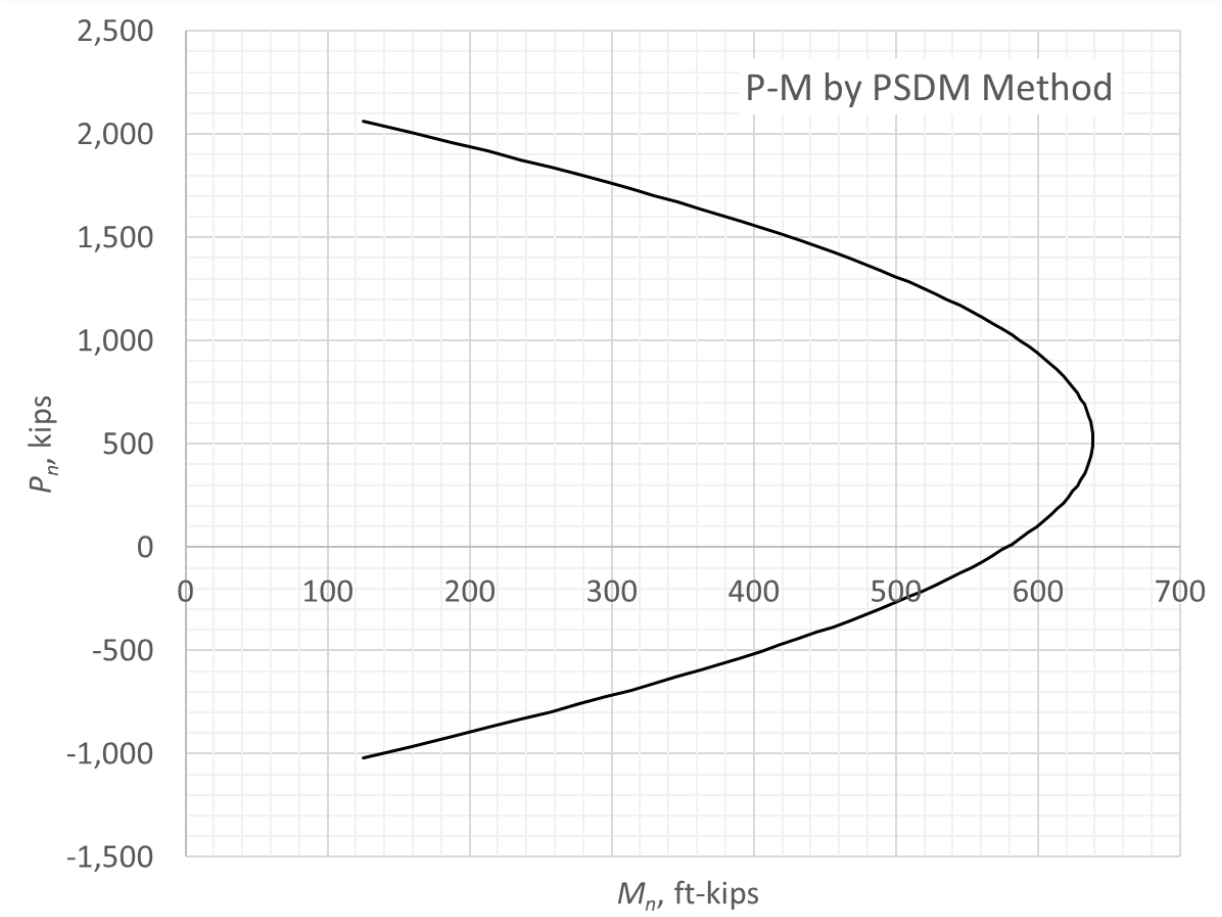

Solution for given Axial Load, P			
Assumed	θ	0.284	radians
c		7.199	inches
y		2.172	inches
P_n		115.0	kips
M_n		7,222.2	in-kips
M_n		601.8	ft-kips

HTPB-Analysis.xlsx

The ***HTPB-Analysis*** spreadsheet may be used to establish axial load-moment (P-M) interaction results for hollow tubes. The methodology employed is from (Rotter & Sadowski, 2017). A plot is produced showing the interaction for both specified and expected yield strength. Section analysis software may also be used to establish P-M interaction results. The spreadsheet includes a comparison between the employed methodology and a section analysis from CONSEC for a 20" x 0.625" tube with yield strengths of 35 ksi (specified) and 52.5 ksi (expected).

The Excel *Data→What-If-Analysis→Goal-Seek* feature can be used to determine the nominal flexural resistance for a given axial load level.

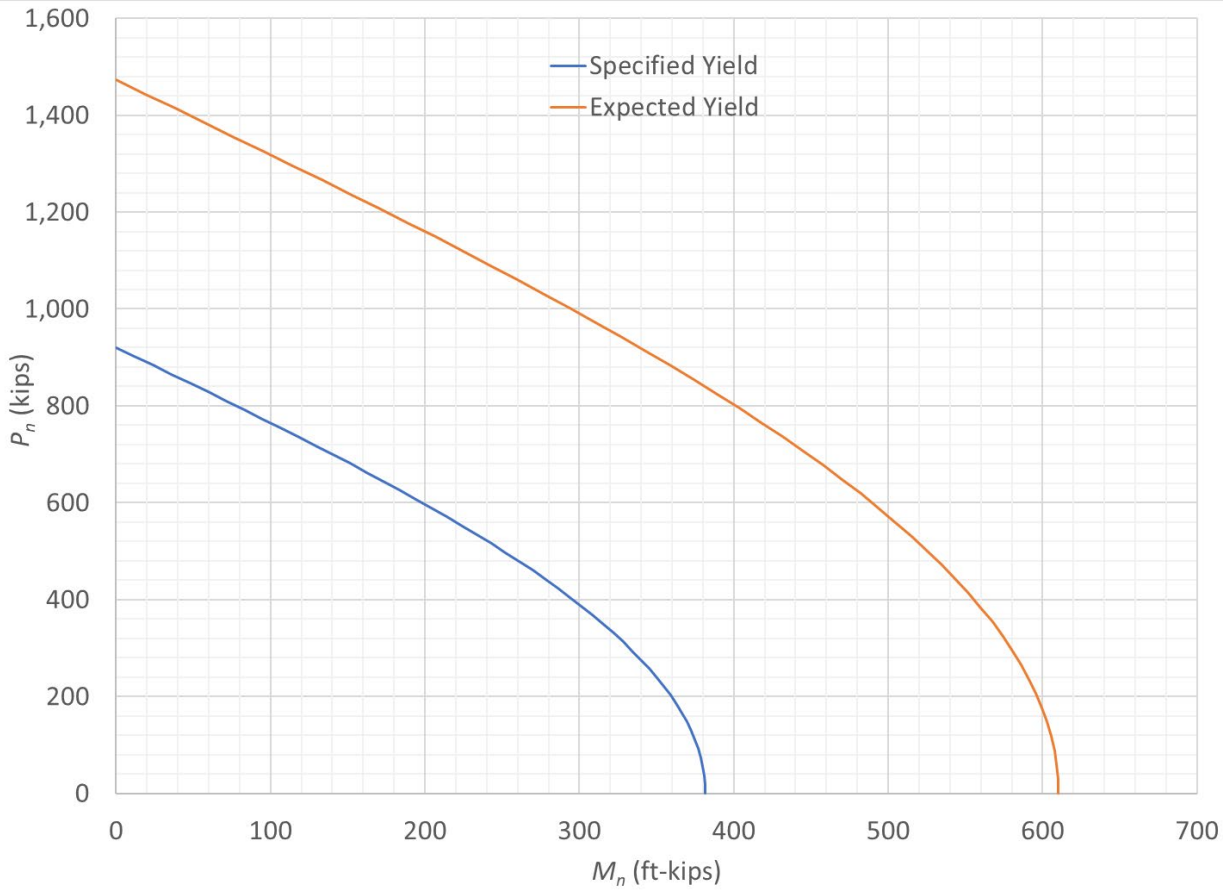

CFST-Embed.xlsx

The calculations on this spreadsheet establish required embedment of tubes into a reinforced concrete pier cap. The required cover concrete above the top of the tube is also determined. Five different criteria from the literature are included. The first method is the method recommended for TODT pile bent bridges constructed with CFST or HTPB. This is the method which most closely and completely mimics circular tubes embedded in a concrete cap without dowels.

1. ***Rapid Construction of Bridge Piers with Improved Seismic Performance*** (Lehman & Roeder, 2012); the method proposed in this study was based on research which required no dowels or internal reinforcement from the tube into the cap; the methodology is appropriate for concrete-filled steel tube (CFST) columns which make use of the embedded annular ring connection; this is the methodology adopted by the Washington State DOT and the methodology recommended for pile bent bridges with pipe piles in Tennessee

2. ***Seismic Performance and Retrofit of Steel Pile to Concrete Cap Connections*** (Shama, et al., 2002); the research upon which this study is based was primarily for H-piles and assumed a linear variation of lateral pressure between the tube and the surrounding concrete

3. ***Performance and Design of Steel Pipe Pile to Concrete Cap Connections Subject to Seismic or High Transverse Loading*** (Kappes, 2016); the proposed embedment equations are based on the use of U-bar reinforcement around the embedded tube; additional research would be required to adopt this methodology;

4. ***Precast Concrete Connections with Embedded Steel Members*** (Marcakis & Mitchell, 1980); the methodology was based on tests on square tubes and relied upon a linear variation of pressure between the tube and the surrounding concrete;

5. ***Laterally Loaded Pile Cap Connections*** (Rollins & Stenlund, 2008); the research was based on tests using pipe piles; a pile embedment of two diameters was found to be adequate for the limited set of conditions tested; additional testing would seem necessary to develop a design methodology

RES2023-04 CFST Tube Embedment / Cap Depth Requirements						
Project Name						
D	12.75	inches		L_e	30	inches
t	0.375	inches				
M_{pE}	3,737	in-kips		***Rollins & Stenlund Criteria***		
λ	1			$(L_e)_{reqd}$	13.07	inches
P_{STR}	280	kips		***Lehman & Roeder Criteria (Recommended)***		
C_{max}	2685	kips		$(L_e)_{reqd}$	29.34	inches
f'_c	4.00	ksi		h_{reqd}	55.22	inches
b	24	inches		***Kappes Criteria***		
L_C	7	feet		$(L_e)_{reqd}$	15.43	inches
F_{us}	112	ksi		***RES2023-04 Strength Criteria***		
D_o	18.75	inches		$(h_{top})_{reqd}$	17.41	inches
λM_{pE}	3,737	in-kips		Controlling h =	55.22	inches
b'	24	inches		L_e = embedment of tube into cap		
e	102	inches		h = total cap depth		
β_1	0.85			h_{top} = cap depth above tube		

Shama, Mander, & Amjad Method		
L_e	23.50	inches
e	95.75	inches
b/D	1.00	
b	12.75	inches
M_{avail}	3,833.2	in-kips

Markakis & Mitchell Method		
L_e	20.00	inches
e	94.00	inches
b/D	1.00	
b	12.75	inches
$(V_c)_{reqd}$	44.49	kips
$(V_c)_{avail}$	48.38	kips

Final-K-Delta-Model.xlsx

A method of determining displacement capacity of pile bents, whether CFST or HTPB construction, recommended by this research involves amplifying the displacement at first yield by a factor, k_D, to determine displacement capacity estimates.

Extensive pushover analyses using fiber-based elements was used to establish the facto, k_D. Yield stress values of 35 ksi, 52.5 ksi, and 80 ksi were included for CFST construction. Yield values of 35 ksi and 52.5 ksi were included for HTPB construction. Subsequent graphs summarize the relationships.

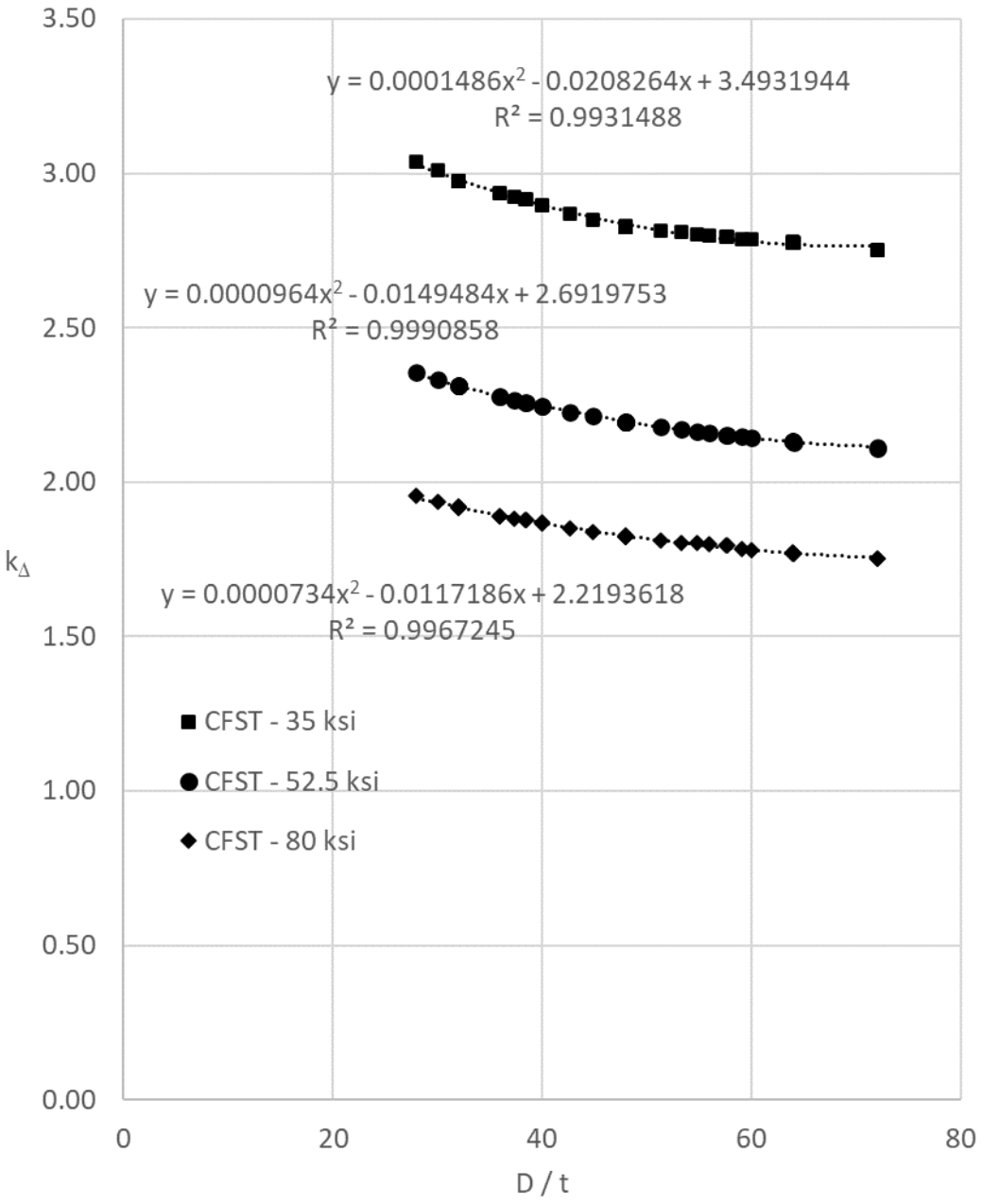
y = 0.0001486x² - 0.0208264x + 3.4931944
R² = 0.9931488
y = 0.0000964x² - 0.0149484x + 2.6919753
R² = 0.9990858
y = 0.0000734x² - 0.0117186x + 2.2193618
R² = 0.9967245
CFST - 35 ksi
CFST - 52.5 ksi
CFST - 80 ksi
k_Δ
D / t
3.50
3.00
2.50
2.00
1.50
1.00
0.50
0.00
0
20
40
60
80

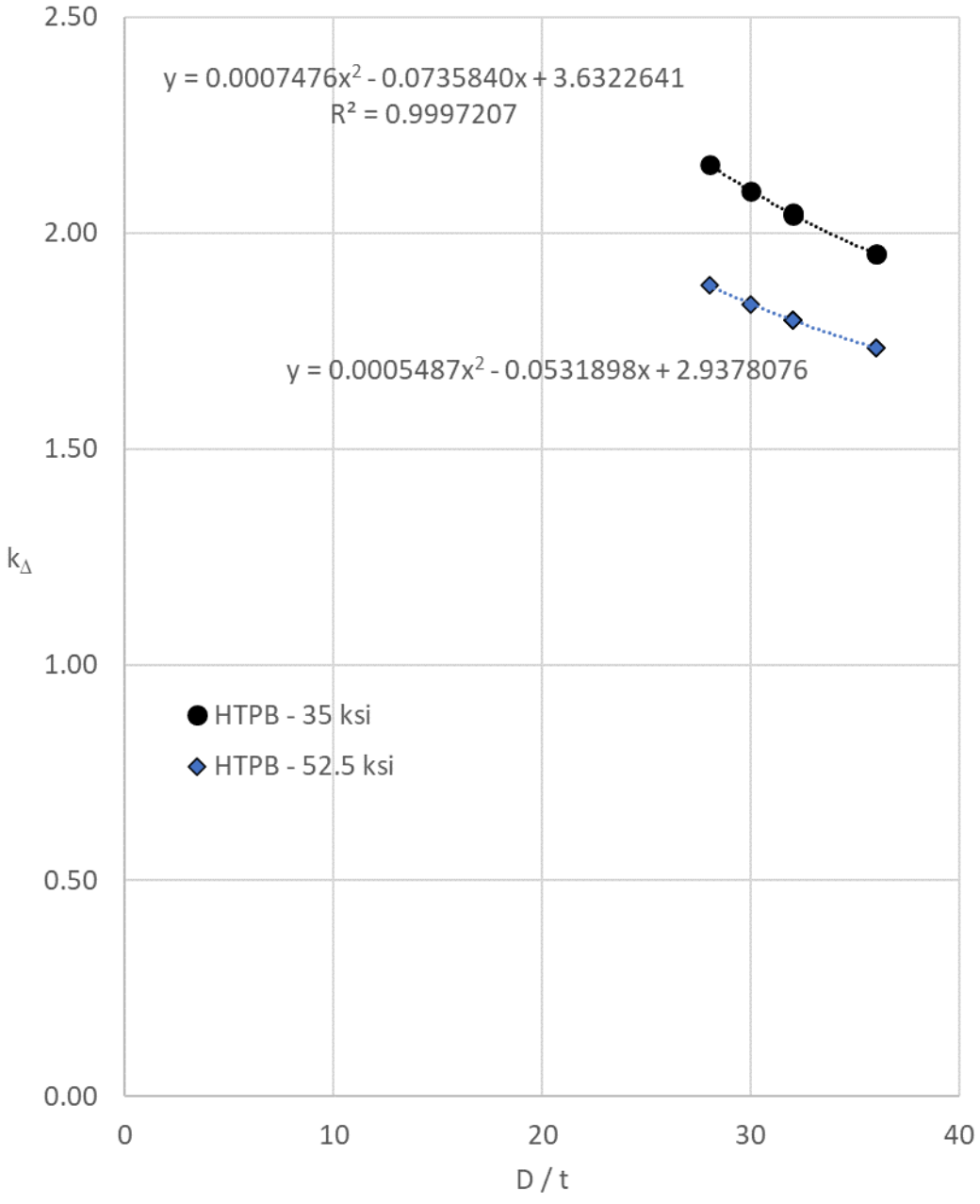
y = 0.0007476x² - 0.0735840x + 3.6322641
R² = 0.9997207
y = 0.0005487x² - 0.0531898x + 2.9378076
HTPB - 35 ksi
HTPB - 52.5 ksi
2.50
2.00
1.50
1.00
0.50
0.00
kΔ
0
10
20
30
40
D / t

RCFST-Analysis.xlsx

The extremely short distance between the top of the tube and the bottom of the cap makes RCFST construction difficult to predict with analytical finite element models. Nonetheless, using an assumed ductility of 4 for this top plastic hinge, it is possible to establish rough displacement capacity estimates. Such an estimate is the primary purpose of this spreadsheet. While other spreadsheets described previously are self-contained, the RCFST-Analysis spreadsheet does require input from CONSEC or other section analysis software for the top plastic hinge. Displacement capacities as well as plastic shears are reported in the spreadsheet.

Tube	CFST20-0625		D / t	32		ρ_s	0.01220	
H_C	25	feet	P	520	kips	f'_{cc} / f'_{cE}	1.366	
Tube F_y	50	ksi	A_s	38.04	in^2	f'_{cc}	6.217	ksi
Tube D	20	inches	I_s	1,787.0	in^4	A_{sp} / s	0.04497	in^2 / in
Tube t	0.625	inches	Core D_c	18.75	inches	Spiral	No. 5	
Fill f'_{cE}	4.55	ksi	A_c	276.12	in^2	s	6.893	inches
α_θ	0.08232		f'_l	0.2744	ksi	Use above in CONSEC		

Longitudinal Bars			Tube Constants			Shear and Embedment		
# of bars	bar size	f_{yE}, ksi	a	b	c	l_{ac}	25.2	inches
7	No. 8	68	-0.000175	0.285514	1,128.5	f_s	0.829	ksi
A_{sr}, in^2	ρ_l	L_{sp}, in.	d	e	f	a'	5.199	
5.53	0.0200	10.2	0.0000964	-0.0149484	2.6920	V_c	24.3	kips
d_{bl}, in.	Transverse Bars		M_y, ft-k	M_n, ft-k	k_Δ	V_S	70.9	kips
1.000	f_{ye}, ksi	68	541.0	1,229.6	2.312	ϕV_n	85.6	kips

Top Hinge (RCFST)			Bottom Hinge (CFST)		Plastic Shear		
M_p, ft-kips	ϕ_y, in^{-1}	L_{C1}, in.	L_{C2}, in.	M, ft-k	V_p	60.4	kips
280.6	0.0002814	55.74	244.3	885.3	λV_p	72.5	kips
δ_{yT}, in.	δ_{uT}, in.		δ_{yT}, in.	δ_{uT}, in.	Load per pile to be applied for Cap Design		
0.408	1.631		4.077	9.428			

Displacement Capacities				M_p and ϕ_y for Top Hinge must be consistent with the data provided here and derived from CONSEC
Transverse (Rigid Frame)		Longitudinal (Cantilever)		
δ_{uT}, in.	11.059	δ_{uL}, in.	14.221	

CFST-IEFF.xlsx

Due to limited driving loads for most CFST tubes, axial loads on these tubes are typically relatively small. This spreadsheet adopts the WSDOT Bridge Manual method for estimating effective flexural stiffness, EI_{EFF}, for concrete-filled steel tubes. The effective flexural stiffness increases as the compressive axial load increases and varies linearly over a wide range of axial load values. A 10% increase over EI_S, where EI_S is the flexural stiffness of the steel tube alone, seems appropriate for cases in which axial compression is relatively low. For cases in which axial loads are relatively high, this spreadsheet may be used to estimate effective flexural rigidity to be used in *WinSeisab*, *CSiBridge*, or other analytical software.

Geotech-k-and-L3.xlsx

Abutment pile spring stiffness may be estimated for a given level of lateral load on the pile. Nine different soil types are included: (1) very loose sand, (2) loose sand, (3) medium dense sand, (4) dense sand, (5) soft clay, (6) medium stiff clay, (7) stiff clay, (8) very stiff clay, and (9) hard clay. As noted in the spreadsheet, the soil in the upper eight pile diameters is most influential and should be the basis for soil type selection. Depth-to-fixity for pile bent piling may also be estimated for any of the same nine soil types.

Stiffness report tab – This tab of the spreadsheet allows the user to input the desired soil type (value of 1 to 9), applied lateral load, pile type, steel modulus, and concrete information. It uses the average load-deflection behavior from Table 8 to plot the load-deflection for the particular pile and soil type. The most applicable approximate linear spring is also plotted. The outputs are:

- Soil and pile-specific value of k
- Estimated top of pile deflection under the specified load

L3 report tab – This tab of the spreadsheet allows the user to input the desired soil type (value of 1 to 9), applied lateral load, pile type, steel modulus, and concrete information. In addition, the pile stickup above grade, L_0, is input. The bending associated with L0 is calculated for reference, and an estimated value of $y_{t\text{-}est}$ is input. An estimated value of L_3/D is selected from **Error! Reference source not found.**, and the estimated values of L_3 and L_2 are provided. This spreadsheet is only partially automated because the next step is to use the estimated L_2 in the structural analysis and determine the calculated deflection, $y_{t\text{-}calc}$. The estimated and calculated deflections are compared with the structural model based on L_2. The spreadsheet is meant to be used iteratively with the structural calculations to determine a best estimate of L_3/D.

Definition of parameters for the spreadsheets

A = the cross-sectional area of a steel tube, in^2

A_S, S_{DS}, and S_{D1} = the pseudo-spectral accelerations defining a three-point design response spectrum

D = the outside diameter of CFST or HTPB tubes, inches

D_o = the diameter of an annular ring welded to the top of a steel tube and embedded in a concrete pier cap, inches

f'_c = the 28-day compressive strength of concrete, ksi; for concrete fill in CFST and HTPB, the recommended value is 4.55 ksi (1.3 times the recommended specified value of 3.5 ksi) when estimating the bent plastic shear

F_{ys} = minimum specified yield strength of a steel tube, ksi

F_{ysE} = expected yield strength of a steel tube, ksi

H_C = the clear column (CFST or HTPB) height as measured from the bottom of the pier cap to the point of fixity in the ground, ft

H_{CAP} = the total depth of the cast-in-place concrete pier cap, feet

h_{top} = the required concrete cover above the top of an embedded steel tube, inches

H_{SS} = the distance from the top of the pier cap to the center of gravity of the superstructure, feet

I = moment of inertia, in^4

K_L = the stiffness of a pile bent in the longitudinal direction, kips per inch

K_T = the stiffness of a pile bent in the transverse direction, kips per inch

k_D = the ratio of ultimate displacement (displacement capacity) to displacement at first yield

L_{c1} = the distance from the point of contraflexure to the bottom of the pier cap for a tube in reverse-curvature bending, feet

L_{c2} = the distance from the point of contraflexure to the point of in-ground fixity for a tube in reverse-curvature bending, feet

L_e = the required embedment of a steel tube into a cast-in-place reinforced concrete pier cap, inches

M_n = the nominal flexural resistance of CFST or HTPB elements as determined from cross-section analysis or equations from the research effort, ft-kips

M_{y1} = the moment in the tube, either CFST or HTPB, at the point of initial yielding on the cross-section, ft-kips

N_{piles} = number of piles at each abutment; abutment pile stiffness is included in the analysis, but backfill contribution to stiffness is neglected

$P_{initial}$ = the estimated, initial axial load on each tube, kips

PSA = pseudo-spectral acceleration, g

P_{STR} = the estimated Strength limit state axial load in each CFST or HTPB, kips; this is used in estimating the required depth of concrete cover above the top of the CFST or HTPB

R = the force-reduction factor in a force-based seismic design procedure

R_d = the short-period amplification factor in a displacement-based seismic design procedure

S = the spacing of piles in the transverse direction, feet

S_s = elastic section modulus of a steel tube, in^3

t = the thickness of a steel tube, inches

T_L = the long-period transition for the design response spectrum, seconds; the value recommended in the literature for the New Madrid Seismic Zone is 12 seconds; also, the natural period of a bridge in the longitudinal direction, seconds

T_T = the natural period of a bridge in the transverse direction, seconds

T^* = the period below which short-period amplification of seismic displacement demand is required

$V_{EQ\text{-}L}$ = the force-based demand on a pile bent in the longitudinal direction, kips

$V_{EQ\text{-}T}$ = the force-based demand on a pile bent in the transverse direction, kips

V_n = the nominal shear resistance of a steel tube, with or without concrete fill, kips

V_P = the plastic shear for a pile bent, kips

W_{SS} = superstructure weight, klf; this includes the deck, the girders, the filler, the overlay, the parapets, any sidewalks, and an allowance for the live load included as part of the active mass during ground shaking; the live load allowance is typically taken as a number of lanes of the HL-93 uniform load

W_{abut} = the estimated weight of each abutment, kips; includes the abutment beam, the backwall, the roadway bracket; since the wingwalls are typically supported on separate piles, it may be acceptable to disregard the wingwalls and wing-beams at the discretion of the designer.

W_{pier} = the weight of each pier cap, kips; this should also include the weight of the support diaphragms at the piers

x = the distance from abutment no. 1 to the pier in question, feet

Z_s = plastic section modulus of a steel tube, in^3

Δ_{uL} = the displacement capacity of a pile bent in the longitudinal direction, inches

$\Delta_{L\text{-}RSA}$ = the seismic displacement demand on a pile bent in the longitudinal direction from a single-mode response spectrum analysis, inches

Δ_{uT} = the displacement capacity of a pile bent in the transverse direction, inches

$\Delta_{T\text{-}RSA}$ = the seismic displacement demand on a pile bent in the transverse direction from a single-mode response spectrum analysis, inches

λ_{mo} = the over-strength factor for CFST and HTPB; the recommended value is 1.2

μ = anticipated displacement ductility demand on a bridge substructure